Changes to the near surface waters of the Canada Basin, Arctic Ocean from 1993-2009

An examination of the consequences of warming and freshening to the water mass structure and optical environment

by

Jennifer Martine Jackson

B.Sc., The University of Victoria, 2002
M.Sc., The University of Alberta, 2006

A THESIS SUBMITTED IN PARTIAL FULFILLMENT OF
THE REQUIREMENTS FOR THE DEGREE OF

DOCTOR OF PHILOSOPHY

in

The Faculty of Graduate Studies

(Oceanography)

THE UNIVERSITY OF BRITISH COLUMBIA

(Vancouver)

March 2011

Abstract

The near-surface water mass structure in the Canada Basin of the Arctic Ocean was examined from 1993 through 2009. This was a period of rapid change due to warming air and ocean temperatures and subsequent sea ice melt. During this time, the Southern Canada Basin transitioned from a perennially ice-covered to an almost seasonally ice-free ocean. It was found that the freshwater from sea ice melt increased the near-surface stratification. Solar radiation was stored below the surface mixed layer as a near-surface temperature maximum (NSTM). From 1993-2009, the NSTM warmed by up to 1.5°C, freshened by up to 4 salinity units, expanded northwards, and formed at successively shallower depths. Below the NSTM is a temperature minimum identified as the remnant of the previous winter's surface mixed layer (rML). Similar to the NSTM, the rML warmed by up to 0.5°C and freshened by up to 2 salinity units from 1993-2009. Using a 1-D model of heat diffusion, it was found that heat from both the NSTM and Pacific Summer Water (PSW) is diffused to the rML. In warmer years, more heat was diffused to the rML from the NSTM. The freshening of both the NSTM and rML was greatest at stations that were located inside the anticyclonic Beaufort Gyre and this is likely because downwelling caused freshwater from sea ice melt to accumulate inside the gyre.

Abstract

An examination of light attenuation to estimate suspended particle concentrations identified six common attenuation features. These features were at the surface, within the summer halocline, within water that has high fluorescence, within cold water that had the salinity range 32.9 - 33.1, within Atlantic water, and at the bottom. It was found that there was no evidence of increased particle concentrations in the basin from 2003-2008. However, the chlorophyll maximum inside the basin deepened from an average of 45 m in 2003 to 61 m in 2008 and it is likely that this is because the nutricline also descended. The deepening of the chlorophyll maximum is one example of how changes to the near-surface water mass structure from climate change can impact the Arctic Ocean ecosystem.

Preface

This is a statement of co-authorship.

Identification and design of research program:

My research used CTD data was collected as part of the Northern Oil and Gas Action Program for 1993, the Joint Western Climate Arctic Study for 2002-2006, and the Canadian International Polar Year Canada's Three Oceans project for 2007-2009. My supervisor Eddy Carmack was a principal investigator in all these projects so helped design where and when the data were collected.

I first observed the NSTM at sea during the summer of 2006 and chose to study it for my thesis. Thus, under the supervision of my committee: Grant Ingram, Eddy Carmack, Fiona McLaughlin, and Susan Allen, I designed a project to analyze the CTD and ice-tethered profile data to examine the NSTM. The fate of the NSTM in chapter 3 was was a natural extension of the work done in Chapter 2 and under the supervision of Susan Allen and Eddy Carmack, I designed a method of examining the CTD data and mooring data. Susan Allen helped me design and write the 1-D model to study heat and salt diffusion used in Chapter 3.

For chapter 4, Fiona McLaughlin and Eddy Carmack designed the idea of studying suspended particles in the Canada Basin and chose the locations

of where to collect transmissometer, TSS and POC data. They also designed the method of collecting and analyzing the data.

Performing the research:

The CTD data were collected during the summer cruises from 1993-2009. I was aboard the icebreaker during the summers of 2006 and 2007 and helped to collect these data. I collected all of the TSS and POC data and prepared them for analysis.

Data analyses:

I analyzed all of the CTD, ITP and mooring data under the supervision of Susan Allen, Eddy Carmack and Fiona McLaughlin. I analyzed the TSS data in 2006 and Maureen Soon analyzed the TSS data in 2007 and the POC data in 2006 and 2007.

Manuscript preparation:

I wrote all 5 chapters of the manuscript. All 5 chapters were edited by Susan Allen, Eddy Carmack, Fiona McLaughlin, Philippe Tortell and Roger Francois. Chapter 2 was edited by Grant Ingram and chapter 3 was edited by Rebecca Woodgate. Chapter 2 was published in the Journal of Geophysical Research in May 2010 with Eddy Carmack, Fiona McLaughlin, Grant Ingram and Susan Allen as co-authors. The citation for this paper is "Jackson, J. M., E. C. Carmack, F. A. McLaughlin, S. E. Allen, and R. G. Ingram (2010), Identification, characterization, and change of the near-surface temperature maximum in the Canada Basin, 1993-2008, *Journal of Geophysical Research,* **115,** C05021, doi:10.1029/2009JC005265". Chapter 4 was published in Ocean Science in September 2010 with co-authors Susan Allen, Eddy Carmack and Fiona McLaughlin. The citation for this paper

is "Jackson, J.M., S.E. Allen, E.C. Carmack, and F.A. McLaughlin (2010), Suspended Particles in the Canada Basin from Optical and Bottle Data, 2003-2008, *Ocean Science,* **6,** 799-813". Thus, anonymous reviewers also helped edit these two manuscripts.

Table of Contents

Abstract ii

Preface iv

Table of Contents vii

List of Tables xii

List of Figures xiii

List of Acronyms xvi

Acknowledgements xviii

Dedication xix

1 Introduction 1

1.1 Physical Oceanography of the Canada Basin 4

1.1.1 General Circulation of the Canada Basin 4

1.1.2 The Chukchi Sea 8

1.1.3 The Beaufort Shelf 11

1.1.4 The Eastern Shelf of the Canada Basin 13

1.1.5 Water Mass Structure of the Canada Basin 14
1.2 Suspended Particles in the Canada Basin 22
1.3 Research Objectives and Layout of Chapters 25

2 NSTM in the Canada Basin... 27
2.1 Chapter Summary 27
2.2 Introduction 29
2.3 Data and Methods 34
2.3.1 Definition of the NSTM 34
2.3.2 Ice Tethered Profiler Data 35
2.3.3 CTD Data 36
2.3.4 Sea Ice Data 38
2.4 Results from ITP Data 38
2.4.1 Seasonal Progression of the NSTM from ITP Data . . 40
2.4.2 Changes to the Upper Ocean Heat Content 46
2.4.3 Ekman Pumping, Winter Storms and Advection . . . 48
2.5 Results from CTD Data 51
2.5.1 The Temperature and Location of the NSTM, 1993-2007 51
2.5.2 How Increased Salt-Stratification has Changed the NSTM from 1993-2007 57
2.6 Discussion 60
2.6.1 Heat Source of the NSTM 60
2.6.2 The NSTM Under a Changing Climate 62
2.7 Conclusions 64

3 Waters Below the NSTM 66

3.1 Chapter Summary 66

3.2 Introduction 67

3.3 Data and Methods 71

3.3.1 Definition of the Near-Surface Water Masses 71

3.3.2 CTD Data 72

3.3.3 Ice Tethered Profiler Data 73

3.3.4 Bering Strait Mooring Data 73

3.3.5 Sea Ice Data 74

3.3.6 Model of Heat and Salt Diffusion 75

3.4 Results: Changes to the Near-Surface Water Masses, 1993-2009 76

3.4.1 The NSTM and rML 76

3.4.2 The Location of the Centre of the Beaufort Gyre . . 81

3.5 Effect of the Beaufort Gyre on Changing Water Mass Properties 85

3.6 Changes to Pacific Summer Water 90

3.6.1 Changes to the Source Waters of Pacific Summer Water 90

3.6.2 Changes to the Pathway and Velocity of Pacific Summer Water 98

3.6.3 Heat Diffusion from the NSTM and PSW to the rML 102

3.7 Discussion and Summary 106

4 Suspended Particles in Canada Basin... 111

4.1 Chapter Summary 111
4.2 Introduction 112
4.3 Data and Methods 116
4.3.1 CTD, Transmissometer and Fluorescence Data 116
4.3.2 POC and TSS Data 118
4.4 Results 120
4.4.1 The Eastern Beaufort Shelf 120
4.4.2 The Western Beaufort Shelf 123
4.4.3 The Eastern Northwind Ridge Slope 125
4.4.4 The Interior of the Canada Basin 127
4.4.5 The Eastern Shelf of the Canada Basin 129
4.4.6 Attenuation from the Shelf to the Basin 131
4.5 Interannual Variation of Beam Attenuation Coefficient and Fluorescence from 2003 to 2008 133
4.5.1 The Eastern Beaufort Shelf 133
4.5.2 The Western Beaufort Shelf 134
4.5.3 The Eastern Northwind Ridge Slope Region 136
4.5.4 The Interior of the Canada Basin 138
4.6 Correlation Between Attenuation and POC and TSS 143
4.7 Conclusions 156

5 Conclusions 160

Bibliography 167

Appendix

A Particles Within the Summer Halocline 189

List of Tables

2.1 Information on collection of ITP data 36

2.2 Information on collection of CTD data part 1 37

2.3 Information on collection of CTD data part 2 37

2.4 Average depth of NSTM and summer halocline, 1993-2007 . . 58

3.1 Number of stations inside gyre, outside gyre and in transition 82

4.1 Attenuation-TSS relationships different regions 147

4.2 Attenuation-POC relationships different regions 148

4.3 TSS-attenuation and POC-attenuation statistics 156

List of Figures

1.1 Map of the Arctic Ocean 5

1.2 Classical and new water masses Canada Basin 16

2.1 Map of the Canada Basin 31

2.2 Water masses of the Canada Basin 32

2.3 NSTM from ITP1 41

2.4 NSTM from ITP6 43

2.5 NSTM from ITP8 44

2.6 NSTM from ITP18 45

2.7 Heat content from ITP data 47

2.8 Ekman pumping and stratification from ITP data 50

2.9 Temperature and location of NSTM from 1993-2003 53

2.10 Temperature and location of NSTM from 2004-7 54

2.11 Average temperature NSTM within latitude ranges, 1993-2007 56

2.12 Average profiles of stratification, 1993-2007 59

2.13 Profile of PAR, temperature and salinity in August 2007 . . . 61

3.1 Changes to near-surface water masses, 1993-2009 70

3.2 Map of Bering Strait moorings 74

3.3 Temperature from ITP8, 2007-2008 78
3.4 Temperature of rML throughout Canada Basin 79
3.5 Salinity of rML throughout Canada Basin 80
3.6 Estimated location of the Beaufort Gyre 83
3.7 Average salinity of the rML relative to the Beaufort Gyre . . 84
3.8 Average water masses relative to Beaufort Gyre, 1993-2009 . 86
3.9 Depth of the NSTM, rML and PSW relative to Beaufort Gyre 88
3.10 Salinity at PSW temperature maximum throughout the basin 92
3.11 Average salinity of PSW relative to the Beaufort Gyre 93
3.12 Comparison of PSW at Bering Strait and the Northwind Ridge 95
3.13 Linear regression between Bering Strait and station CB5 . . . 97
3.14 Estimate of diffusion at PSW in the Canada Basin 101
3.15 Temperature diffusion over 1 year at station CB21 104
3.16 Salinity diffusion over 1 year at station CB21 105

4.1 Map bottle and sensor data and different regions 113
4.2 Attenuation, fluorescence, POC, TSS eastern Beaufort Shelf . 122
4.3 Attenuation, fluorescence, POC, TSS western Beaufort Shelf . 124
4.4 Attenuation, fluorescence, POC, TSS Northwind Ridge 126
4.5 Attenuation, fluorescence, POC, TSS Canada Basin 128
4.6 Attenuation, fluorescence, POC, TSS east shelf Canada Basin 130
4.7 2007 attenuation across different shelf-basin sections 132
4.8 Interannual attenuation eastern Beaufort Shelf 135
4.9 Interannual attenuation western Beaufort Shelf 137
4.10 Interannual attenuation Northwind Ridge 139

4.11 Interannual attenuation Canada Basin 141

4.12 Depth chlorophyll maximum in basin, 2003-08 142

4.13 Average attenuation in 5 different regions 144

4.14 Attenuation-TSS and attenuation-POC for all samples 146

4.15 Relationship between attenuation and TSS in each region . . 150

4.16 Relationship between attenuation and POC in each region . . 152

4.17 Variations POC-attenuation relationships in Canada Basin . 155

A.1 Average attenuation and stratification profiles, 2003-8 190

List of Acronyms

ACC - Alaskan coastal current

ACW - Alaskan coastal waters

AIDJEX - Arctic Ice Dynamics Joint Experiment

AOO - Arctic Ocean Oscillation index

BSW - Bering Sea Water

CAA - Canadian Arctic Archipelago

CESAR - Canadian Expedition to Study the Alpha Ridge

CTD - Conductivity temperature depth profiler

ITP - Ice tethered profiler

NCEP - National Centers for Environmental Prediction

NODC - National Oceanographic Data Center

NSTM - Near surface temperature maximum

PAR - Photosynthetically available radiation

POC - Particulate organic carbon (μgkg^{-1})

PSW - Pacific Summer Water

PWW - Pacific Winter Water

PML - Polar mixed layer

rML - Remnant of the previous winter's mixed layer

SHEBA - Surface Heat Budget of the Arctic

SML - Surface mixed layer

SST - Sea surface temperature

TSS - Total suspended solids (μgkg^{-1})

Acknowledgements

It is a pleasure to thank those who made this thesis possible. I am especially grateful to my supervisors, Susan Allen, Eddy Carmack, Fiona McLaughlin, and Grant Ingram. The completion of my thesis would not have been possible without their knowledge, support, guidance, and willingness to put in many extra hours to achieve what seemed to be an unobtainable deadline. I would also like to thank Susan Allen for agreeing to supervise me after Grant's sudden, tragic passing. I feel very fortunate.

I would also like to acknowledge those who helped with my field work. These include the Captain, crew and science team aboard the CCGS Louis S St Laurent in the summers of 2006 and 2007. In particular, I would like to thank Sarah Zimmerman, Jane Eert, Linda White, Mike Dempsey, Kristina Brown, Helen Drost, Luc Rainville, and Rick Krishfield. On land, Maureen Soon was a great help with processing my samples.

Finally, I would like to thank my family for their unwavering help and support. In particular, my parents and my sister helped us tremendously when trying to combine having children with doing a Ph.D. My children Brody and Autumn are a joy. And I owe my deepest gratitude to my partner Simon for encouraging me to pursue this dream.

Dedication

To Simon - you are my rock. I couldn't have done this without you.

Chapter 1

Introduction

Sea ice first appeared in the Arctic about 47 Million years ago (Ma) and became a year-round feature about 13-14 Ma (Polyak et al. 2010). During this time, there were brief periods (order 1000 years) where the Arctic Ocean was seasonally ice-free (Polyak et al. 2010) and the cause of these interludes is thought to be changes in Earth's orbit around the sun (Polyak et al. 2010) that led to increased solar energy in the Arctic (Miller et al. 2010a). The most recent warm period was during the Holocene from 8500-6000 years ago and although there was reduced sea ice, there is no evidence that the Arctic Ocean was seasonally or perennially ice-free (Polyak et al. 2010). During each warming period, air temperatures in the Arctic increased about 3-4 times more than the rest of the Northern Hemisphere and it is likely that a similar amplification will be observed (Miller et al. 2010b) over the coming century as a result of human-induced climate change (White et al. 2010). While the current human-induced climate change has similar forcing (in terms of size) to some natural climate changes (such as volcanoes and orbital variability), it is difficult to predict the future Arctic climate and its feedbacks since there are no past episodes of human-forced climate change (White et al. 2010).

During the current climate change, the reduction of the Arctic Ocean ice cover has been dramatic. Between 1978-1996, the sea ice areal extent decreased by 2.8% per decade throughout the Northern Hemisphere, with greatest decreases observed in the Okhotsk Sea, Japan Sea, Barents Sea and Kara Sea and a rate of decrease in the Arctic Ocean basin of 1.3% per decade (Parkinson et al. 1999). Prior to 1995, this warming can be explained by an interdecadal atmospheric variability called the Arctic Oscillation, with a cool trend from 1930-1965 and a warm trend from 1965-1995 (Steele et al. 2008). The 1965-1995 warming affected the sea ice thickness, which thinned from an average of 3.1 m in 1958-76 to an average of 1.8 m in the 1990s (Rothrock et al. 1999). The ice loss resulted in a surface freshening of 2 salinity units and an increased heat content of 67 MJm^{-2} between 1975 and 1997 McPhee et al. (1998). Throughout this thesis, salinity is reported as salinity units that are based on the practical salinity scale of 1978 (Unesco 1981). In the last decade, sea ice cover has decreased rapidly. Since 1995, warming that was not correlated with Arctic Oscillation occurred throughout the Arctic such that by 2007, the SST was up to 5 °C warmer than the 100 year average (Steele et al. 2008). This warming has melted snow and thinned ice, and the reduced albedo has resulted in an increase of solar heat input to the ocean by as much as 200 MJm^{-2} from 1979 to 2005 (Perovich et al. 2007). It is estimated that that rate of loss of sea ice areal extent was 10.1% per decade from 1997-2007, with the lowest summer sea ice extent and area ever observed in 2007 (Comiso et al. 2008). The rapid warming over the past decade has caused a decrease in the amount of multiyear ice, from an average of 31% that was at least 5 years old in 1988 to an average of 10%

in 2007 (Maslanik et al. 2007). Climate models have predicted the loss of summer sea ice throughout the Arctic Ocean as early as 2100, however, the recent rapid decline was faster than predicted and implies that summer sea ice could be gone by 2040 (Stroeve et al. 2007). Winton (2006) suggests that a rise above an annual mean polar temperature of -9°C (-5°C) could be the tipping point between a perennially ice-covered and seasonally ice-free (perennially ice-free) ocean.

The decrease in summer sea ice is expected to have significant impacts on the Arctic atmosphere (Ogi and Wallace 2007, Overland 2009), ocean (Shimada et al. 2006, Perovich et al. 2007, Proshutinsky et al. 2009, McPhee et al. 2009, Toole et al. 2010), and ecosystem (Carmack et al. 2006, Carmack and Wassmann 2006, Lavoie et al. 2010). For example, phytoplankton growth is limited by both light and nutrients. In the Canada Basin, the loss of sea ice would be expected to increase both the amount of photosynthetically available radiation and the stratification. The former process would be expected to increase primary production because phytoplankton would be supported at deeper depths while the latter process would decrease primary production because the replenishment of nutrients through vertical mixing would be inhibited. Thus even the direction and magnitude of change, positive or negative, is not known. For my Ph.D. thesis, I studied changes to both the near surface waters, which I define as the upper 100 m (Chapters 2 and 3), and to particle concentrations (Chapter 4) in the Canada Basin and its surrounding shelves during the rapid warming from 1993-2009.

1.1 Physical Oceanography of the Canada Basin

The Arctic Ocean can be considered a Mediterranean sea due to its relatively enclosed, or in the middle of land, nature (Figure 1.1; Aagaard et al. 1985). It is composed of two main basins - the Eurasian and Canadian - that are separated by the 1600 m Lomosomov Ridge and is surrounded by shallow shelves. It has been estimated that shelves account for as much as 53% of the total area (Jakobsson 2002) and only 25% of the volume (Aagaard et al. 1985) of the Arctic Ocean. The Canada Basin alone, with a bottom depth of up to 4000 m, makes up 43% of the total volume of the Arctic Ocean. The Canada Basin is surrounded by shallow shelves on three sides - the Chukchi Sea to the west (details in Section 1.1.2), the Beaufort shelf to the south (details in Section 1.1.3), and the shelves adjacent to the Canadian Arctic Archipelago (CAA) to the east (details in Section 1.1.4).

1.1.1 General Circulation of the Canada Basin

The anticyclonic gyre (herein known as the Beaufort Gyre) that dominates the general circulation of the surface waters of the Canada Basin was first identified based on the drift of ice floe stations and ocean vessels (Coachman and Barnes 1961). An initial estimate of the velocitiy was 1-5 cms^{-1} throughout most of the gyre, with a higher velocity of 10 cms^{-1} just north of Alaska (Coachman and Barnes 1961). Using a coupled ocean-ice model that was forced with NCEP winds, Jahn et al. (2010a) confirmed these velocity estimates for the upper 108 m, which was the depth of the top two layers of their ocean model. By comparing the temperature profiles of two stations

Figure 1.1: A bathymetric map of the Arctic Ocean and the features that are relevant for this thesis. The contour lines represent the bathymetry from 500-3550 m in 500 m intervals. Red lines indicate the inflow of Atlantic water into the Canada Basin based on findings by McLaughlin et al. (2002) and McLaughlin et al. (2009). Green lines estimate inflow of Pacific water into the Canada Basin basin on findings by Coachman and Barnes (1961), Weingartner et al. (1998), and Münchow and Carmack (1997).

in the Canada Basin, I estimated a minimum velocity of about 1 cms^{-1} if the near-surface waters traveled in a unrealistically straight line between stations (Chapter 3.6.2). Since the Beaufort Gyre is anticyclonic, Ekman pumping (downwelling) causes water to accumulate and descend within the gyre. Using satellite passive microwave data, Yang (2006) gave the first estimate of downwelling in the Canada Basin as 0.9 to 4.5 m per month, or about 29 m per year, with highest values in November and December and lowest values in August and September. I confirmed this annual Ekman pumping rate based on ice-tethered profile (ITP; details in Toole et al. 2006) data from 2005 to 2008 (Chapter 2.4.3). McPhee et al. (2009) also found a similar downwelling rate of 27 m per year based on different ITPs. The depth of the Beaufort Gyre is largely unknown. Coachman and Barnes (1961), Shimada et al. (2001), and Steele et al. (2004) suggest that the gyre forces the circulation of Pacific Summer Water (PSW, described in Section 1.1.5) that is found at depths of about 40-100 m. I found evidence that the Beaufort Gyre affects PSW to about 80 m (Chapter 3.4). McLaughlin et al. (2009) suggested that the gyre actually impacts the circulation of Atlantic water (described in Section 1.1.5) based on the spreading of thermal intrusions.

The strength of the circulation of the Beaufort Gyre is influenced by interdecadal climate variability that can be predicted by the Arctic Ocean Oscillation index (AOO), which is based on sea level height (Proshutinsky and Johnson 1997). The AOO has two modes - during the cyclonic regime, the Beaufort Gyre weakens while during the anticyclonic regime, the Beaufort Gyre strengthens. This results in more freshwater stored in

the Beaufort Gyre during the anticyclonic regime that is largely released and exported out of the Arctic during the cyclonic region (Proshutinsky et al. 2002). From 1997 to 2008, the gyre was in a strong anticyclonic mode (Overland 2009, Arndt et al. 2010) and switched to a cyclonic mode in 2009 (Arndt et al. 2010). This, combined with the increased sea ice melt and subsequent stronger near-surface stratification increased the storage of freshwater (relative to the salinity 34.8) within the Beaufort Gyre by about 1000 km^3 (Proshutinsky et al. 2009). Several recent papers have commented on a shift in the location of the Beaufort Gyre from traditionally being centred at 76°N, 150°W to gradually moving towards the southeast Canada Basin in the last decade (Proshutinsky et al. 2009, Yamamoto-Kawai et al. 2009a, McPhee et al. 2009). It has been suggested that the accumulation of freshwater within the gyre has altered the near-surface circulation, with higher velocities along the southern, western, and eastern edges of the gyre (McPhee et al. 2009). Based on mapping the depth of a given isohaline, I found that the location of the gyre was quite variable during my study period and not necessarily in the southeast corner of the Canada Basin in recent years (Chapter 3.4.2). In addition, this fresher Beaufort Gyre altered the near-surface water properties to at least a depth of 40 m and may even have a longer term impact on the water masses (Chapter 3.4).

The other main circulation pattern in the Canada Basin is the cyclonic transport of Atlantic origin water that flows from the Eurasian Basin into the Canada Basin. It is thought that there are 2 main branches of Atlantic water - the Fram Strait branch and Barents Sea branch - whose properties depend on where they were formed (Rudels et al. 1996). McLaughlin et al.

(2009) describe the cyclonic flow as a boundary current that travels at a velocity of about 0.5 cms^{-1}. Its proximity to the shelf allows Atlantic water to be periodically upwelled onto the shelf (further discussed in Section 1.1.2).

1.1.2 The Chukchi Sea

To the west of the Canada Basin is the Chukchi Sea. This large, shallow sea has an average depth of about 50 m (Woodgate et al. 2005a) and it accounts for 5% of the total Arctic Ocean area (Jakobsson 2002). The Chukchi Sea serves as a gateway between the Pacific and Arctic Oceans. Pacific water generally flows northward to the Arctic Ocean through the shallow (about 45 m) Bering Strait (Coachman and Barnes 1961). Flow across the Bering Strait into the Arctic is thought to be primarily controlled by a sea level-induced pressure gradient between the Pacific and Arctic Oceans such that water flows 'downhill' towards the Arctic (Coachman et al. 1975, Woodgate et al. 2005a), however, the transport may reverse to southward flow if wind speeds exceed 8 ms^{-1} from the north (Coachman 1993, Weingartner et al. 1998). Once through the Bering Strait, Pacific waters cross the shallow Chukchi Sea, are modified along the way, and in general flow off the shelf either to the west into the East Siberian Sea or to the east into the Canada Basin (Coachman and Barnes 1961). The geochemical and physical properties of these Pacific origin waters depend on the season in which they were modified and will be further discussed in Section 1.1.5. Of the eastern branch, it is thought that most of the water flows through Barrow Canyon (Aagaard and Roach 1990, Weingartner et al. 1998, Woodgate et al. 2005a, Weingartner et al. 2005). Based on a 2-D barotropic model, Win-

sor and Chapman (2004) found that most of the Pacific-origin water exits the Chukchi Sea through Barrow Canyon when winds are from the south, north, or west, however, strong northeasterly or easterly winds push flow to the northern Chukchi Sea. Thus, wind direction is important in determining where Pacific-origin water enters the Arctic Ocean.

Barrow Canyon is a 250 km, 30 km wide feature that runs parallel to the coast near Point Barrow, Alaska (Aagaard and Roach 1990). Flow is generally down-canyon, towards the Canada Basin, at an average velocity of 13-23 cms^{-1} (depending on location in the canyon) and a peak velocity of up to 100 cms^{-1} (Woodgate et al. 2005a). Reversals to up-canyon flow, caused by upwelling-favourable winds, are common (about 10-15 events per year from 1986-87 moorings (Aagaard and Roach 1990) and 1990-91 moorings (Woodgate et al. 2005a)) and bring waters from the Canada Basin onto the Chukchi Sea shelf. These flow reversals last about 5 days, are most common in fall, and can bring warm (temperature about 1°C), salty (salinity about 34) Atlantic-origin water onto the Chukchi Sea shelf (Aagaard and Roach 1990, Woodgate et al. 2005a). Transport times from Bering Strait to Barrow Canyon vary considerably depending on season, with estimates of 150 days for waters entering Bering Strait in September and 270 days for waters entering in February or March (Panteleev et al. 2010). It is likely that much of this variability can be explained by wind direction because winds are often from the northeast in the late fall to early winter (Weingartner et al. 1998), which would be expected to slow the northward flow across the Chukchi Sea. (Weingartner et al. 1998, Winsor and Chapman 2004, Woodgate et al. 2005a, Panteleev et al. 2010).

Once Chukchi Sea water (which is largely of Pacific-origin (Aagaard and Roach 1990, Woodgate et al. 2005a, Okkonen et al. 2009)) enters Barrow Canyon, it can travel one of three directions - one that travels eastward along the Beaufort shelf, one that travels eastward along the Beaufort slope, and one that turns north into the Canada Basin (Münchow and Carmack 1997). Not much is known about the fate of the water that travels east along the shelf although Okkonen et al. (2009) found that its velocity and pathway are related to wind direction. Due to the shallow nature of the shelf, it is likely that these Pacific waters are heavily modified from sea ice formation, input of river runoff, and wind mixing. More research has been done on the water that flows eastward along the slope. The annual average velocity and transport of this western Arctic boundary current is 6-8 cms^{-1} eastward and 0.39 Sv, respectively (Pickart 2004), although Nikolopoulos et al. (2009) found that the flow can become westward under upwelling-favourable winds. Pickart et al. (2009) correlated upwelling events with northward-travelling Pacific-born storms that originated near the eastern end of the Aleutian Island Arc. These storms were frequent in the fall of 2002 and upwelled warm, salty Atlantic-origin water onto the Beaufort shelf (Pickart et al. 2009) where it likely mixed with Beaufort shelf water. The fate of Pacific-origin water that travels in the western Arctic boundary current is not well-understood although it is generally thought that some water is advected into the Canada Basin and some is transported all the way to the Canadian Arctic Archipelago (Jones et al. 1998, Steele et al. 2004). Mechanisms that transport Pacific-origin water from the boundary current into the Canada Basin are largely unknown, although it has been

suggested that hydrodynamic instabilities of the current can form basin-bound eddies (Pickart 2004, Nikolopoulos et al. 2009), and upwelling events (Pickart 2004) could feasibly advect the boundary current into the basin. The velocity of water that flows northward from Barrow Canyon into the Canada Basin has been estimated (based on 2 days in September 1993) as 5-10 cms^{-1} (Münchow and Carmack 1997) although specific details of this transport and its volume are unknown.

1.1.3 The Beaufort Shelf

The Beaufort shelf is the region that is bordered to the west by Barrow Canyon and to the east by the Amundsen Gulf (Carmack et al. 2006). The shelf is narrow (about 70 km) at the western end and widens to about 120 km at the eastern end (Carmack et al. 2006). At the western end, the feature that likely has the greatest impact on Canada Basin waters is Barrow Canyon that, as discussed in Section 1.1.2, enables cross-shelf transport of Pacific-origin water from the Chukchi Sea and forms an eastward-flowing boundary current along the slope. Heading east, there are several small rivers such as the Sagavanirktok, Colville, and Kuparuk Rivers that can modify shelf properties during spring when the rivers flood (Alkire and Trefry 2006, Carmack et al. 2006). There is no evidence that outflow from these rivers affect waters in the Canada Basin (Alkire and Trefry 2006).

At the eastern end, the features that likely have the greatest impact on Canada Basin waters are the Mackenzie Trough and the Mackenzie River (Figure 1.1). The Mackenzie Trough lies to the west of the main Mackenzie River mouth. Unlike Barrow Canyon, most of the flow through the 60 km

wide, 400 m deep Mackenzie Trough is along-shelf although frequent upwelling events (about 6 in the winter of 1995-96) advect Atlantic and Pacific-origin waters into the canyon (Williams et al. 2006). In winter, Melling and Lewis (1982) found that ice formation along the shelf near the Mackenzie Trough can cause the water to become so dense (σ_t ~26.5) that it flows cross-shelf and into the basin as a density current. It is possible then that the Mackenzie Trough enables the transport of dense winter-derived shelf water into the Canada Basin. The Mackenzie River is the largest river in the North American Arctic and the fourth largest river in the Arctic Ocean. It discharges about 3.3 x 10^{11} m^3 per year of freshwater, with the greatest flows from May to September (Macdonald et al. 1998). The pathway and spreading of Mackenzie River water is controlled by ice thickness (Macdonald et al. 1995a) and wind direction (Macdonald et al. 1999, 2002, Mulligan et al. 2010), with landfast ice in spring restricting and strong winds accelerating the spreading of the river plume. Mackenzie River water is modified as it heads north, becoming saltier as wind-mixing and ice formation erodes the surface stratification and entrains saltier water below (Macdonald et al. 1995a, Mulligan et al. 2010). Based on geochemical data, it is thought that much of Mackenzie River water is advected into the Canadian Arctic Archipelago (McLaughlin et al. 2006), though there are some years when a change in wind direction can transport the water into the southern Canada Basin (Macdonald et al. 1999, 2002). Indeed, more Eurasian river-origin water is generally found in the central Canada Basin than Mackenzie River-origin water (Yamamoto-Kawai et al. 2005, Guay et al. 2009). This suggests that although the Mackenzie River is a prominent feature in my study area,

its impact on near-surface waters and particle concentrations in the Canada Basin may be minimal.

1.1.4 The Eastern Shelf of the Canada Basin

The eastern shelf of the Canada Basin was sampled during the summer of 2007. This was the first time in recent history that the area between the entrance to Amundsen Gulf to the south and the western Archipelago shelf up to about 76°C to the north was virtually ice-free and passable by ice-breaker (Eddy Carmack and Fiona McLaughlin, personal communication). Thus, I collected the first known particular organic carbon (POC) and total suspended solids (TSS) samples and analyzed some of the first CTD, transmissometer and fluorometer data from this region of the Arctic Ocean.

The CAA has been termed an outflow shelf because Arctic Ocean water passes through it on its way to the North Atlantic (Carmack and Wassmann 2006). Little Atlantic water flows over the shallow sills into the CAA so most water is of Arctic or Pacific origin (Carmack and Wassmann 2006). Near surface physical and geochemical processes such as the freeze-melt cycle and nutrient uptake by phytoplankton modify water during its transit so that it has different properties when it enters the North Atlantic (McLaughlin et al. 2006). However, the relatively high silicate content in Baffin Bay suggests that this water still has a Pacific signature after passing through the archipelago (Tremblay et al. 2002). For the eastern shelf of the Canada Basin, it is likely that water generally flows from the shelf into McClure Strait and the Amundsen Gulf of the CAA (McLaughlin et al. 2006, Steele et al. 2004), which may explain why sea ice tends to be heavily ridged in

this region. I found evidence of nepheloid layers transporting particles from the eastern shelf into the Canada Basin (Chapter 4.4.5), which suggests that cross-shelf gravity currents may be important here. There are no major rivers (McLaughlin et al. 2006) or known topographic features such as canyons along this shelf.

1.1.5 Water Mass Structure of the Canada Basin

Traditional Definition of Water Masses

The original classification of water masses in the Canada Basin was based on data from 1894 through 1960 and defined by Coachman and Barnes (1961) as follows (Figure 1.2, black line). At the surface was a deep (about 50 m) mixed layer, called the polar mixed layer (PML), that was relatively fresh and at the freezing temperature. Below the PML was a temperature maximum that was at depths of 75-100 m, had a temperature of 0.5°C to 1.0°C and was within the salinity range 31.6 to 32.4. Below the temperature maximum was a temperature minimum at a depth of about 150 m that had a temperature of about -1.4°C to -1.5°C. Coachman and Barnes (1961) suggested that these waters were originally from the Bering Sea and entered the Canada Basin after transiting through the Bering Strait and Chukchi Sea. Thus, they named both the temperature maximum and minimum Bering Sea Water (BSW). They pointed out that source of the temperature maximum is likely water that flowed through the Chukchi Sea in summer whereas the source of the temperature minimum is water that flowed through in winter. Using geochemical data, Jones and Anderson (1986) confirmed

that the source of BSW was Pacific water that was modified in the Chukchi Sea. In addition, they found that the nutrient maximum was associated with cold BSW centred at the salinity 33.1. Details of the biogeochemical modification of Pacific-origin waters during their transit across Chukchi Sea are sparse, however Grebmeier et al. (2006a) report that the organic carbon concentration increases as the water moves north. Below the BSW was a temperature maximum located at depth of about 250 m to 900 m that had a temperature greater than 0°C and a salinity of 34.5-35. The source of this water is the Atlantic Ocean and it has long been called simply Atlantic water. Below Atlantic water is cold (temperature less than 0°C), salty (34.93 to 34.99) deep water that fills the basin from about 900 m to the bottom (the average basin depth is about 3700 m). It is likely that sporadic (order 1000 years) renewal events cause deep water to flow from the Eurasian Basin to ventilate the deep Canada Basin (Timmermans and Garrett 2006).

Recent Changes to Near-Surface Water Masses

The recent warming and freshening of near-surface waters in the Canada Basin has had a significant effect on the near-surface (which I define as the upper 100 m) water masses. Beginning at the surface, I will discuss below the known changes to the near-surface waters.

I chose to change the name PML to surface mixed layer (SML) for my thesis. This is because the term PML is ambiguous. It implies that there is only one mixed layer in the Canada Basin but recent changes have caused at least one other mixed layer to form. From 1993 through 2009, the SML has shoaled, warmed and freshened. Based on data from ice island T-3

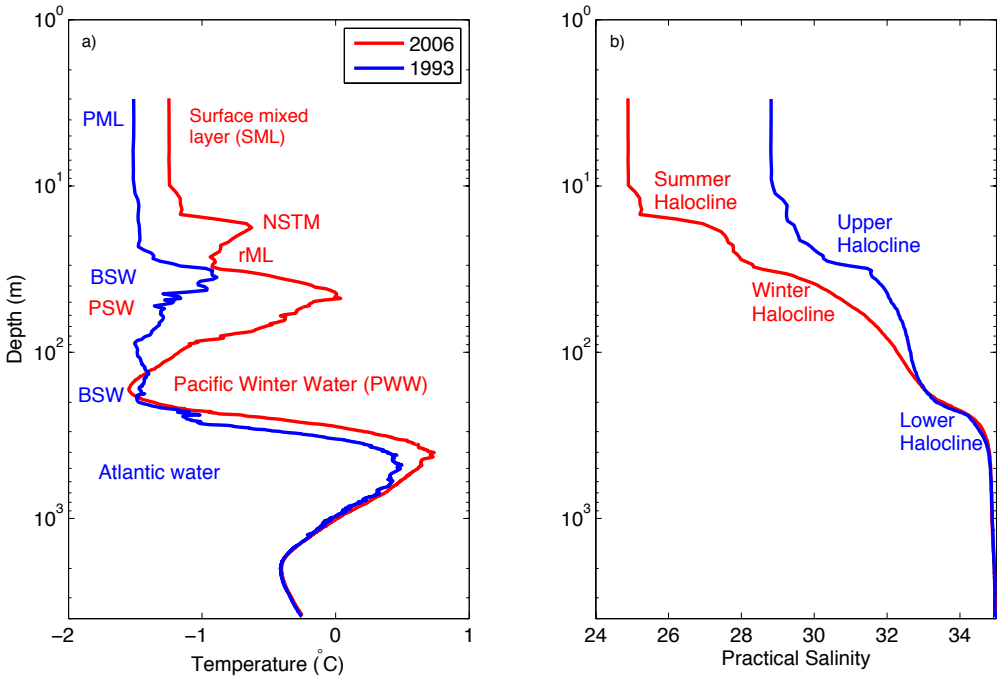

Figure 1.2: The classical (first defined by Coachman and Barnes (1961)) and new water masses observed in the Canada Basin. Both a) observed temperature and b) salinity are shown. Note that the vertical axis is log depth so that the surface features are exaggerated. The blue line and words represent the classical water masses that are represented by data collected at station 18 (76.4°N, 151.3°W) on September 2, 1993. The red line and words are from data collected at station CB4 (76°N, 150°W) on August 29, 2006 and represent the new water masses that I defined in Chapter 2. Here, PML stands for polar mixed layer, SML for surface mixed layer, NSTM for the near-surface temperature maximum, rML for remnant of the previous winter's mixed layer, BSW for Bering Sea Water, PSW for Pacific Summer Water, and PWW for Pacific Winter Water. This figure represents changes observed at one station during the summers of 1993 and 2006. In Chapter 3, I detail similar changes that occurred throughout the Canada Basin from 1993-2009.

(located in the northeast corner of the Canada Basin), collected from 1970-1973, Morison and Smith (1981) found that the SML varied little seasonally - the average SML depth was about 40 m in summer and 50 m in winter, the SML temperature was at the freezing temperature in winter and about 0.5°C warmer in summer, and the SML salinity varied from about 31.25 in summer to 31.65 in winter. In October 1997, the SML depth was about 30 m, the salinity was about 27.5, and the temperature was at the freezing temperature (Kadko 2000). During the summer of 2002, the SML depth in the southern Canada Basin was 15-20 m with a temperature of -1.3°C and a salinity of 26 (McLaughlin et al. 2005). Based on year-round ITP data from 2004 to 2009, Toole et al. (2010) found that the average summer SML depth was 16 m and the average winter SML depth was 24 m. It is likely that the summer SML depth is overestimated because ITPs do not sample above 8 m depth. I suggest that the shoaling of the SML can be explained by the rapid freshening of the surface waters, which formed a new halocline (that I name the summer halocline in Chapter 2). The stratification of the summer halocline is so strong that an eddy diffusivity of 13x10^{-4} m^2s^{-1} in summer (2x10^{-4} m^2s^{-1} in winter) is needed to erode the summer halocline and deepen the SML (Toole et al. 2010). This is 2-3 orders of magnitude greater than the diffusivity of 1-3 x10^{-6} m^2s^{-1} that has been estimated for the Canada Basin (Chapter 3.6.3; Gargett 2003, Zhang and Steele 2007). In addition, the location of the Beaufort Gyre had a impact on the depth of the SML. Freshwater accumulates within the gyre (Proshutinsky et al. 2002), thereby increasing the strength of the summer halocline, and I found that the depth of the SML was about 10-15 m shallower at stations that were

located inside the gyre than those that were outside of the gyre (Chapter 3.5).

The temperature maximum below the SML (Figure 1.2; grey line) was not discussed in the literature until the 1990s. This temperature maximum has been called the summer mixed layer water (Shimada et al. 2001) and I chose to rename it the near-surface temperature maximum (NSTM) because it normally lies at the base of the summer halocline and is therefore not in a mixed layer (Chapter 2.4.1). According to the literature, the NSTM was first observed in late July 1975 during the AIDJEX experiment. McPhee et al. (1998) found that the winter mixed layer was near the freezing temperature until the end of May 1975 and warmed steadily through summer so that by mid-August a NSTM had formed that was 0.2°C above the freezing temperature at a depth of 25 m. A NSTM, with a temperature of 0.5°C above the freezing temperature, was also observed during the SHEBA experiment in mid-October, 1997 at a depth of 30 m (Kadko 2000, Kadko and Swart 04) and in early November, 1997 at a depth of 34 m (McPhee et al. 1998). In December 1997, Shimada et al. (2001) described a NSTM with a temperature of about 0.6°C above the freezing temperature at a depth of 38 m in the western Canada Basin. From 1993-2007, I found that the NSTM spread northwards such that by 2003, it was found throughout the Canada Basin (Chapter 2.5.1). This change was the greatest north of 75°N and I found that from 2004 through 2007, the temperature of the NSTM increased by an average of 0.13°C per year (Chapter 2.5.1). The salinity of the NSTM also freshened from 1993 through 2009 by as much as 4 salinity units (Chapter 3.4.1). Similar to the SML, the NSTM was freshest at

stations that were located inside the Beaufort Gyre.

The heat source that produces the NSTM has been debated. The AIDJEX data showed the gradual evolution of the NSTM, from warmed summer upper water in early summer to a trapped temperature maximum in late summer as the colder winter mixed layer formed at the surface (McPhee et al. 1998). Results from ^{7}Be sampling (a radioactive nuclide with a short half life (53 days) that is useful for studying seasonal processes) during SHEBA in 1997 showed that the water within the NSTM formed during that same summer, confirming that the NSTM formation mechanism is seasonal (Kadko 2000). Thus, it has been suggested that the source of heat in the NSTM is the penetration of solar radiation through leads during summer (Maykut and McPhee 1995, McPhee et al. 1998, Kadko 2000, Kadko and Swart 04). McPhee et al. (1998) suggested that the warm, low salinity water in the NSTM was associated with sea ice melt, whereas Macdonald et al. (2002), based on data collected in 1997, used oxygen isotopes to show that the warm, low salinity water was due to influx of Mackenzie River water. The presence of Mackenzie River water in the basin is anomalous because the dominant eastward wind direction normally pushes these waters towards the archipelago (McLaughlin et al. 2006). Shimada et al. (2001) also noted that baroclinic flow would advect near-surface waters around the perimeter of the Beaufort Gyre so that the NSTM is not necessarily formed by local processes. For stations that were located within the Canada Basin (and thus far removed from coastal processes), I found that the NSTM is formed in mid-June to mid-July when sufficient solar radiation penetrates through leads and melt ponds to warm the near-surface waters (Chapter

2). The summer halocline then forms a few weeks later when enough sea ice has melted to stratify the near-surface waters. The summer halocline prevents mixing and entrainment of the NSTM into the SML, essentially trapping solar radiation below the SML. The NSTM became a year-round feature in the winter of 2007-2008 so solar radiation is now stored throughout the year in the Canada Basin. The storage of the NSTM is also enabled by downwelling, which causes the NSTM and summer halocline to descend by as much as 29 m during the winter, thereby further protecting these features from surface mixing processes such as sea ice formation and wind stress. Thus, the summer halocline traps solar radiation as the NSTM in the Canada Basin where the heat can either be used to melt ice if the summer halocline erodes or to amplify the temperature of the following summer's NSTM if it is stored year-round.

Below the NSTM is a cold mixed layer that I call the remnant of the previous winter's mixed layer (rML). I was the first person to identify this layer (Chapter 2) and to describe how it has changed in recent years (Chapter 3). The rML is the temperature minimum directly below the NSTM (grey line, Figure 1.2), which implies that the presence of the rML is dependent on presence of the NSTM. I suggest that as the NSTM forms each summer, there is a part of the previous winter's SML that is too deep to be warmed by solar radiation. This cold water should have the same properties as the previous winter's SML (i.e. the temperature should be near the freezing temperature and it should have a uniform salinity). In essence, the annual formation of the NSTM traps a remnant of the previous winter's mixed layer below it that forms a separate temperature minimum. The depth of

the rML is about 35-45 m in summer (Chapter 3.5) and, similar to the NSTM, deepens in winter from Ekman pumping (Chapter 2.4.3). Since the rML is trapped below the NSTM and summer halocline, it is unlikely that it will be ventilated by the newly-formed SML. During my study period, I found that, similar to the SML and NSTM, the rML warmed (by about 0.5°C) and freshened (by about 2 salinity units) (Chapter 3.4.1). Using a 1-D vertical model of heat diffusion, I found that the warming of the rML can be largely explained by the diffusion (with a value of $3x10^{-6}$ m^2s^{-1}) of heat from both the NSTM and the temperature maximum below the rML (Chapter 3.6.3). As the NSTM warmed, the rML also warmed because more heat was diffused to the rML. Similar to the NSTM and SML, the rML was fresher at stations that were located within the Beaufort Gyre (Chapter 3.5). It is likely then that the freshwater accumulated in the Canada Basin can explain the freshening of the rML because the rML has been formed in progressively fresher near-surface waters.

Much research has been done on the temperature maximum below the rML that was originally called BSW. For my thesis, I called this feature Pacific Summer Water (PSW) because it's origin is the Pacific Ocean (not just the Bering Sea) and it is modified in the Chukchi Sea during summer. Pacific water entering the Arctic Ocean through Bering Strait has different sources. The Bering Strait is separated into two channels by the Diomede Islands (Woodgate et al. 2005b) that are too small to appear on Figure 1.1. Flowing through the western channel is colder, saltier Anadyr water, while warmer, fresher Alaskan coastal waters (ACW) are found in the eastern channel, and the warmest, freshest Alaskan coastal current (ACC) hugs the

eastern shelf (Coachman et al. 1975, Woodgate et al. 2005b). Of these waters, the source of the temperature maximum that I call PSW in the Canada Basin is thought to largely be a combination of ACW and ACC (Shimada et al. 2001, Steele et al. 2004) that primarily enters the basin through Barrow Canyon (for example Münchow and Carmack 1997). By comparing mooring data in the Bering Strait from 1992 through 2009 to summer CTD data in the Canada Basin from 1993 through 2009, I found that the properties of PSW in the basin are very well-correlated (i.e. R^2 values greater than 0.8) with properties of ACW (Chapter 3.6.1), thus changes to PSW can be explained by changes to ACW. Several recent papers have suggested that some of the reduction of ice cover can be attributed to warming of PSW (Shimada et al. 2001, 2006, Woodgate et al. 2010). Based on an assessment of both ACW water in the Bering Strait and PSW in the Canada Basin, I found no evidence that these waters were either warming or freshening (Chapter 3.6.1). Indeed, it is likely that the strengthening of the summer halocline (Chapter 2.5.2) combined with the deepening of PSW (Chapter 3.5) will further remove PSW from surface processes and the heat in PSW will be less available to melt ice.

1.2 Suspended Particles in the Canada Basin

Predictions for how primary production will change as the Canada Basin becomes ice-free are varied. Some recent papers have postulated that primary production will increase due to a longer growing season from reduced sea-ice cover (Arrigo et al. 2008, Lavoie et al. 2010) and increased export of nutri-

ents from increased river runoff, coastal erosion, and coastal upwelling that could be advected into the basin (Carmack and Wassmann 2006, Dunton et al. 2006). Conversely, other studies have suggested that primary production will decrease due to increased near-surface stratification that reduces vertical nutrient transport (Chapter 2.6.2, Tremblay et al. 2008, Cai et al. 2010), the deepening of the subsurface chlorophyll maximum (Chapter 4.4.4) that could be related to the deepening of nutrient-rich Pacific waters (Chapter 3.5), an observed shift in the phytoplankton species from larger cells to smaller cells (Li et al. 2009), and the acidification of near-surface waters (Yamamoto-Kawai et al. 2009b). In addition, it is predicted that subarctic species are invading the Arctic Ocean, which could have profound effects on the Arctic Ocean ecosystem and its primary production (Grebmeier et al. 2006b). Thus, not even the direction of change - increased or decreased primary production - is known.

The first estimates of organic biomass, which can indicate regions of high primary production, in the Arctic Ocean were based on particulate organic carbon (POC) samples. The first reported POC data from the Canada Basin, collected in the spring of 1968 and 1969 at Ice Station T-3 ranged from 2-14 μgC kg^{-1}, with the highest values of both observed at 50 m (Kinney et al. 1971). Similar values for POC were found in April 1983 along the Alpha Ridge during the CESAR program (Gordon and Cranford 1985). The above concentrations were among the lowest ever observed for an open ocean system, and thus the Canada Basin was described as a biological desert (Kinney et al. 1971, Gordon and Cranford 1985). In 1994, POC samples were collected in summer during the joint Canada-US expedition

from the Chukchi Sea to the North Pole and values in the upper 100 m were about five times greater than previous estimates, suggesting that the Canada Basin is seasonally productive (Wheeler et al. 1997) and actively cycles carbon (Wheeler et al. 1996). Thus, early sampling of production in the Canada Basin was both spatially and temporally sparse.

Transmissometer data, which is a measure of light attenuation, have been collected along the eastern Beaufort shelf and the southern Canada Basin since the mid-1980s and fluorometer data, a proxy for the concentration of chlorophyll *a*, have been collected since the early 1990s. These sensors are attached to the CTD so allow for the entire water column to be examined at every station. Studies have shown that both the concentration of suspended particulate matter (herein known as total suspended solids or TSS), which includes both organic and inorganic particles, and the concentration of POC can be estimated from transmissometer data (Bishop 1986, 1999). Previous research has shown that the relationships between TSS and attenuation and POC and attenuation are well-correlated in Puget Sound (Baker and Lavelle 1984), along the continental rise of the northwest Atlantic (Gardner et al. 1985), in the Gulf Stream (Bishop 1986), in the Laptev Sea near the Lena River delta (Burenkov 1993), in the equatorial Pacific (Bishop 1999) and in the subarctic Pacific (Bishop et al. 1999). Prior to my thesis, the relationships between TSS and POC and attenuation in the Canada Basin had not been examined. To account for spatial variability, I divided my study area into 5 separate regions (the eastern Beaufort shelf, the western Beaufort shelf, the eastern slope of the Northwind Ridge, the interior of the Canada Basin and the eastern shelf of the Canada Basin) and found

that TSS and attenuation were not well-correlated anywhere (Chapter 4.6). In addition, the relationship between POC and attenuation was only well-correlated along the eastern slope of the Northwind Ridge, in the interior of the Canada Basin and along the eastern shelf of the Canada Basin (Chapter 4.6).

To date, there have been no known interannual studies of attenuation or fluorescence data that could answer the question of whether production has increased or decreased due to sea ice melt. I examined both attenuation and fluorescence data that were collected during the summer cruises of 2003 through 2008 (Chapter 4.5). I found no obvious trend of increasing attenuation and instead found some evidence that attenuation may have decreased over my study period. In the interior of the Canada Basin, I found that the depth of the chlorophyll maximum had deepened at a rate of 3.2 m per year. The cause of this deepening and its impact on primary production is an important area of future research.

1.3 Research Objectives and Layout of Chapters

My research objectives for my Ph.D. are:

1. To examine changes to the near-surface water masses in the Canada Basin during a period of rapid warming and freshening that is linked to human-induced climate change from 1993-2009. In particular, I will examine changes to the NSTM and rML.

2. Using transmissometer data from 2003-2008, I will construct a baseline of persistent regions with high attenuation throughout the Canada Basin

and its surrounding shelves. I will correlate these high attenuation regions with POC and TSS data from 2006 and 2007 to determine where the particles are primarily organic or inorganic. I will also examine the attenuation data from 2003 to 2006 to determine if attenuation has changed during my study period.

In chapter two I present the changes to the NSTM in the Canada Basin from 1993 through 2007. In chapter three I examine how the warming and freshening from sea ice melt changed the near-surface water mass structure from 1993 through 2009. In chapter four I present suspended particle concentrations from bottle and optical data from 2003 through 2008. In chapter 5 I conclude and discuss how the near-surface waters in the Canada Basin have changed during the reduction of sea ice cover from 1993 through 2009.

Chapter 2

Identification, Characterization and Change of the Near-Surface Temperature Maximum in the Canada Basin, 1993-2008[1]

2.1 Chapter Summary

Sea ice in the Canada Basin of the Arctic Ocean has decreased significantly in recent years, and this will likely change the properties of the surface waters. A near-surface temperature maximum (NSTM) at typical depths of 25-35 m

[1]This chapter is published as "Jackson, J. M., E. C. Carmack, F. A. McLaughlin, S. E. Allen, and R. G. Ingram (2010), Identification, characterization, and change of the near-surface temperature maximum in the Canada Basin, 1993-2008, *Journal of Geophysical Research,* **115,** C05021, doi:10.1029/2009JC005265."

has been previously described; however its formation mechanisms, seasonal evolution and interannual variability have not been established. Based on summertime CTD surveys and year-round Ice Tethered Profiler data from 2005-2008, I found that the NSTM forms when sufficient solar radiation warms the upper ocean. A seasonal halocline forms in summer once enough sea ice melt has accumulated to separate the surface mixed layer from the NSTM. The surface mixed layer returns to the freezing temperature in fall and the NSTM becomes trapped below the summer halocline, thereby storing heat from solar radiation. This heat can be stored year-round in the Canada Basin if the halocline is strong enough to persist through winter. In addition, energy from storm-driven mixing can weaken the summer halocline and entrain the NSTM, thereby melting sea ice in winter. Throughout this cycle, Ekman pumping within the convergent Beaufort Gyre acts to deepen the NSTM. From 1993 through 2007, the NSTM warmed and expanded northwards and both the NSTM and the summer halocline formed at successively shallower depths. North of 75°N, the temperature of the NSTM increased from 2004-7 by 0.13°C per year and the NSTM and summer halocline shoaled by 2.1m/year and 1.7m/year, respectively from 1997-2007. The formation and dynamics of the NSTM are manifestations of both the ice-albedo feedback effect and changes to the freshwater cycle in the Canada Basin.

2.2 Introduction

Recent changes observed in the Arctic Ocean have been dramatic. The sea ice cover has declined at a rate of ∼11% per decade from 1979-2007 and the sea ice extent observed in September 2007 was 37% less than the climatological average for the same period (Comiso et al. 2008). This decrease in sea ice has led to an increase in the annual amount of solar energy absorbed in the upper ocean, estimated by Perovich et al. (2007) to be 400 MJm^{-2} from 1992-2005 compared to 200 MJm^{-2} 1979-1992. Steele et al. (2008) calculated that this amount of heat would delay freeze-up by 13-71 days and would prevent 56 - 75 cm of sea ice from forming during the following winter in peripheral seas. Overall, the Chukchi and southwestern Beaufort seas have experienced the greatest increase in absorbed solar radiation (Perovich et al. 2007). The loss of sea ice has increased ice velocities and this has increased the rate of Ekman convergence (downwelling) within the Beaufort Gyre (Yang 2009). Despite these documented changes, very little is known about how warming will affect the structure and properties of the upper water column in the central basins of the Arctic Ocean, or how the upper ocean will affect the sea ice cover (Serreze et al. 2007).

The upper 200 m of the Canada Basin in the western Arctic Ocean (Figure 2.1) is a complex layering of water masses (Figure 2.2). The upper 50 m was historically described as the relatively fresh surface mixed layer with temperatures near the freezing point (Coachman and Barnes 1961). Then, based on data from AIDJEX from April 1975 - May 1976, a summertime temperature maximum at a depth of ∼25 m was described in the Canada

Basin (Maykut and McPhee 1995, McPhee et al. 1998). I call this feature the near surface temperature maximum (NSTM) and observe that it lies within the summer halocline - a seasonal feature that is the most stratified part of the water column. Below the NSTM is a temperature minimum that I suggest is the remnant of the previous winter's mixed layer. There are also several distinct water masses of Pacific origin in the upper 200 m. Below the remnant of the winter mixed layer is a temperature maximum that is composed of Pacific origin water that was modified in the Chukchi Sea during summer, which Coachman and Barnes (1961) referred to as Pacific Summer Water (PSW). PSW is typically warmer than -1.0°C (Steele et al. 2004) and has a salinity of ∼31-33 (Shimada et al. 2001, Steele et al. 2004). The deepest Pacific origin feature is a temperature minimum found at a depth of ∼150 m and at a salinity of ∼33.1. This water mass, which Coachman and Barnes (1961) call Pacific Winter Water (PWW), is composed of Pacific origin water that was modified in the Chukchi Sea during winter.

It is important here to make the distinction between the winter mixed layer, which has near-uniform salinity and temperatures near the freezing point, and the summer upper layers (the layers that occupy the upper ∼50 m), which are freshened by ice melt and river inputs and warmed by solar radiation and are thus highly stratified. During AIDJEX, McPhee et al. (1998) found that the winter mixed layer was near the freezing temperature until the end of May 1975. By late July, the summer upper layer had warmed to about 0.15°C above the freezing temperature and by mid-August a NSTM had formed that was 0.2°C above the freezing temperature at a depth of 25 m. A NSTM, with a temperature of 0.5°C above the

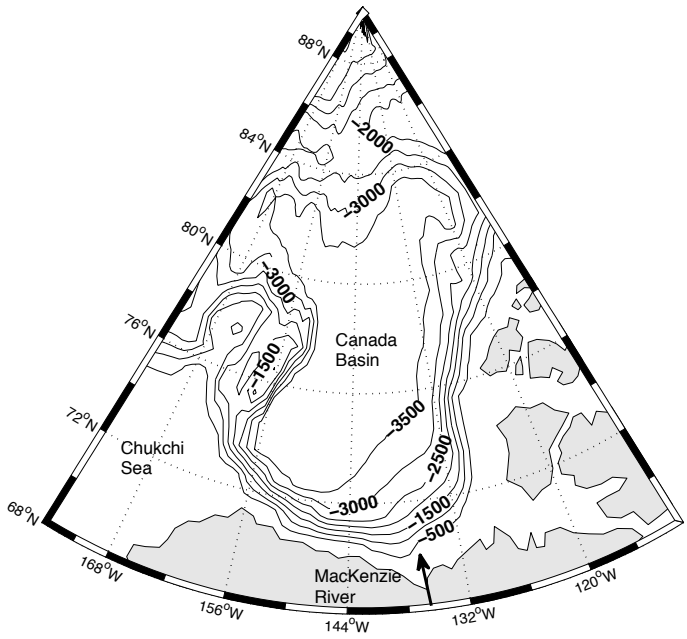

Figure 2.1: A map of the southern Canada Basin. The black lines represent the bathymetry at 500m intervals, from 500m to 3500m. The black arrow represents the approximate location of outflow from the Mackenzie River although the actual path of modified river water depends on ice and wind conditions.

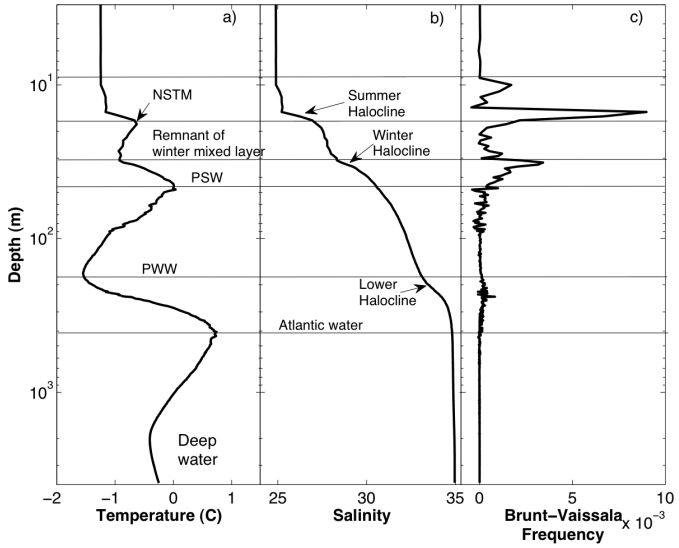

Figure 2.2: Water mass structure of the Canada Basin as characterized by a) temperature, b) salinity and c) Brunt-Väisälä frequency profiles. Note the depth axis is log scale. In summer, there are up to 3 temperature maximums (the near-surface temperature maximum (NSTM), Pacific Summer Water (PSW) and Atlantic water), 2 temperature minimums (the remnant of the previous winter's surface mixed layer and Pacific Winter Water (PWW)), and 3 haloclines (the summer halocline, the winter halocline and the lower halocline). The strongest stratification is associated with the NSTM. Profiles are from a station located at 75° N, 150° W, occupied on August 29, 2006.

freezing temperature, was also observed during the SHEBA experiment in mid-October, 1997 at a depth of 30 m (Kadko 2000, Kadko and Swart 04) and in early November, 1997 at a depth of 34 m (McPhee et al. 1998). In December 1997, Shimada et al. (2001) described a NSTM with a temperature of about 0.6°C above the freezing temperature at a depth of 38 m in the western Canada Basin. Thus, a NSTM was observed from August to December in the central and western Canada Basin with characteristic

temperatures increasing from 0.2°C to 0.6°C above the freezing temperature between 1975 and 1997.

The heat source that produces the NSTM has been debated. The AIDJEX data showed the gradual evolution of the NSTM, from warmed summer upper water in early summer to a trapped temperature maximum in late summer as the colder winter mixed layer formed at the surface (McPhee et al. 1998). Results from ^{7}Be sampling (a radioactive nuclide with a short half life (53 days) that is useful for studying seasonal processes) during SHEBA in 1997 showed that the water within the NSTM formed during that same summer, confirming that the NSTM formation mechanism is seasonal (Kadko 2000). It has then been suggested that the source of heat in the NSTM is the penetration of solar radiation through leads during summer (Maykut and McPhee 1995, McPhee et al. 1998, Kadko 2000, Kadko and Swart 04). In addition to the increased temperature of the NSTM in 1997 compared to 1975, the near surface water column was about 2 salinity units fresher. McPhee et al. (1998) suggested that the warm, low salinity water in the NSTM was associated with sea ice melt, whereas Macdonald et al. (2002) used oxygen isotope data to show that the warm, low salinity water was due to influx of Mackenzie River water. Shimada et al. (2001) also noted that baroclinic flow would advect near-surface waters around the perimeter of the Beaufort Gyre so that the NSTM is not necessarily formed by local processes.

Given the reductions of sea ice cover during the past decade, which have substantially altered the regional ice-water albedo ratio, I suggest that the properties of the NSTM have continued to change since the late 1990s.

In addition, I will show that the stronger near-surface stratification from accelerated sea ice melt traps heat in the NSTM for longer periods of time, thereby storing solar radiation in the Arctic Ocean as a result of the albedo-feedback effect. Here, I will examine conductivity, temperature and depth (CTD) sensor data from the Canada Basin sampled during the summers of 1993, 1997 and 2002-2007 to identify the characteristics and geographical location of the NSTM and to determine whether its temperature warmed during this time. Also, I will analyze CTD data collected year-round from Ice-tethered profilers (ITP; Toole et al. 2006) deployed in the Canada Basin from 2005-8 to investigate the distribution and seasonal evolution of the NSTM. Based on these data, I will describe its mechanism of formation, show its seasonal progression and then discuss its interannual and spatial variability.

2.3 Data and Methods

2.3.1 Definition of the NSTM

The NSTM was observed each year and its depth, spatial distribution, and temperature varied significantly. To compare the NSTM in space and time, I first calculated the observed temperature of the NSTM relative to the freezing temperature ($T_f(S,p)$), which is a function of salinity (S) and pressure (p), for all ship-based and ITP CTD profiles as:

$$T_f(S,p) = -0.0575S + 1.710523\times10^{-3}S^{3/2} - 2.154996\times10^{-4}S^2 - 7.53\times10^{-3}p \quad (2.1)$$

where p is in decibars and $T_f(S, p)$ fits measurements to an accuracy of 0.004°C (Gill 1982). I then defined the NSTM as present if it met three criteria - i) The NSTM was the temperature maximum that was nearest to the surface and was above a temperature minimum that was at least 0.1°C colder than the NSTM. This criterion ensured that the NSTM was a distinct layer separate from the deeper temperature maxima; ii) The NSTM was defined as having a salinity less than 31 to ensure that the temperature maximum was not PSW; iii) The NSTM was defined as present when the maximum temperature was at least 0.2°C above the freezing temperature. This temperature difference, though somewhat subjective, was chosen because it was the maximum temperature above freezing observed during the AIDJEX in the summer of 1975 (McPhee et al. 1998), and thus serves as a baseline for comparison.

2.3.2 Ice Tethered Profiler Data

Data from ITPs deployed in the Canada Basin provide year-round observations from the upper Canada Basin (Krishfield et al. 2008, Toole et al. 2006). Here, archived (level 3) CTD data were examined from ITP1, ITP6, ITP8 and ITP18. The measurement error for both temperature and salinity from level 3 data is estimated at 0.005 (Richard Krishfield, personal communication). The locations and dates of deployment of these ITPs varied through the study period (Table 2.1). Data collection commences at about 8 m and continues to 800 m with 1 m resolution. These data are biased to waters that have a high ambient ice concentration and it is likely then that the ITP data only show NSTMs formed in relatively ice-covered waters. In

Table 2.1: Date range and location range for ITP1, ITP6, ITP8 and ITP18. Temperature and salinity data from these ITPs were used to investigate the seasonal progression of the NSTM.

ITP	Date range of data collection	Start Location	End location
ITP1	Aug 16, 2005 - Aug 15, 2006	78.8° N, 150.1° W	77.2° N, 132.7° W
ITP6	Sept 5, 2006 - Aug 10, 2007	78.2° N, 140.1° W	74.8° N, 139.9° W
ITP8	Aug 12, 2007 - July 24, 2008	78.4° N, 153.8° W	79.1° N, 132.9° W
ITP18	Aug 17, 2007 - July 28, 2008	79.9° N, 140.1° W	75.3° N, 143.4° W

contrast, the ship-based CTD data gives a yearly snapshot of conditions at pre-determined locations in various ice conditions during the summer, and thus show NSTMs formed in a range of sea ice conditions. ITP data with preliminary processing are available online at http://www.whoi.edu/itp. I analyzed profiles on a 3 day interval and only examined profiles that started at a minimum depth of 10 m.

2.3.3 CTD Data

Temperature and salinity CTD data were collected by researchers from Fisheries and Oceans Canada in collaboration with researchers from Woods Hole Oceanographic Institution and the Japan Agency for Marine-Earth Science and Technology in 1993, 1997, 2002-07 using instruments reported in Tables 2.3 and 2.3. In 2007, photosynthetically active radiation (PAR, 400-700nm) data were collected at select stations with a biospherical PAR sensor that was attached to the CTD.

Table 2.2: Data collection dates and information on CTD used during each cruise and from the ice tethered profilers.

Year	Date range	References
1993	Aug 3 - Sept 25	Macdonald et al. (1995b)
1997	Sept 24 - Oct 15	Macdonald et al. (2002)
2002	Aug 18 - Sept 5	Shimada et al. (2005)
2003	Aug 13 - Sept 3	McLaughlin et al. (2008)
2004	Aug 5 - 30	McLaughlin et al. (2008)
2005	Aug 3 - 31	McLaughlin et al. (2008)
2006	Aug 7 - Sept 12	McLaughlin et al. (2008)
2007	July 27 - Aug 28	McLaughlin et al. (2008)
2005-8	ITP - year round	Krishfield et al. (2008)

Table 2.3: Data collection dates and information on CTD used during each cruise and from the ice tethered profilers.

Year	CTD make	CTD model	Temp precision (°C)
1993	FSI CTD	ICTD	0.002
1997	Neil Brown	MkIII	0.002
2002	Seabird	SBE-911 Plus	0.001
2003	Seabird	SBE-911 Plus	0.001
2004	Seabird	SBE-911 Plus	0.001
2005	Seabird	SBE-911 Plus	0.001
2006	Seabird	SBE-911 Plus	0.001
2007	Seabird	SBE-911 Plus	0.001
2005-8	Seabird	SBE-41-CP	0.002

2.3.4 Sea Ice Data

Sea ice concentrations were obtained from the National Snow and Ice Data Center (http://www.nsidc.org). I used the final data produced from the Nimbus-7 Scanning Multichannel Microwave Radiometer (SMMR) and the Defence Meteorological Satellite Program (DMSP) -F8, -F11 and -F13 Special Sensor Microwave/Imager (SSM/I) radiances (Cavalieri et al. 2008) . These data have a 25 km spatial resolution. Here, both daily and monthly averaged data were used to determine the representative sea ice concentrations during the ship-based CTD sampling. Monthly averaged data from August were used except in 1997, when the later cruise meant that September data were more representative of conditions during the sampling period.

2.4 Results from ITP Data

ITP data give continuous, year-round conditions in the Arctic Ocean, but only where sufficient sea ice persists to support the system. Here, I use summer 2005 - summer 2008 ITP data to investigate the seasonal evolution of the NSTM. Initial observations showed that the depth of the NSTM was closely linked to the depth of a near-surface pycnocline, which I call the summer halocline (Figure 2.2). Thus, the Brunt-Väisälä frequency (N) was calculated as

$$N^2 = \frac{-g}{\rho}\frac{d\rho}{dz} \tag{2.2}$$

to compare the strength of the stratification. For this equation, a value of 9.8 ms^{-2} was used for gravity (g), ρ represents the observed density and z is

the vertical distance measured upwards. Once the Brunt-Väisälä frequency was calculated, the depth of the maximum Brunt-Väisälä value was used to represent the most stratified region of the water column.

Here, I describe the seasonal evolution of the summer halocline. The summer halocline is formed when enough sea ice melt water is injected into the ocean to stratify the near-surface waters, thereby becoming a barrier between the fresh surface mixed layer and the saltier waters below. The summer halocline continues to strengthen until either solar radiation weakens and there is not enough heat in the surface waters to melt sea ice or until all the ice has melted. At this time, the summer halocline stops forming and is either entrained into the surface mixed layer if there is enough mixing from air-sea and ice-water stress to break down the stratification or, if not, the halocline remains intact below the descending surface mixed layer. At this time, the summer halocline represents a remnant of the previous summer's stratification.

In the following evaluation of the annual progression of the NSTM based on ITP data, I will call each summer halocline according to the year in which it was formed. It is also important to note here that I neglect advective effects in the following section. While lateral advection is no doubt important in the Canada Basin, I instead focus on the average seasonal evolution of the NSTM. How advection, and in particular baroclinic advection, affects the NSTM would be an important topic for future research.

2.4.1 Seasonal Progression of the NSTM from ITP Data

From August 2005 to August 2006, ITP1 moved from the north-west to the east part of the Canada Basin, within the range of 75-80°N, 131-153°W (Figure 2.3). From at least mid-August through late-October 2005, a NSTM was present in the salinity range of 28-30 and was generally deeper than 20 m. The water at 10 m reached the freezing temperature in early October, indicating the onset of freezing and the end of summer 2005 halocline formation. The NSTM gradually cooled and deepened, with average temperatures above the freezing temperature of 0.32°C, 0.27°C and 0.24°C and depths of 20 m, 24 m and 29 m in August, September and October, respectively. During this period, the summer 2005 halocline (denoted by the Brunt-Väisälä frequency maximum) was always above the NSTM, with an average depth between the two features of 3 m (Figure 2.3b). From the beginning of November, a NSTM was observed sporadically until mid-June. During this period, the NSTM deepened to an average depth of 41 m yet the temperature varied, with the warmest NSTMs observed at the beginning of February and in early May. Higher temperatures coincided with the most southwesterly location of ITP1. The NSTM first reappeared near the surface in mid-July and persisted above 22 m through at least mid-August. In comparison, the maximum Brunt-Väisälä frequency remained deep, below 35 m, until mid-August, when the summer 2006 halocline formed at 12 m. It is interesting to note that while the summer 2006 halocline appears to have formed intermittently in August 2006 (Figure 2.3b), the depth of the maximum in Brunt-Väisälä frequency alternated between two stratified

waters - the summer 2006 halocline and the deeper summer 2005 halocline.

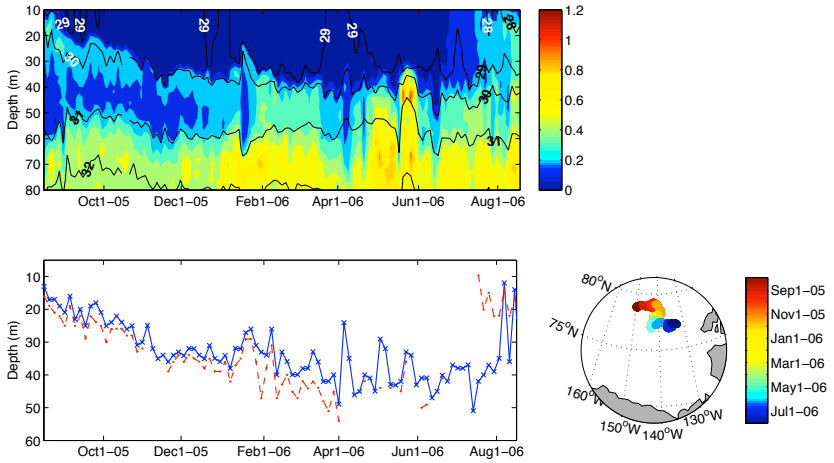

Figure 2.3: Results from ITP1. Figure a) is a contour plot of the observed temperature above the freezing temperature from 10-80 m at ITP1. The black lines indicate the salinity contours at 1 salinity unit intervals. Figure b) is a comparison of the depth of the Brunt-Väisälä Frequency maximum (blue line with blue exes that denote the sample dates) and the depth of the NSTM (red dashed line with red dots that denote the sample date) over the sample period. Figure c) shows the movement of ITP1 over the sample period. Data from every 3 days were plotted from August 16, 2005 to August 15, 2006.

From September 2006 to August 2007, ITP6 moved south in the central region of the Canada Basin, in the range of 74-79°N, 136-145°W (Figure 2.4). ITP6 was deployed later than other ITPs and the NSTM was already deep at the beginning of September. The water at 8 m reached the freezing temperature in late September. A progressively deepening NSTM was observed consistently until the end of January and then sporadically until the middle of April. Again, the NSTM cooled and deepened through fall, with

average temperatures above the freezing temperature of 0.32°C, 0.26°C and 0.26°C and depths of 26 m, 33 m, and 37 m in September, October and November, respectively. The depth of the summer 2006 halocline was again on average just 3 m shallower than the NSTM until the end of January and there were no instances when the NSTM was above this stratified water. A deeper temperature maximum that could be PSW was present throughout the study period and was cooler and deeper until the end of January, then became warmer and shallower as ITP6 moved south from May through August. The NSTM first reappeared near the surface in mid-June and persisted above 21 m until at least mid-August. The summer 2007 halocline was first observed in mid-July at 11 m, however the most stratified water was associated with the PSW so this feature is not evident in Figure 2.4b. The warmest NSTM was 0.95°C above the freezing temperature on August 8th at 18 m, more than two times the temperature of the NSTMs observed by ITP1 in 2006.

From August 2007 to July 2008, ITP8 moved from the northwest to the northeast region of the Canada Basin, within the range of 78-81°N, 130-154°W (Figure 2.5). In the summer of 2007, the NSTM was relatively shallow until the end of August and the warmest NSTM was 0.73°C above the freezing temperature at 16 m on August 30th. The NSTM was observed, for the first time, year-round from ITP8. The NSTM again cooled and deepened through the fall, with average temperatures above the freezing temperature of 0.57°C, 0.49°C and 0.49°C and depths of 24 m, 31 m and 31 m in September, October and November, respectively. The depth of the summer 2007 halocline was just above the NSTM, with an average difference

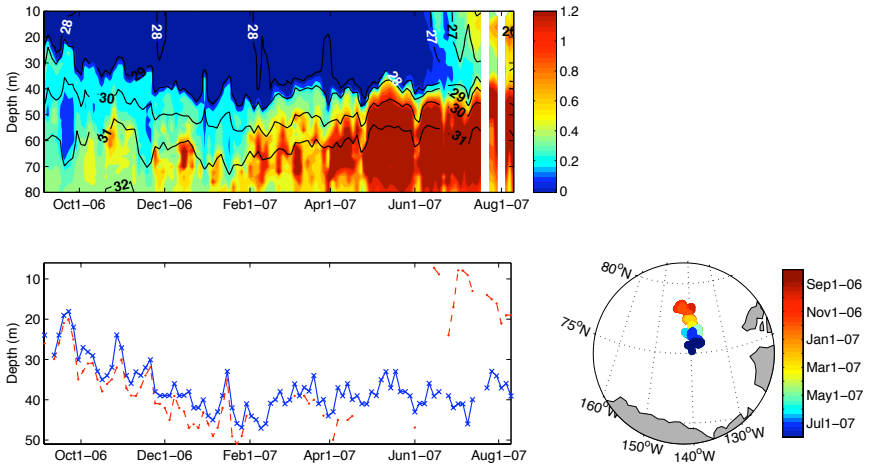

Figure 2.4: As in Figure 2.3 but for ITP6 from September 5, 2006 to August 10, 2007. White regions in a) denote times when data were not available. White region denotes time when data were not available.

of 4 m, until the beginning of February, when these features, with an average difference of 10 m, became less correlated. The NSTM first reformed at the end of June 2008, and the summer 2008 halocline formed in early July.

From August 2007 to July 2008, ITP18 followed the anticyclonic path of sea ice in the Beaufort Gyre (Proshutinsky et al. 2002), within the range of 74-79°N, 131-145°W (Figure 2.6). Overall, the near-surface water properties were different at ITP18 than other ITPs and three features were of note. First, the NSTM was shallower throughout late summer to early fall 2007, and did not consistently descend below 20 m until late October. It is interesting to note that the water at 8 m reached the freezing temperature on October 9th, thus for almost 3 weeks ice was forming less than 20 m above water that was up to 0.7°C above the freezing temperature. Second,

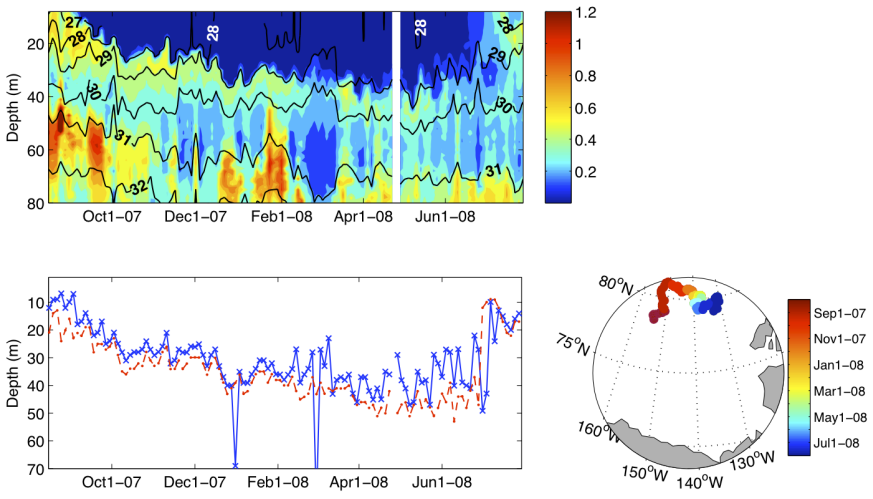

Figure 2.5: As in Figure 2.3 but for ITP8 from August 12, 2007 to July 28, 2008. White region denotes time when data were not available.

the NSTM was on average 6 m deeper than the summer 2007 halocline from mid-August to the beginning of December, which was more than the 3 m - 4 m difference observed from the other ITPs. Third, the depth of the NSTM and summer 2007 halocline were much more variable from December through June than at the other ITPs. Some of the latter variability can be explained by the movement of ITP18. At the end of December, ITP18 moved south, into a region which contained a warm, shallow NSTM below the freshest observed surface water. From February to mid-March, ITP18 moved west, into a region with a deeper NSTM below relatively unstratified water. In late March, near 145 °W, ITP18 again moved into a region with a relatively shallow NSTM. The NSTM was then only seen intermittently from mid-April through the end of May. Overall, there were multiple pycnoclines

in the upper water column through this winter. Thus, my method of simply choosing the maximum Brunt-Väisälä frequency to represent the summer 2007 halocline doesn't distinguish between this and other regions stratified by eddies and other water masses. Likewise, there were several instances, for example in early March, where the NSTM may have merged with a deeper temperature maximum that could be PSW, thus my analysis may have identified a NSTM when one was not present. I left these examples to show the complex near-surface structure of the south-central Canada Basin in early 2008. The NSTM reformed in late-June and the summer 2008 halocline formed in early July. Both these features were observed at a shallow depth through the remainder of my study period.

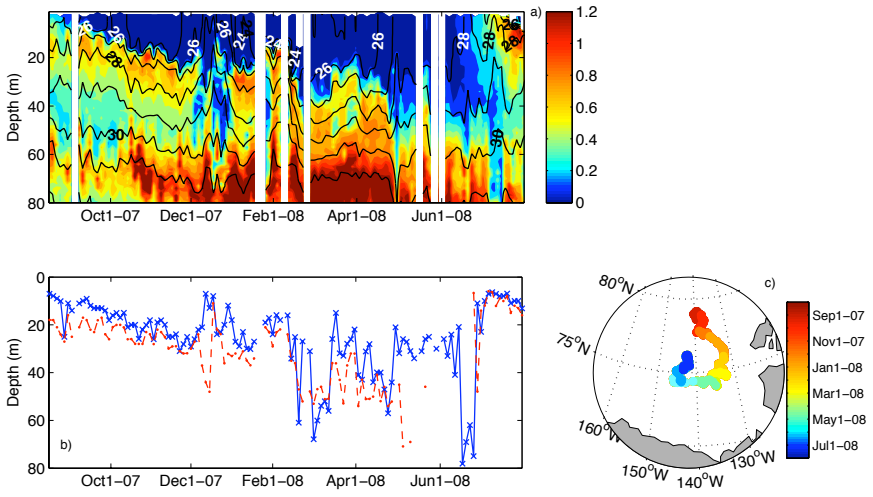

Figure 2.6: As in Figure 2.3 but for ITP18 from August 17, 2007 to July 31, 2008. White region denotes time when data were not available.

2.4.2 Changes to the Upper Ocean Heat Content

In the previous section, I found that i) The NSTM warmed form 2005-8, ii) The NSTM was warmer at more southerly locations, and iii) The NSTM was a year-round feature in the winter of 2007-8. This variability would be expected to have a significant impact on heat stored in the upper waters of the Canada Basin. To examine these changes, I calculated the heat content (HC) relative to the freezing temperature above PWW. HC was calculated as:

$$HC = \rho_o C_p \int (T - T_f)(S, P) dz \tag{2.3}$$

where ρ_o, the reference density, was 1027 kgm^{-3}, C_p, the specific heat of seawater, was 3986 J°C^{-1}kg^{-1}, and $(T - T_f)(S, P)$ was the temperature relative to the freezing temperature interpolated in 1 m intervals. The base of the initial calculation was chosen to be PWW since this is a relatively consistent feature whose presence can be approximated based on temperature and salinity profiles. My initial findings suggested that the depth of PWW varied considerably from about ∼130 m in 2005 to ∼190 m in 2008. To correct for this, I calculated the average heat content per meter instead of the total heat content above PWW. Also, the initial examination found that changes to the heat content of the NSTM were often dwarfed by variations in the temperature maxima below the remnant of the winter mixed layer (rML, temperature minimum below the NSTM). Thus, to highlight near-surface changes, I separated the water column into two different layers and calculated the average heat content per meter in each layer. The first

layer was from 10 m to the rML (Figure 2.7a) and the second layer was from rML to PWW (Figure 2.7b). There were a few instances when no rML was present, for example in May 2007 from ITP6. In these cases, I instead plotted the average heat content from PWW to 10 m in Figure 2.7b.

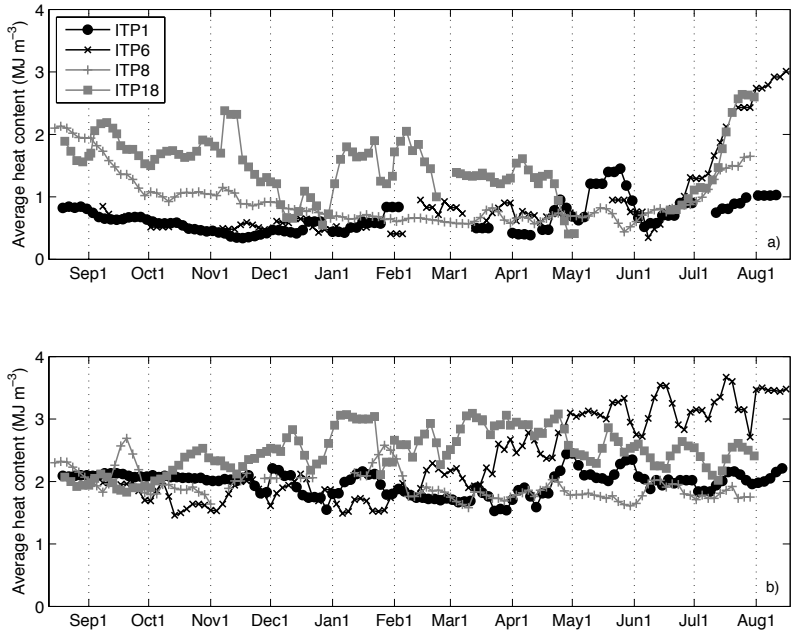

Figure 2.7: The average heat content per meter (in MJm^{-3}) for two different layers. The first layer a) is between 10 m the temperature minimum below the NSTM that I call the remnant winter mixed layer (rML). The second b) is between the rML and Pacific Winter Water (PWW). Here I calculated the heat content relative to the freezing temperature. If no rML was present, the average heat content for Figure 2.7b was calculated from PWW to 10 m. A 9 day centered running mean was applied to the average heat content in both figures to smooth the data.

An important difference between the upper and lower layers was that, with the exception of ITP18, the heat content in water above the rML had a distinct seasonal cycle. This cycle showed that at ITP1, ITP6 and ITP8, the heat content decreased around the end of October and was generally less than 1 MJ m^{-3} until the beginning of June, when the heat content began to increase. This closely matched the timing of the NSTM formation described in Section 2.3.1. As previously discussed, near-surface observations from ITP18 were different. In particular, while the average summer heat content was similar at ITP6, ITP8 and ITP18 ($\sim$ 1.5 - 3 MJ m^{-3}), the average winter heat content above the rML at ITP18 was greater than at other ITPs, indicating that about 1 MJ m^{-3} more heat was being stored there during the winter. Below the rML, about 2 - 3.5 MJ m^{-3} of heat were stored year-round at all ITPs. I suggest that the amount of heat stored here was dependent on both advective and vertical processes. Advective processes would be the shelf to basin transport of modified Pacific water into the Canada Basin and the circulation of the Beaufort Gyre while vertical processes would be the quasi-perennial storage of heat below the rML that is trapped by the summer halocline. Further investigation of the different temperature maxima below the rML is needed to determine how these are changing the structure of the upper ocean and how these may impact the sea ice cover (more details in Chapter 3).

2.4.3 Ekman Pumping, Winter Storms and Advection

In this chapter, I propose that the seasonal progression of the NSTM is primarily forced by the 1-D thermodynamics dominated by the annual cycle of

solar radiation. However, it is evident from the variable depth and temperature of the NSTM, especially in fall, that other processes, including Ekman pumping, winter storms, and advection, affect the behaviour of the NSTM. To examine these processes, I plotted the average monthly downwelling rate (based on calculations by Yang 2006) with the Brunt-Väisälä frequency and the depth of the NSTM (Figure 2.8). The downwelling rates I used were 0.9 m month^{-1} for September, 3.6 m month^{-1} for October, 4.5 m month^{-1} for November and December, 3.6 m month^{-1} for January, 2.7 m month^{-1} for February, and 1.8 m month^{-1} for March through July. Based on ITP observations, McPhee et al. (2009) estimated downwelling rates of 3.5 m month^{-1} from September through May, indicating that an NSTM at 20 m at the end of September would descend to 48 m by the end of May compared to 44 m based on the values in Yang (2006).

Overall, the depth of the fall NSTM closely followed the average downwelling rate at all ITPs. However, there were some instances when the fall NSTM was deeper or shallower than can be explained by Ekman pumping alone. Storm-driven vertical mixing can also cause the NSTM to deepen. Based on buoy data analyzed from April 1996 - April 1997 in the Canada Basin, Yang et al. (2004) found that winter and spring storms can cause ice to move up to 40 cm s^{-1}, thereby amplifying ice-ocean stress and deepening the surface mixed layer to at least 45 m, even under full winter ice cover. The average number of stormy days (defined as daily average geostrophic winds above 15 m s^{-1}) in the Canada Basin is 8-16 per year (Yang et al. 2004). In addition, since there is variable sea ice cover, sea ice melt, and incoming solar radiation throughout the Canada Basin, the NSTM is not

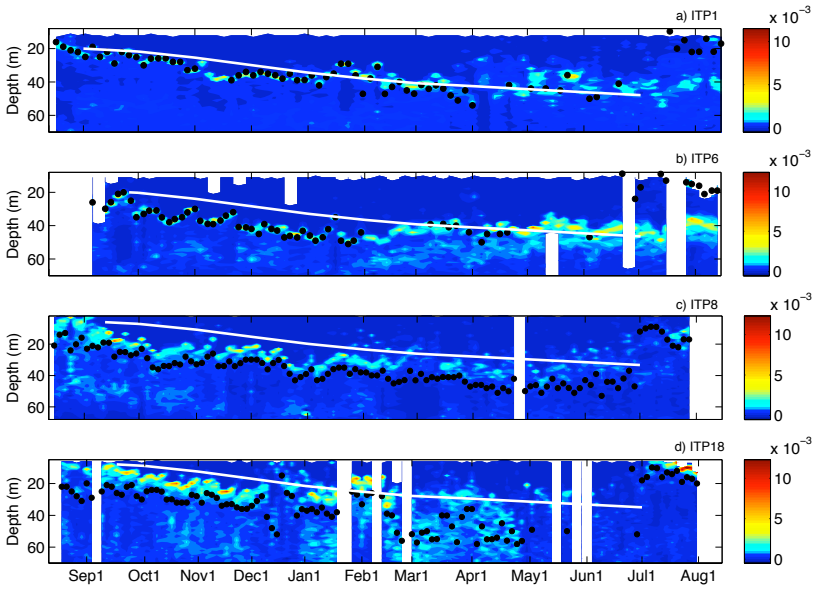

Figure 2.8: A comparison of the strength of the Brunt-Väisälä frequency (s^{-2}) between the four ITPs - a) ITP1, b) ITP6, c) ITP8, and d) ITP18. Here, the black dots represent the depth of the NSTM and the white line shows the average rate each month of downwelling from Ekman pumping as calculated by Yang (2006). White regions denote times when no data were available.

formed at a uniform depth. Thus, wind-driven advection of sea ice can cause the ITP to drift into a region with either a shallower or deeper NSTM.

At ITP18, the NSTM was less correlated with the downwelling rate than the other ITPs. For example, the decreased stratification observed in mid-December 2007 was correlated with a very deep NSTM that was followed 3 days later by a very shallow NSTM located just below a near-surface halocline. At the same time, the salinity decreased by about 0.5. It is possible that this near-surface variability was due to mixing from a winter

storm that caused sea ice to melt, freshen the upper waters, and form a near-surface halocline. However, based on 6-hourly data from the NCEP/NCAR reanalysis 1 (Kalnay et al. 1996), no major storms occurred near ITP18 in mid-December. Thus, it is likely that ITP18 drifted across a front in mid-December that separated saltier near-surface water with a deep NSTM from fresher near-surface water with a shallow NSTM. Given the shallow depth of the NSTM during the winter of 2007-8, it is possible that heat from the NSTM could melt ice during winter if there was sufficient mixing to erode the halocline and I suggest this is an important subject for future research.

2.5 Results from CTD Data

2.5.1 The Temperature and Location of the NSTM, 1993-2007

Ship-based CTD data provide an annual snapshot of conditions in the Canada Basin in varying sea ice. Initial observations showed that the upper 8 m was complex and there were often various peaks in the Brunt-Väisälä frequency (not shown). This suggests that, unlike the smooth progression seen below 8 m in the ITP data, the summer halocline is formed over time near the surface under variable summer atmospheric conditions (for example Overland 2009, Yang et al. 2004). In other words, summer snapshot sampling emphasizes NSTM spatial variability, not the gradual NSTM and summer halocline formation that is observed from ITP data.

Since I analyzed data collected from 1993, I can investigate how the NSTM changed from 1993-2007 under increased sea ice melt (Perovich et

al. 2008, McPhee et al. 2009, Yamamoto-Kawai et al. 2009a). To do this, I first plotted the maximum temperature of the NSTM relative to the freezing temperature (Figures 2.9 and 2.10) and several patterns emerged - i) the highest temperatures were located to the south and at coastal stations; ii) north of 75° N the NSTM was observed only sporadically until 2002, after which it was seen in all northern samples, iii) the NSTM warmed throughout the study period, with warmest offshore temperatures seen in 2007. This warming of the NSTM appears to be correlated with decreased sea ice concentrations, however, a linear regression of the NSTM temperature with daily sea ice concentration at each station was inconclusive (not shown, R^2=0.18). The lack of correlation between these is likely caused by the poor spatial resolution of both the CTD (∼100 km) and sea ice data (25 km). Since I suggest that temperature of the NSTM is dependent on variations in both time (the annual cycle of solar radiation and the gradual melting of sea ice) and space (the latitude and the inconsistent sea ice cover), it is unrealistic to expect that a snapshot of data on the order of 25-100 km will correlate with these processes. However, a recent analysis by Yamamoto-Kawai et al. (2009a) found that the proportion of sea ice melt in Canada Basin freshwater (relative to the salinity 32.5) increased threefold from 2003 to 2007. Within the Canada Basin, the southeast region where they found the greatest sea ice melt water in 2007 was also where I found the warmest NSTMs (Figure 2.10), supporting my suggestion that the warming of the NSTM is linked to sea ice melt.

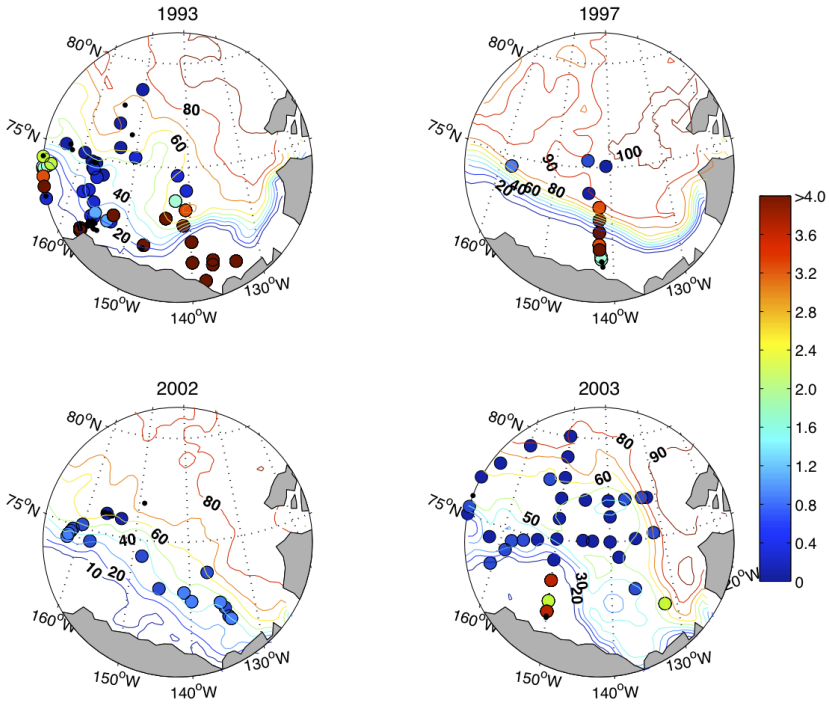

Figure 2.9: Temperature (relative to the freezing temperature) of the NSTM from CTD data at all stations for 1993-2003 cruises. Contour lines represent the monthly sea ice concentration (from the National Snow and Ice Data Center's final SMMR and DMSP SSM/I Passive Microwave data) labeled in percent concentration. August sea ice data were used for 1993, 2002 and 2003 and September data were used for 1997. Black dots indicate stations that were sampled where no NSTM was observed. Note that due to the changing ice concentration, the contour colours are different among years. Regions with no contour lines over water represent ice-free regions. The temperature range varied each year: 0.20 - 10.98°C in 1993; 0.25 - 4.28°C in 1997; 0.46 - 0.90°C in 2002, and 0.23 - 4.35°C in 2003.

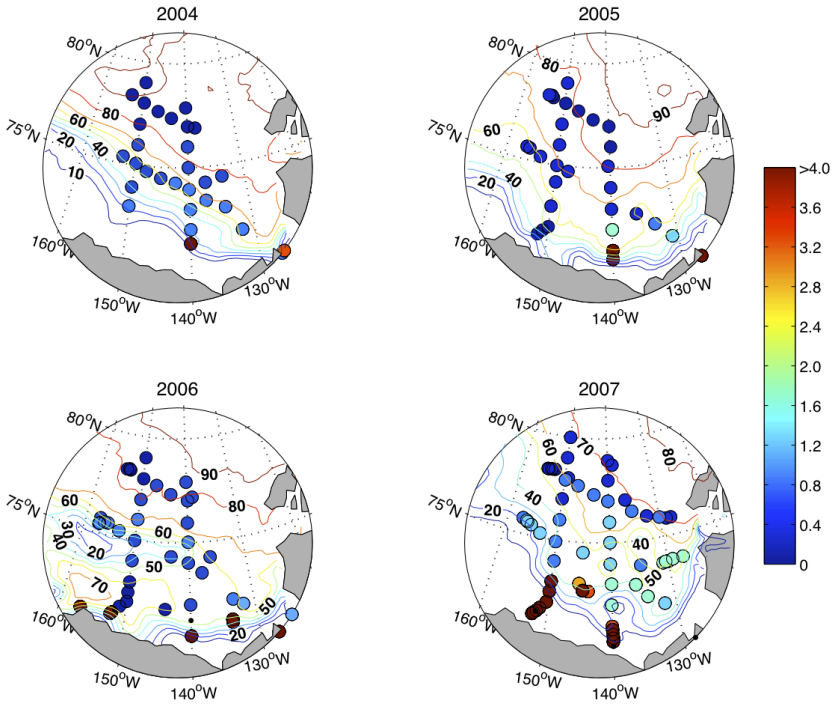

Figure 2.10: As in Figure 2.9 but for 2004-7. August sea ice data were used for all years. The temperature range varied each year: 0.27 - 6.96°C in 2004; 0.25 - 6.20°C in 2005; 0.20 -11.79°C in 2006; and 0.51 - 11.21°C in 2007.

To investigate the rate of change over my study period, the observed temperature above the freezing temperature of the NSTM was averaged in 1° latitude ranges from 70° - 80°N for each year (Figure 2.11). It was found that south of 75°N (Figure 2.11a), the temperature was more variable, with the highest average temperatures at 70° - 71°N in 2006 and 1993. This variability can be explained by the melting of multiyear ice that is periodically transported by the Beaufort Gyre atmospheric circulation into the open water at more southerly latitudes (Ogi and Wallace 2007, Yamamoto-Kawai et al. 2009a) and by the advection of anomalies (such as river runoff) from the shelves that is not accounted for in my 1-D analysis. North of 75°N was different, with the highest temperature at all latitudes observed in 2007 and the temperature minimum observed in either 2003 or 2004 (Figure 2.11b). I compared the rate of change from 2004 to 2007 for all latitude increments north of 75°N. It was found that the temperature of the NSTM increased by an average of 0.18°C per year at 75° - 76°N, by 0.14°C at 76° - 77°N, by 0.17°C per year at 77° - 78°N, and by 0.08°C per year at 78° - 80° N. Thus, north of 75°N, the temperature of the NSTM increased by an average of 0.13°C per year from 2004 through 2007.

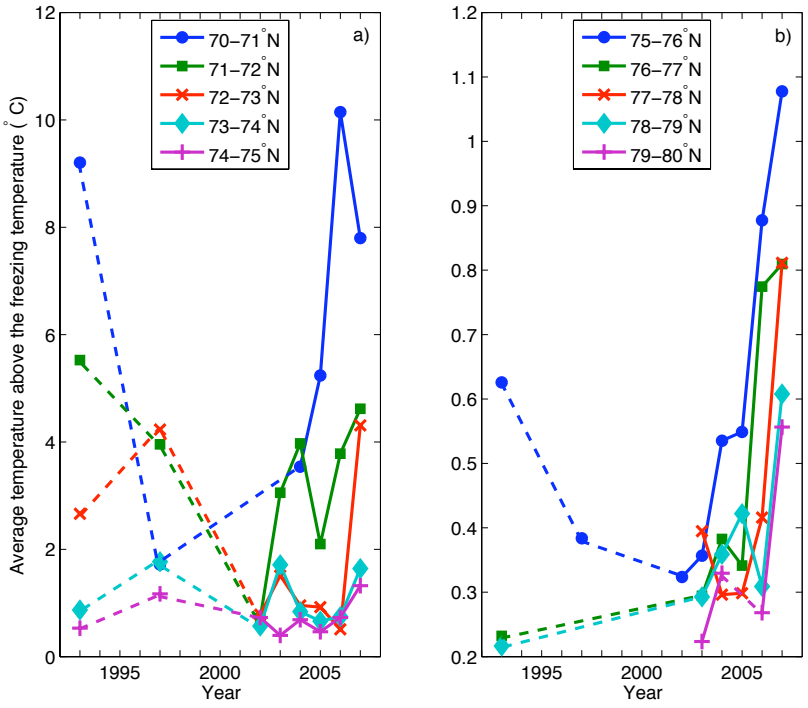

Figure 2.11: The average observed temperature relative to the freezing temperature of the NSTM within each latitude range for each year. Dashed lines connect data points that were not sampled yearly. Standard errors ranged from 0.1 - 1.6°C for 70-71°N; 0.1 - 3.0°C for 71-72°N; 0.1 - 1.0°C for 72-73°N; 0.0 - 1.5°C for 73-74°N; 0.0 - 0.2°C for 74-75°N; 0.0 - 0.3°C for 75-76°N; 0.0 - 0.1°C for 76-77°N; 0.0°C for 77-78°N; and 0.0 - 0.1°C for 78-79°N.

2.5.2 How Increased Salt-Stratification has Changed the NSTM from 1993-2007

In addition to the warming of the NSTM, changes to the stratification of the near-surface waters were observed. To demonstrate these changes, I calculated the average profile of Brunt-Väisälä frequency (Figure 2.12). Since the most consistent temperature increase of the NSTM was found in the northern Canada Basin, I chose to only include stations that were north of 75°N and had a bottom depth greater than 3500 m in this calculation. From these profiles, the following trends emerged - i) The most stratified region of the water column was in the upper 40 m and this feature was associated with the summer halocline formed from sea ice melt during all years except 2002 and 2003. In 2002, a temperature maximum that could be PSW was found at a shallow depth so this stratified feature marked the transition from surface mixed layer to the deeper temperature maximum. In 2003, conditions were more variable and the surface mixed layer was often quite deep so that the Brunt-Väisälä frequency maxima were sometimes associated with the transition from surface mixed layer to a deeper temperature maximum; ii) The surface mixed layer became progressively shallower, from a maximum of about 23 m in 1997 to virtually no surface mixed layer in 2007. To emphasize this point, I calculated the average depth of the NSTM and the average depth of the maximum Brunt-Väisälä frequency (Table 2.4) at the same deep, northern stations. Both features shoaled over time, from maximum depths of about 33 m in 1997 to minimum depths of about 15 m in 2007, for a shoaling rate of 2.1 m year^{-1} for the NSTM and 1.7 m year^{-1}

Table 2.4: Comparison of the average depth (with standard error) of the NSTM and the average depth of the maximum Brunt-Väisälä frequency in the northern Canada Basin during the summers of 1993, 1997, and 2002-07. Here, only stations that were north of 75°N and had a bottom depth greater than 3500 m were used to calculate the average. For standard error, the value of n was 3 in 1993, 2 in 1997, 3 in 2002, 12 in 2003, 13 in 2004, 11 in 2005, 13 in 2006 and 17 in 2007. In 2002, only one station had an NSTM that was 1 m deep.

Year	Depth of NSTM (m)	Depth of maximum Brunt-Väisälä frequency (m)
1993	26.8±6	27.6±4
1997	35.0±1	33.0±1
2002	1	28.0±4
2003	16.6±3	33.5±4
2004	21.3±1	18.8±8
2005	18.2±3	17.4±3
2006	20.9±1	18.6±1
2007	13.6±2	16.3±4

for the summer halocline. The shallow NSTM may explain the dramatic bottom melting of ice observed by Perovich et al. (2008) during the summer of 2007; iii) Another strongly stratified feature was prominent below the summer halocline in all years except 1993 and 2002. This deeper feature was either the previous year's summer halocline or was associated with PSW and there was a relatively well-mixed layer between the two haloclines in 1997 and 2004. The region between the two haloclines became more stratified with time, so that by 2007 the entire upper 50 m was stratified. Thus, I suggest that the warm, shallow NSTM observed through the winter of 2007-8 from ITP data can be explained by the increased stratification of the upper 50 m that prevented a deep surface mixed layer from forming in winter.

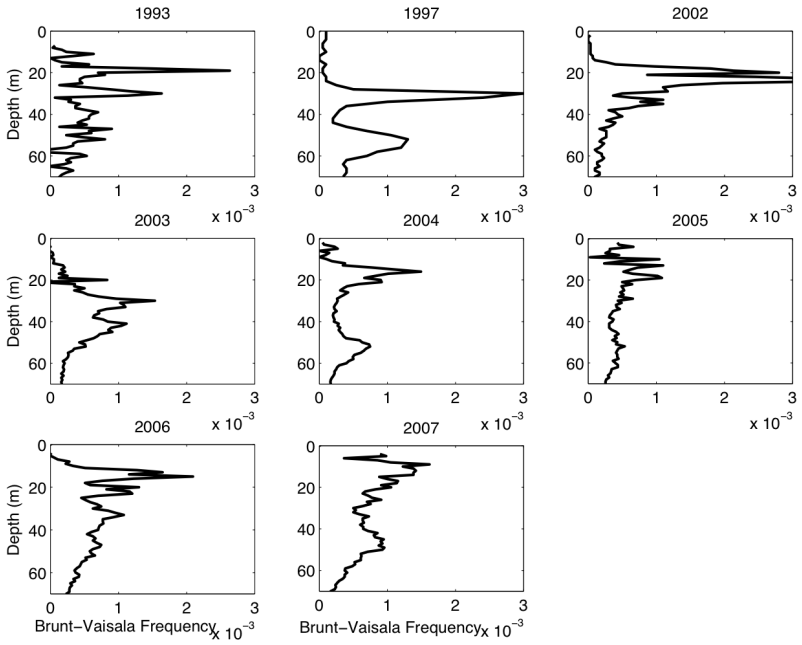

Figure 2.12: The average profile of the Brunt-Väisälä frequency in the northern Canada Basin during the summers of 1993, 1997 and 2002-7. Here, only stations that were north of 75°N and had a bottom depth greater than 3500 m were used to calculate the average. The number of stations that fit this criteria was 3 in 1993, 2 in 1997, 3 in 2002, 12 in 2003, 13 in 2004, 11 in 2005, 13 in 2006 and 17 in 2007.

2.6 Discussion

2.6.1 Heat Source of the NSTM

To determine whether there was sufficient solar radiation entering the water to warm the NSTM, I approximated the amount of incoming solar radiation through sea ice and open water. I based these calculations on data from station CB11b at 80°N, 150°W. On August 12, this station in the northern Canada Basin had one of the highest concentrations of sea ice (55%) in 2007 and an NSTM that was 0.56°C above the freezing temperature at a depth of 21 m (Figure 2.13). It was sampled in the early morning, and, based on transmissometer profiles (not shown), the water was very clear so attenuation was minimal. In addition, CB11b was one of only a few stations during the summer of 2007 cruise where PAR profiles were taken from which I could calculate the extinction coefficient in the water column.

Since I found in section 2.3 that the NSTM begins forming around mid-June, I need to determine the sea ice conditions in the 2 months before the CTD and PAR profiles were taken. Based on daily sea ice data, I found that the average sea ice concentration for these 2 months was 78%. If I assume that the sea ice from June 12th through August 12th was melting multiyear ice, I can use an albedo of 0.75 for the ice and 0.25 for the open water (Light et al. 2008). Thus, based on the average daily incoming solar radiation of $\sim$200 Wm^{-2} found by Maykut and McPhee (1995) during the AIDJEX experiment in 1995, I find that 150 Wm^{-2} (i.e Of the 200 Wm^{-2}, 25% is reflected) enters the ocean and 50 Wm^{-2} (i.e Of the 200 Wm^{-2}, 75% is reflected) enters the surface of the melting multiyear ice. Of the solar

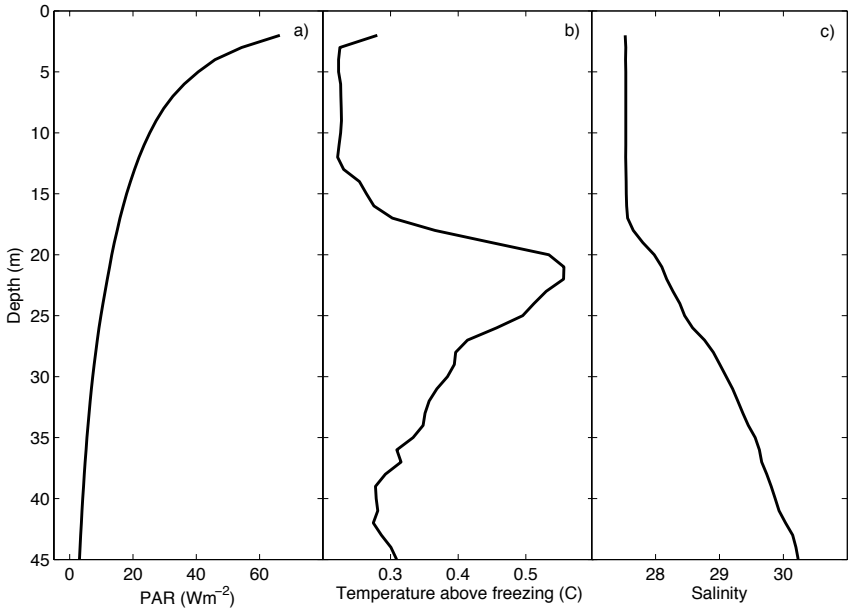

Figure 2.13: Profiles of a) PAR, b) observed temperature above the freezing temperature and, c) salinity sampled at station CB11b (80.0°N, 150.0°W). CB11b was sampled at 09h30 on August 12th, 2007.

radiation that enters the sea ice, about 9 Wm^{-2} (based on an extinction coefficient for melting multiyear ice that is 0.753 m^{-1} (Light et al. 2008) and an ice thickness of 2 m) would be transmitted to the ocean surface. Thus given the proportions of sea ice and open water, an average of 42 Wm^{-2} enters the ocean from mid-June to mid-August at station CB11b. The observed PAR profile (Figure 2.13a) at CB11b had an extinction coefficient of 0.08 m^{-1} so the incoming solar radiation deposited at 21 m would be 0.6 Wm^{-3}. To compare this to the observed temperature, I first calculate the heat content at the NSTM as 2.3 MJm^{-3}. Based on a continuous incoming

value 0.6 Wm^{-3} and assuming that no heat was lost by vertical diffusion, it would take 45 days to warm the NSTM to 0.56°C above the freezing temperature. Thus there is sufficient incoming solar radiation to form the NSTM over two months.

2.6.2 The NSTM Under a Changing Climate

Based on my findings, I suggest that the NSTM is a manifestation of i) the thermodynamic ice-albedo feedback effect, where decreased sea ice allows more solar radiation to enter and warm the ocean, and ii) changes to the ocean's freshwater cycle, where increased freshwater input from sea ice melt changes the buoyancy of the surface waters and traps solar radiation in the ocean. As the Arctic Ocean continues to warm, I propose several altered processes in the near surface waters.

- The year-round presence of the NSTM will modify the annual sea ice cycle. Overland et al. (2008) showed that the melt date near the North Pole was now on average one week earlier in the 2002-7 period than in the 1937-88 period. An earlier melt date would likely mean that both the NSTM and the summer halocline are formed sooner, thereby forming a warmer NSTM because albedo is reduced earlier. Conversely, the average freeze-up date has not changed, however, as was seen from ITP18 in October 2007, a shallow NSTM can still persist several weeks after sea ice begins forming. This suggests that heat from the NSTM can be entrained into the surface mixed layer as it deepens, thereby melting the underside of ice and reducing ice thickness. In

addition, if there is enough mixing from winter storms, heat from the NSTM will maintain thinner sea ice through winter, which would then melt sooner in spring.

- Thinner ice will alter the effect of wind stress on sea ice. Shimada et al. (2006) suggested that reduced internal ice stress from thinner sea ice would increase ice drift and air-ocean coupling. In other words, thinner sea ice moves faster, thereby transferring more stress into the ocean than thicker sea ice. It would be expected then that with thinner sea ice, both downwelling and storm-driven mixing would increase (Yang 2009) and the former would cause the NSTM to descend while the latter would cause the summer halocline and NSTM to erode. Thus, a weakening of internal ice stresses would activate two feedback mechanisms, one that would cause the heat associated with solar radiation to be stored deeper in the ocean and the other that would bring the heat associated with solar radiation closer to the surface.

- Increased near-surface stratification would decrease primary production in the Canada Basin because it would constrain the yearly replenishment by convection of nutrients in the surface mixed layer. If the summer halocline becomes a persistent, year-round feature, as was observed from ITP8 in 2008, it is probable that the near-surface waters will be even more nutrient-limited because the summer halocline limits interaction with the nutrient-rich modified Pacific waters. In addition, amplified downwelling from thinner ice would be expected to cause the Pacific waters to descend farther away from incoming solar radiation.

Thus, I suggest that the new, more stratified Canada Basin will be less productive.

2.7 Conclusions

The near-surface temperature maximum (NSTM) in the Canada Basin of the Arctic Ocean was examined year-round from 2005-8 and during the summers of 1993, 1997 and 2002-7. Based on the year-round ITP data, I determined the seasonal evolution of the NSTM. The NSTM is first formed from mid-June to mid-July when sufficient solar radiation enters the upper ocean through leads and melt ponds to warm the near-surface waters. The accumulation of sea ice melt from the warmed surface waters forms a near-surface summer halocline below the surface mixed layer. This feature, which first forms between the beginning of June and mid-August, prevents the NSTM from eroding, thereby storing solar radiation. The summer halocline continues to form and the NSTM continues to warm until there is insufficient incoming solar radiation to melt ice. This occurs near the end of September, when sea ice begins to form and the NSTM and the summer halocline become the stored residual of the previous summer's solar radiation and sea ice melt, respectively. The summer halocline continues to trap the NSTM until penetrative convection from brine rejection and air-ocean and ice-ocean stresses deepen the surface mixed layer. Throughout this cycle, Ekman pumping within the convergent Beaufort Gyre acts to deepen the NSTM. The erosion of the summer halocline did not occur at the same time each year and the NSTM was even a perennial feature during the winter of

2007-2008. Processes such as storm-driven mixing and advection alter the properties of the summer halocline and the NSTM and would be interesting areas of future research.

My examination of ship-based data from the summer of 1993, 1997 and 2002-2007 showed that although the temperature of the NSTMs were warmest and most variable south of 75°N, the temperature of the NSTM in the Canada Basin increased more uniformly north of 75°N at a rate of 0.13 °C per year since 2004. In addition, while the strength of the stratification north of 75°N did not increase since 1993, the depth of the water column over which there was strong stratification increased so that by 2007, the upper 50 m was strongly stratified. This caused both the depth of the NSTM and the depth of the summer halocline to shoal since 1997 at a rate of 2.1 m per year and 1.7 m per year, respectively. These changes can be attributed to increased sea ice melt during the same years. To verify that enough solar radiation could enter the ocean to form the NSTM, I approximated (based on average sea ice concentration and estimated radiation flux through ice and water) the amount of solar radiation at a station in the northern Canada Basin from mid-June through mid-August 2007. It was found that it would take about 45 days to warm the NSTM to the observed temperature.

In summary, my analyses suggests that the NSTM is a ubiquitous feature in the Canada Basin which influences stratification of the upper ocean and may be related to the rapid sea ice decline. The dynamics of the NSTM should be considered when modelling climate change in the Arctic.

Chapter 3

Changes to the near-surface waters in the Canada Basin, Arctic Ocean from 1993-2009: Waters below the NSTM

3.1 Chapter Summary

Decreased albedo and increased sea ice melt have changed the water mass structure of the Canada Basin. From 1993-2009, the near-surface temperature maximum (NSTM) and remnant of the previous winter's mixed layer (rML) warmed by up to 1.5°C and 0.5°C and freshened by up to 4 and 2 salinity units, respectively. A vertical heat diffusion model shows that the warming of the rML can be explained by heat diffusion from both the NSTM above and PSW below. In years with a warmer NSTM, more heat was diffused to the rML. The salinity of the rML was correlated with distance from

the centre of the Beaufort Gyre; the rML was on average 1.9 salinity units fresher at stations that were inside than outside the gyre. I suggest this is because convergent Ekman drift and downwelling caused the freshened surface water (from sea ice melt) to accumulate within the gyre. In addition, the salinity range of Pacific Summer Water (PSW) - defined by its local temperature maximum - freshened from about 30-32 in 1993 to about 28-32 in 2008. Order of magnitude calculations suggest this freshening cannot be explained by changes in the PSW source waters, changes in advection of PSW within the Canada Basin, or salt diffusion from the PSW. Thus, it is likely that the freshened rML widened the salinity range surrounding PSW. Observations from 2009 were different, with the appearance of a third temperature maximum from an as yet unknown source.

3.2 Introduction

Changes in the near-surface (here defined as the upper 100 m) waters of the Canada Basin of the Arctic Ocean in recent years include the increased annual absorption of solar radiation in the upper ocean (Perovich et al. 2007), the earlier onset of the melt season by about 7.3 days per decade and the delay of freeze-up by about 6 days per decade over the past 30 years (Markus et al. 2009), and the freshening of the upper waters from both increased river runoff and sea-ice melt (Yamamoto-Kawai et al. 2009a). These changes can be partly explained by the rapid decrease of summer sea ice (e.g. Stroeve et al. 2007). The increased accumulation of freshwater has led to higher stratification and a shallower winter mixed layer (Toole et al.

2010) that now traps summer solar radiation throughout winter (Chapter 2).

It is likely that the increased sea ice melt and absorption of solar radiation will also affect the near-surface water mass structure. In the Canada Basin, water masses have been typically defined as follows (Figure 3.1, 1993 curve). At the surface is a mixed layer that had a depth of 40-50 m based on data collected from the 1890s through 1970s (Coachman and Barnes 1961, Morison and Smith 1981). Year-round ice-tethered profile (ITP) data collected from 2004-2008 showed that the surface mixed layer shoaled since the 1970s to an average summer depth of (at most) 16 m and a winter depth of 24 m (Toole et al. 2010). The base of the surface mixed layer is called the summer halocline and is formed from sea ice melt diluting the layer above (Chapter 2). Below the summer halocline is a feature called the near-surface temperature maximum (NSTM). This NSTM is formed each summer by solar radiation that is trapped by the summer halocline (Chapter 2). During winter, the NSTM will either disappear if the summer halocline erodes from winter mixing or is trapped year-round below the summer halocline if winter mixing is weak. The temperature minimum below the NSTM is thought to be the remnant of the previous winter's local mixed layer (rML) (Chapter 2), and thus its temperature should be near the freezing point when formed because the high arctic winter vertical mixing is likely due to brine rejection or surface freezing rather than mechanical mixing. The temperature maximum below the rML has long been defined as water of Pacific origin that is modified in the Chukchi and Bering Seas during summer (Coachman and Barnes 1961). I call this second temperature maximum Pacific Summer

Water (PSW). PSW is believed to come from the eastern Chukchi Sea (and has also been called the eastern Chukchi Sea water or ECSW by Shimada et al. 2001), waters that have previously been defined as Alaskan Coastal Water (ACW) by Coachman et al. (1975). A major component of the ACW is in the Alaskan Coastal Current (ACC) (Woodgate and Aagaard 2005), a warm, fresh seasonal coastal current present in the Chukchi Sea in summer. I call the halocline between the rML and PSW the winter halocline (Chapter 2). Finally, the temperature minimum below PSW is Pacific Winter Water (PWW) and its source is Pacific water that is modified in the Chukchi and Bering Seas during winter (Coachman and Barnes 1961).

The warming and freshening of the near-surface waters is affecting the ecology of the Canada Basin. Recent studies have shown the deepening of the subsurface chlorophyll maximum by about 18 m from 2003 to 2008 (Chapter 4) and a transition in foodweb structure from primarily nanoplankton (2 - 20 μm diameter) to primarily picoplankton (<2 μm diameter) (Li et al. 2009). Phytoplankton rely on nutrients that are transported into the Canada Basin within modified Pacific waters (Jones and Anderson 1986), thus changes to the Pacific waters would be expected to impact productivity.

In this paper, I use summer CTD data to examine changes to the near-surface (0-100 m) water masses in the Canada Basin from 1993-2009. Section 3.3 discusses details of the data and of the 1-D vertical model used to estimate heat diffusion. The data show warming and freshening of the NSTM and rML and the freshening of the salinity range surrounding the PSW temperature maximum; I examined the warming of the NSTM in Chapter 2. In section 3.4, I discuss changes to the rML and PSW. In section 3.5, I investi-

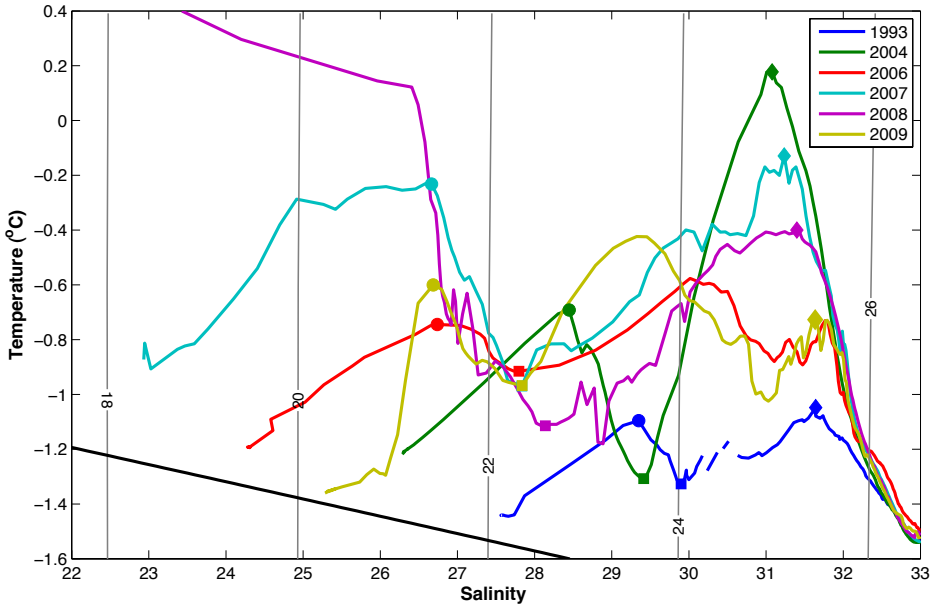

Figure 3.1: A comparison of temperature and salinity above Atlantic water at station CB21 (74°N, 140°W). Samples were taken on 11 September, 1993 (blue line), 24 August, 2004 (green line), 8 September, 2006 (red line), 23 August, 2007 (cyan line), 14 August, 2008 (purple line), and 9 October, 2009 (mustard line). The coloured symbols mark the temperature maximum near-surface temperature maximum (NSTM; circle), the temperature minimum remnant of the previous winter layer (rML; square) and temperature maximum that is likely Pacific summer water(PSW; diamond) for each year. PSW is not indicated in 2006 because it appears as though cold water intruded on the temperature maximum. While this appears to be similar in 2009, an examination of other stations found that three temperature maxima were ubiquitous in 2009 and an anomaly in 2006. The black solid line represents the freezing temperature as a function of salinity and pressure and the grey lines denote density (sigma-theta) at 2 unit intervals.

gate the role of the Beaufort Gyre in changing water mass distribution and properties. In section 3.6, I examine three different mechanisms that could be changing the salinity range of PSW - viz., changes to the sources waters of PSW, changes to the pathway and velocity of PSW, and changes to the vertical diffusion of heat and salt in the waters surrounding PSW. These mechanisms are examined in isolation but all could be acting together.

3.3 Data and Methods

3.3.1 Definition of the Near-Surface Water Masses

As in Chapter 2, I define the current NSTM as being present if:

- is the temperature maximum that is nearest to the surface and is at least 0.1°C warmer than the temperature minimum directly below (the rML);
- has a salinity less than 31;
- has a maximum temperature that is at least 0.2°C warmer than the freezing temperature.

I then define the rML as the temperature minimum directly below the NSTM that exists if it is at least 0.1°C colder than the NSTM. Thus, by definition, the NSTM cannot exist without the rML and vice-versa. If there appear to be multiple temperature maxima and minima that fit these criteria (e.g. the 2009 profile in figure 3.1) then the NSTM is the temperature maximum nearest the surface and the rML is temperature minimum below the NSTM.

The PSW is defined as the temperature maximum directly below the rML that was at least 0.1°C warmer than the rML. If no NSTM or rML is present then PSW is the only temperature maximum in the near-surface waters. This definition was consistent until 2009, when three near-surface temperature maxima were observed. In 2009 I chose to define PSW as the only temperature maximum that had a salinity greater than 31. The definition of PSW in 2009 will be examined further in section 3.6.

3.3.2 CTD Data

I use CTD data collected by a collaboration of Fisheries and Oceans Canada, the Japan Agency for Marine-Earth Science and Technology, and the Woods Hole Oceanographic Institution during the summers of 1993 and 2002-2009 (details in McLaughlin et al. 2008) using a FSI CTD ICTD (1993) and a Seabird SBE-911 Plus (2002-09). Cruises took place in late summer, specifically

- 1993: 3 August - 25 September;
- 2002: 18 August - 5 September;
- 2003: 13 August - 3 September;
- 2004: 5-30 August;
- 2005: 3 - 31 August;
- 2006: 7 August - 12 September;
- 2007: 27 July - 28 August;

- 2008: 23 July - 20 August;
- 2009: 20 September - 12 October.

3.3.3 Ice Tethered Profiler Data

I also use year-round archived (level 3) CTD data from the Ice Tethered profiler (ITP) (http://www.whoi.edu/itp Toole et al. 2006, Krishfield et al. 2008) instrument number 8, which collected data from 12 August, 2007 - 24 July, 2008 in the northern Canada Basin. Uncertainties in the CTD data are estimated at 0.005 salinity units and 0.005°C (Krishfield et al. 2008). Data collection commences at about 8 m and continues to 800 m with 1 m resolution. It is important to note that these data are biased to waters that have a high ambient ice concentration. Profiles from every 3 days were examined and those that started deeper than 10 m were ignored.

3.3.4 Bering Strait Mooring Data

I also use time-series temperature and salinity data from the Bering Strait from 2001-2009 (Woodgate et al. 2010) and references therein, http://psc.apl .washington.edu/BeringStrait.html and NODC. Year-round moorings have been deployed in the 2 channels of the strait and at a site just to the north almost continuously since 1990 (not all moorings were deployed all years). I use data from moorings in the eastern strait (site A2- centre of the strait, sampling mostly ACW, and site A4 in the Alaskan Coastal Current) and from the northern site (A3), believed to be a useful average of the total flow through the strait (Woodgate et al. 2005b). The time series are from

Figure 3.2: A bathymetric map of the location of Bering Strait moorings, which are denoted by a blue x.

about 9 m from the seafloor thus do not measure the upper waters, which in summer and fall are likely up to 2°C warmer and 1 salinity unit fresher (Woodgate et al. 2005a).

3.3.5 Sea Ice Data

Sea ice concentrations were obtained from the National Snow and Ice Data Center (http://www.nsidc.org). I used the August averaged 25 km final data produced from the Nimbus-7 Scanning Multichannel Microwave Radiometer (SMMR) and the Defence Meteorological Satellite Program (DMSP) -F8, -F11 and -F13 Special Sensor Microwave/Imager (SSM/I) radiances (Cava-

lieri et al. 2008) for the years 1993 and 2002-07. Since -F13 was lost at the end of 2007, for 2008 and 2009 I used the near-real-time 25 km DMSP SSM/I daily polar gridded sea ice concentrations (Maslanik and Stroeve 1999) from the -F17 satellite. I used sea ice concentrations from the middle of the cruise - August 5, 2008 and October 1, 2009 - to estimate the sea ice conditions since monthly averages are not available.

3.3.6 Model of Heat and Salt Diffusion

In section 3.6, I use a 1-D vertical diffusion model to study changes in temperature and salinity in the upper 100 m of the Canada Basin. Although vertical diffusion coefficients are small and often ignored in the Arctic (Gargett 2003), the large temperature and salinity gradients in the near-surface waters suggest the effect of diffusion might be significant. By central derivative finite difference, I solve

$$\frac{\partial T}{\partial t} = \kappa \frac{\partial^2 T}{\partial z^2}, \frac{\partial S}{\partial t} = \kappa \frac{\partial^2 S}{\partial z^2} \tag{3.1}$$

where t is time, T is temperature, S is salinity, z is depth and κ is the vertical diffusivity (from both molecular and turbulent processes) for temperature or salinity. Previous studies have found κ values of 1-3 x 10^{-6} m^2s^{-1} in the polar ocean below the mixed layer (Gargett 2003, Zhang and Steele 2007) so two separate model experiments, one with a diffusivity of 1 x 10^{-6} m^2s^{-1} and the other with a diffusivity 3 x 10^{-6} m^2s^{-1} were run. This simple model does not include advection, horizontal variability or mixing driven by brine-rejection from sea-ice on freezing.

The model was run for the upper 100 m for summer profiles from two different stations - CB5 (75.3°N, 153.3°W; Figure 3.3b) near the southern Northwind Ridge and CB21 (74°N, 140°W; Figure 3.3b) in the centre of the basin. At the upper and lower boundaries, zero gradient boundary conditions were used. The upper and lower boundaries were set to the temperature or salinity that was one space step away (above or below) from the boundary. The model used a vertical resolution of 0.25 m and a time step of 50 minutes, both of which were sufficiently small that the solution was independent of resolution. It was run for 1 year to estimate conditions during the following year's cruise.

3.4 Results: Changes to the Near-Surface Water Masses, 1993-2009

3.4.1 The NSTM and rML

The CTD data showed dramatic changes to the near-surface properties from 1993 through 2009, e.g. at station CB21 in the central Canada Basin (Figure 3.1). Since 2004, the depth of the winter mixed layer has shoaled in the central Canada Basin due to increased near-surface stratification (Chapter 2; Toole et al. 2010), which has resulted in the year-round storage of the NSTM (Chapter 2). Since successive strongly-stratified NSTMs are formed at progressively fresher salinities (Figure 3.1) that may then descend by gyre-driven downwelling, I would expect to identify annual NSTM layers stacked one on top of each other. If deep enough, these layers may be iso-

lated from surface mixing - Toole et al. (2010) found the average winter mixed layer depth from the summer 2004 through the summer 2009 was 24 m and I showed, based on all the ITP data available that almost without exception, the NSTM was consistently deeper than 30 m in winter (Chapter 2). Data from ITP8 show how the NSTM could form successive stacking layers (Figure 3.3). This was the first time that the NSTM was observed year-round (Chapter 2) and the NSTM that formed during the summer of 2008 (salinity 28) was at least 1 salinity unit fresher than the 2007 NSTM (salinity 29). Thus, unless there was diffusive mixing below the 2008 summer halocline, the 2007 NSTM should form a separate, denser layer below the lighter 2008 NSTM. Separate stacked NSTM and rML layers were not evident and instead, with the exception of 2009, both the NSTM and rML warmed and freshened each summer together (Figure 3.1). It is only in 2009 that two temperature maxima and two temperature minima that could be successively stacked NSTMs and rMLs were observed. I will now explore the NSTM and rML from 1993 through 2009 to describe how these layers are changing.

Both the NSTM and the rML warmed by about 1.5°C and 0.5°C, respectively. To determine the spatial extent of the warming, the temperature (Figure 3.4) at the rML was plotted during each summer in relation to the sea ice concentration. To minimize shelf effects, only stations whose bottom depth was greater than 2000 m were examined. Similar to the NSTM, the rML warmed during my study period and it appeared that the warmer rMLs were in regions with reduced sea ice. This warming is at first puzzling because the temperature of the rML should be independent of sea ice con-

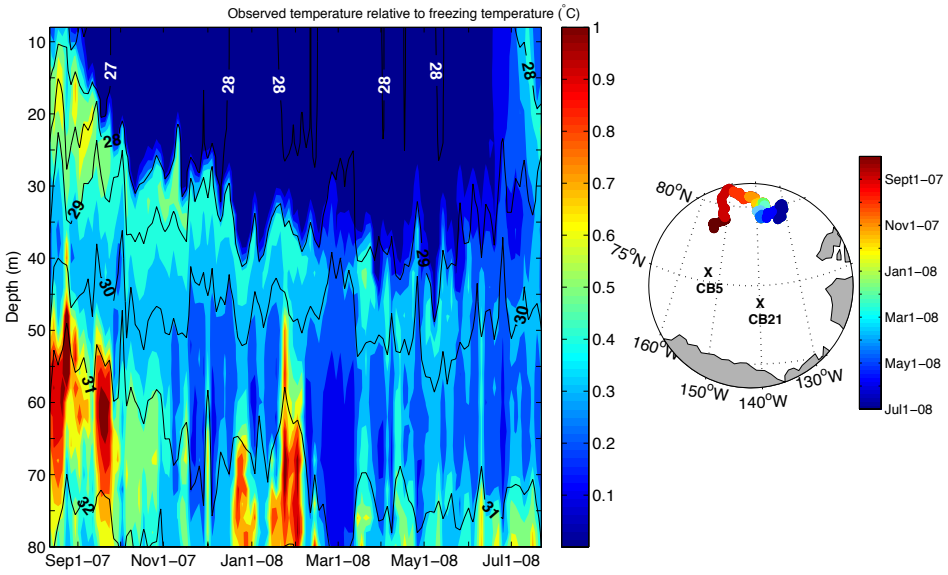

Figure 3.3: Observations from ITP8, where data were collected from 12 August, 2007 - 24 July, 2008. On the left in colour is the observed temperature relative to the freezing temperature. The black lines indicate salinity contours. On the right is the location of ITP8 over time. Stations CB5 (75.3°N, 153.3°W) and CB21 (74°N, 140°W) are denoted by black x.

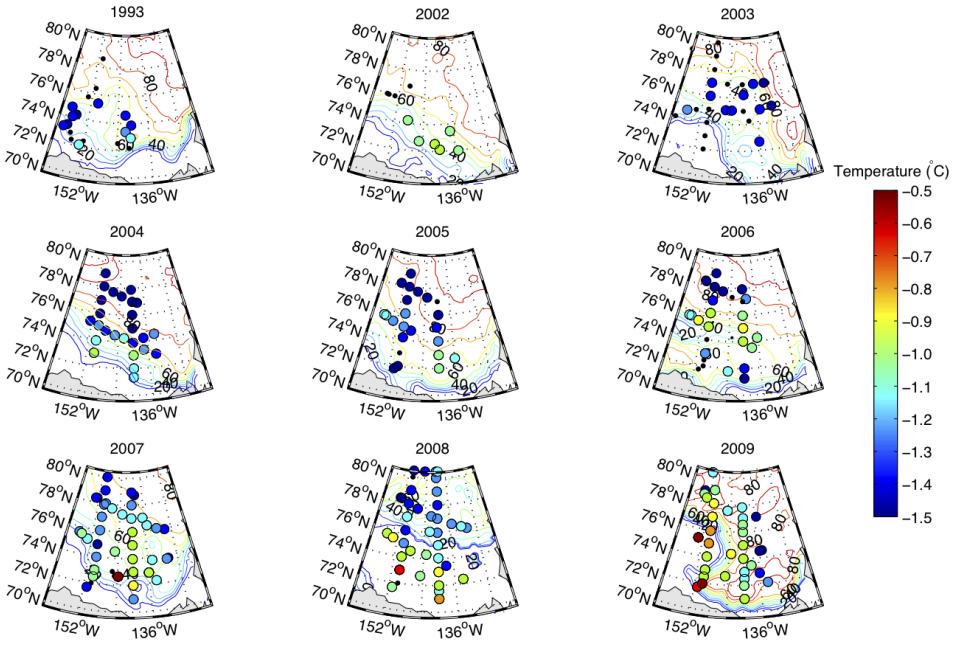

Figure 3.4: The temperature at the rML during the summer cruises of 1993 and 2002-9. To minimize coastal processes, only stations whose bottom depth was greater than 2000 m were plotted. Black dots represent stations where no rML was present. Contour lines estimate the sea ice concentration during each cruise.

centration since it is formed in winter when the surface mixed layer is at the freezing temperature. Modifications to the temperature of the rML will be examined in section 3.6.3.

From 1993 through 2009, the NSTM and rML freshened by about 4 and 2 salinity units, respectively. The spatial extent of the freshening was also plotted relative to sea ice concentration (Figure 3.5). The salinity trend seemed to be more variable and less linked to ice conditions, with the freshest rMLs observed in 2002-3 and 2006-9. The freshest rMLs appeared to be

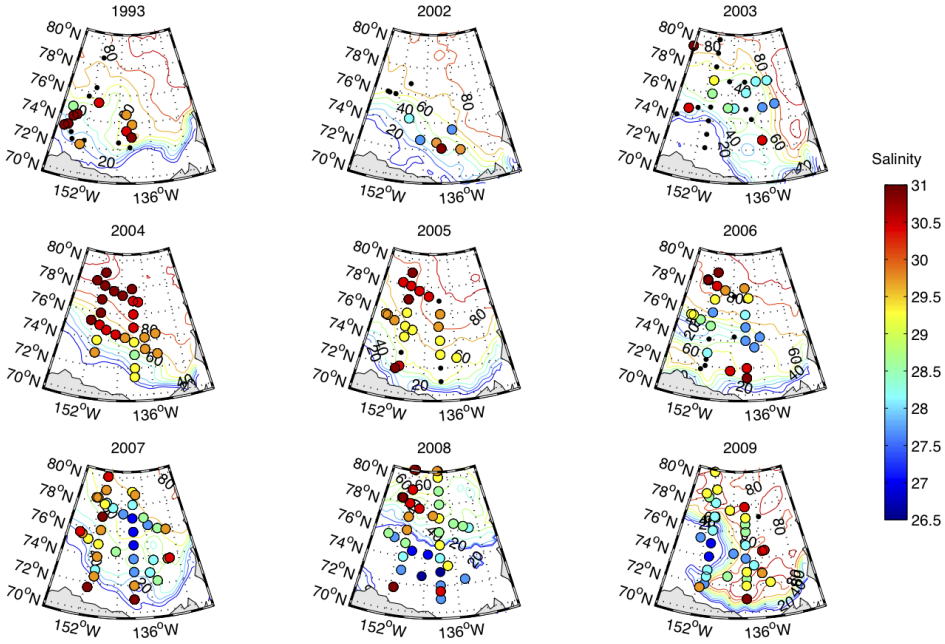

Figure 3.5: As in Figure 3.3 but for the salinity at each rML.

clustered at a slightly different location each summer, suggesting that the salinity of the rML may be influenced by the location of the Beaufort Gyre. The relationship between the salinity of the rML and the location of the Beaufort Gyre will be examined in section 3.4.2.

From 2004-2008, the salinity range of the temperature maximum that includes PSW was about 2 salinity units fresher (about 28-32) than the salinity of 31-32 defined by Shimada et al. (2001) and Steele et al. (2004). In 2009, two temperature maxima were observed below the NSTM, and the source of the middle temperature maximum is unknown. It could be an intrusion of warmer and fresher PSW or another water mass that formed between the rML and PSW. Changes to PSW will be explored in Section

3.6.

3.4.2 The Location of the Centre of the Beaufort Gyre

Several recent papers have discussed the importance of the Beaufort Gyre to changes in the near-surface salinity of the Canada Basin and have identified decreasing salinities within the gyre (e.g. Proshutinsky et al. 2009, McPhee et al. 2009, Jahn et al. 2010a), so it is possible that the salinity of the rML is affected by the location of the Beaufort Gyre. Anticyclonic gyres have a bowl shape, with isohalines deeper in the centre and shallower at the edge; thus, the location of the Beaufort Gyre can be identified by plotting isohalines in the upper layer. The recent freshening (e.g. Proshutinsky et al. 2009, Yamamoto-Kawai et al. 2009a, McPhee et al. 2009) has resulted in the deepening of isohalines (discussed further in section 3.5), thus the same isohalines could not be examined each year. Initial observations of the Beaufort Gyre were based on contoured isopycnals across the Canada Basin that showed the bowl shape of the gyre (not shown). These suggested that the depth of the bottom of the gyre, which was estimated as the deepest part of the bowl shape, was usually less than 50 m, so the isohaline that was at 40 m in the centre of the gyre was plotted (Figure 3.6). The results were not sensitive to this depth choice. This isohaline was 30 salinity units in 1993, 29.5 in 2002 and 2003, 29 in 2004 and 2005, 28.5 in 2006, 27.5 in 2007 and 2009 and 27 in 2008. The location of the Beaufort Gyre was variable and appeared to be in the southeast Canada Basin in 2002 and 2004-6, in the central Canada Basin in 1993, 2007 and 2008, in the northeast Canada Basin in 2003, and in the southwest Canada Basin in 2009. The number of

Table 3.1: The number of stations that were defined as inside the gyre, outside the gyre and in the transition zone from 1993-2009.

Year	Inside the gyre	Outside the gyre	In transition zone
1993	4	0	13
2002	5	0	2
2003	20	1	2
2004	8	9	8
2005	9	4	6
2006	13	2	7
2007	9	6	13
2008	6	9	17
2009	13	5	8

stations within each region are presented in Table 3.1.

The salinity of the rML appeared to be negatively correlated with the local depth of the chosen isohaline, suggesting the rML was fresher inside the Beaufort Gyre. To elucidate this relationship, the average salinity of the rML was calculated for three different regions - i.) The inside of the Beaufort Gyre, which was defined as the region where the depth of the chosen isohaline was 25-40 m; ii.) The outside of the Beaufort Gyre, which was the region where the depth of the chosen isohaline was 0-15 m; and iii.) The transition zone between the inside and outside of the gyre, which was defined as the region where the depth of the chosen isohaline was 16-24 m (Figure 3.7). When calculating the average, only basin stations that had bottom depths greater than 3000 m were included. The rML was on average 1.9 salinity units fresher inside than outside the gyre, with the greatest difference (3.0 salinity units) in 2008 and the smallest difference (1.1 salinity units) in 2004. Given these salinity differences, I suggest that the freshening of the rML can be partially attributed to the location of the Beaufort Gyre. This is because

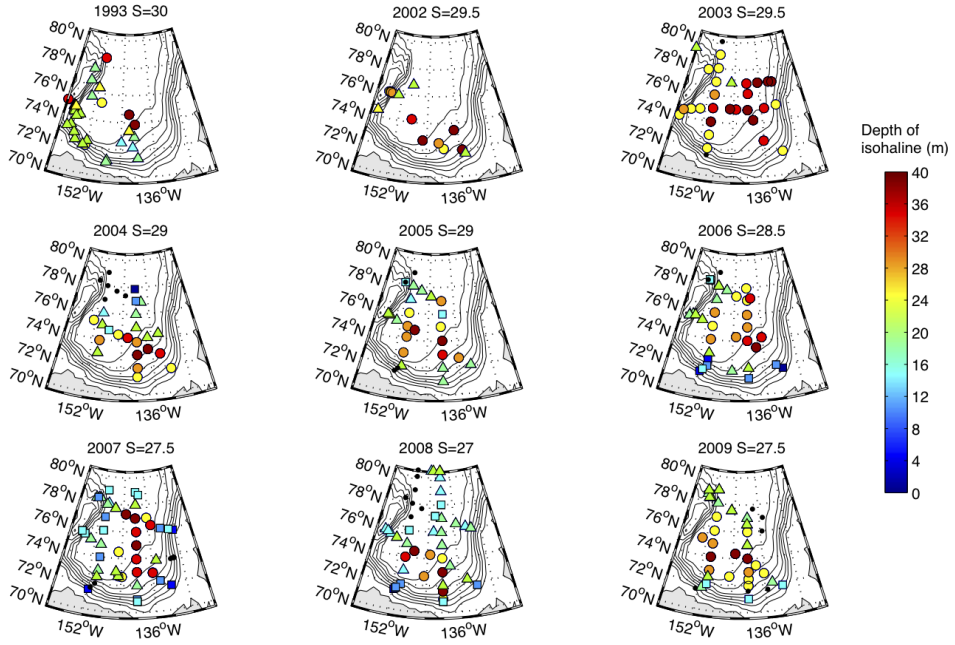

Figure 3.6: The depth of a chosen isohaline to outline the location of the Beaufort Gyre (details in text). This isohaline was 30 salinity units in 1993, 29.5 in 2002 and 2003, 29 in 2004 and 2005, 28.5 in 2006, 27.5 in 2007 and 2009 and 27 in 2008. Coloured circles represent stations that were inside the Beaufort Gyre, triangles represent stations that were in the transition zone, squares represent stations that were outside of the gyre and black dots indicate stations that were sampled where the surface was saltier than the chosen isohaline (and thus outside of the gyre). Black lines show the bathymetry at 500 m intervals from 500 m to 3500 m.

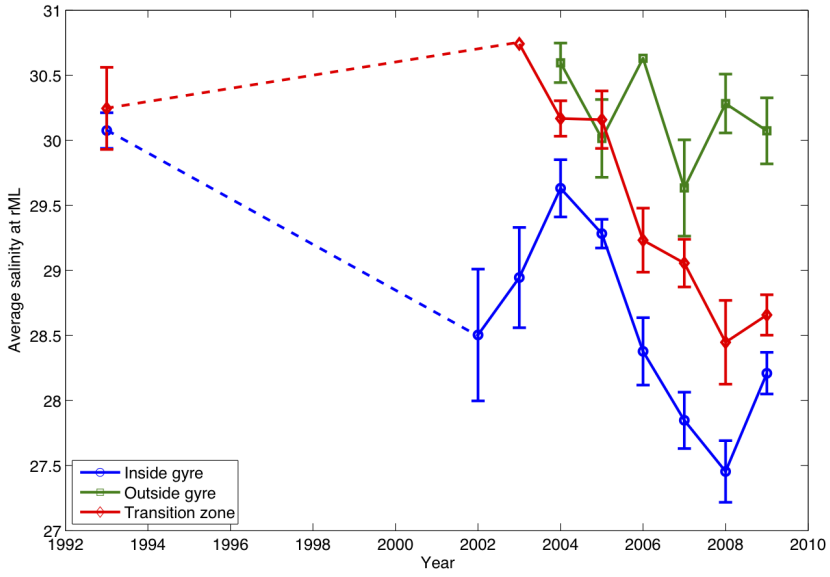

Figure 3.7: Average salinity with error bars of the rML for stations that were within the Beaufort Gyre (blue line), outside of the Beaufort Gyre (green line) and in the transition zone between the centre and edge of the Beaufort Gyre (red line). The dashed line represents years when no samples were taken.

the properties of the rML should reflect the surface salinity where it was formed. If formed in the centre of the gyre, the rML should be fresher than if it was formed outside the gyre. The effect of the Beaufort Gyre on near-surface water masses will be explored in Section 3.5.

3.5 Effect of the Beaufort Gyre on Changing Water Mass Properties

To examine how the Beaufort Gyre influences water mass properties, the average temperature and salinity profiles for stations inside the Beaufort Gyre, outside the Beaufort Gyre and within the transition zone during each summer cruise were calculated (Figures 3.8). These profiles showed that from 2003-2008, the NSTM, rML and PSW were coldest and saltiest outside of the gyre and warmest and freshest inside the gyre. In addition, the temperature maximum associated with PSW changed to encompass a greater salinity range, from about 29.5-32 in 2004 to 28-32 in 2007. Data from 2009 were different - inside the gyre there were three temperature maxima (at salinities 26.6, 29.5 and 31.5) and two temperature minima (at salinities 28.1 and 30.9), in the transition zone there were two temperature maxima (at salinities 28.1 and 30.5) and one temperature minimum (at salinity 28.7), and outside the gyre there was only one temperature maximum (at salinity 30.3) that extended over the salinity range of about 28-32.

The chlorophyll maximum deepened in the Canada Basin between 2003-2008 (Chapter 4) and this could be linked to the deepening of the winter halocline and nutrient-rich Pacific waters. The average depths of the NSTM, rML and PSW relative to the location of the centre of the Beaufort Gyre was calculated to determine if these water masses have deepened. The NSTM ranged from about 1-35 m and did not appear to be influenced by the location of the Beaufort Gyre (Figure 3.9a). The NSTM shoaled in all regions and this trend was linear (2.9 m per year from 2004-2007) and sta-

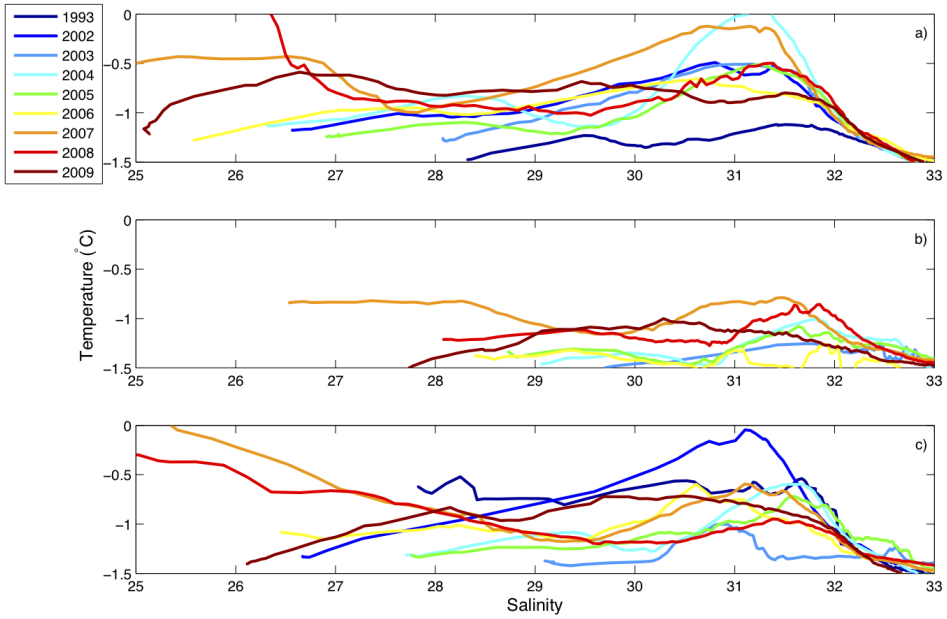

Figure 3.8: Average temperature-salinity plots for stations that were a) inside the Beaufort Gyre, b) outside the Beaufort Gyre, and c) in the transition zone for 1993-2009. Only stations with bottom depths greater than 3000 m were used to calculate the average. The number of stations used to calculate the average are presented in Table 3.1.

tistically significant (p-value=0.002) only in the transition zone. The later sampling in 2009 resulted in a deeper NSTM throughout the basin due to downwelling and the winter deepening of the surface mixed layer. From 1993-2003, the average depth of the rML ranged from about 25-55 m but was consistently 35-45 m from 2004-2009 when there was better spatial coverage of the Canada Basin (Figure 3.9b). Similar to the NSTM, the depth of the rML did not appear to be influenced by the location of the Beaufort Gyre and unlike the NSTM, the rML had no statistically significant shoaling trend (p-value from 2004-2009 ranged from 0.11 for stations in the transition zone to 0.60 for stations inside the gyre). This suggests that changes to the near-surface stratification in summer do not affect the depth of the rML. Unlike the NSTM and rML, the depth of PSW appeared to be influenced by the location of the Beaufort Gyre. The depth of PSW inside of the gyre and in the transition zone appeared to deepen from 2002-2008 and 2002-2009, respectively (Figure 3.9c). This deepening was statistically significant (p-value = 0.01 for the relationship $Z_{PSW} = 5.186 * \text{year} - 10340$ m) only for stations inside the gyre. Outside of the gyre, the depth of PSW was more variable and was deepest in 2005 and 2008. In 2009, PSW inside the gyre remained at the 2008 depth while PSW in the transition zone and outside of the gyre shoaled by about 30 m.

The deepening of PSW inside the Beaufort Gyre and in the transition zone from 2006-2008 could be related to interdecadal climate variability that affects the circulation of the Beaufort Gyre. This interdecadal variability is described by the Arctic Ocean Oscillation index (AOO) (Proshutinsky and Johnson 1997). The AOO has two modes - a cyclonic regime where the

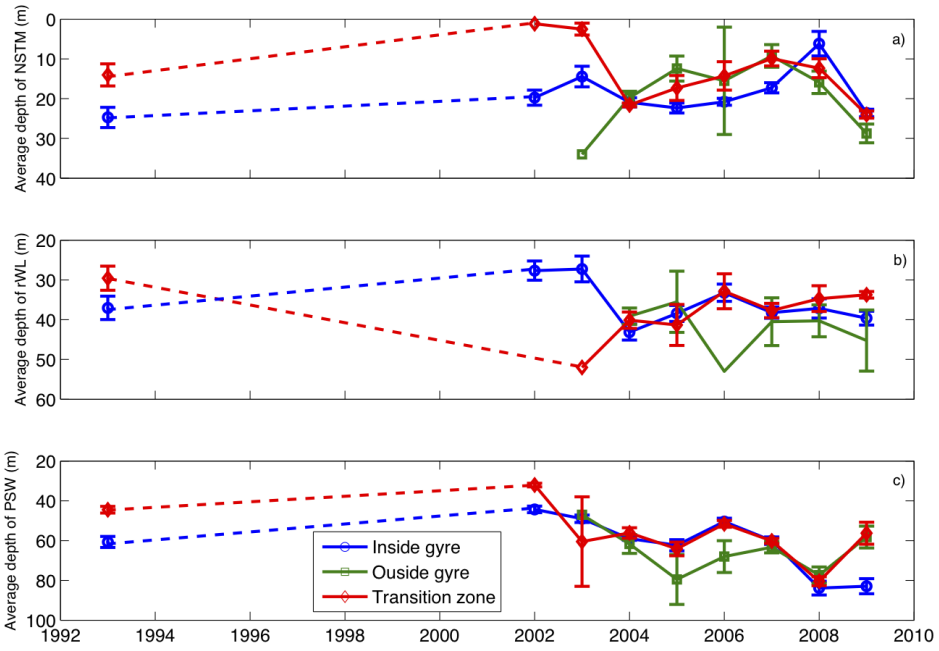

Figure 3.9: A comparison of the average depth of the a) NSTM, b) rML and c) PSW from inside of the gyre (blue line), outside of the gyre (green line) and in the transition zone (red line) during the summers of 1993 to 2009. The error bars represent the standard error for year, with the same sample sizes that were noted in Figures 3.8-3.10 The dashed lines represent years when no data were collected.

Beaufort Gyre weakens and the Transpolar Drift strengthens and a anticyclonic regime where the Beaufort Gyre strengthens and the Transpolar Drift weakens. During the anticyclonic regime more freshwater is stored in the Beaufort Gyre that is largely released and exported through Fram Strait during the cyclonic regime (Proshutinsky et al. 2002). The AOO was anticyclonic from 1997-2008, with very high values for 2007 and 2008 (Overland 2009, Arndt et al. 2010), and switched to a cyclonic mode in 2009 (Arndt et al. 2010). The strengthened anticyclonic winds in 2007 led to enhanced Ekman pumping (downwelling) and increased freshwater storage within the Beaufort Gyre (Proshutinsky et al. 2009). In addition, the sea ice concentration (Figures 3.4 and 3.5) was lowest and the surface salinity (not shown) was lowest in 2007 and 2008. I suggest that the strong downwelling and sea ice melt led to increased freshwater storage inside the gyre from 2006-2008, which freshened the NSTM and rML. The salinity of the NSTM and rML should be similar to the summer salinity and winter salinity, respectively, at the location that they were formed. Unless the source of PSW freshened, which will be examined in Section 3.6.1, this increased freshwater would likely accumulate in the gyre, causing PSW to enter the Canada Basin at a deeper depth. PSW remained deeper in 2009 inside of the gyre but shoaled in both the transition zone and outside of the gyre - the non-synchronized depth of PSW could be a response to the switch to the cyclonic regime.

3.6 Changes to Pacific Summer Water

In the previous section I showed that the NSTM and rML freshened and the salinity range of PSW has also freshened from about 29.5-32 in 2004 to 28-32 in 2007. Has PSW itself freshened or have other waters merged with PSW to change the properties of the temperature maximum? Here, I propose and examine three possible mechanisms that could change these properties. The first is that the source waters of PSW have freshened so that PSW enters the Canada Basin along a lighter isopycnal. The second is that the velocity and pathways of PSW entering into the Canada Basin have changed so that the amount of PSW and the modification of PSW once in the Canada Basin have changed. The third is that the diffusion of heat from PSW and the NSTM and diffusion of salt in the more stratified basin have changed the properties of the rML and have increased the salinity range surrounding the temperature maximum of PSW.

3.6.1 Changes to the Source Waters of Pacific Summer Water

There is significant interannual variability in the properties of the waters entering the Arctic through the Bering Strait (Woodgate et al. 2006, 2010). The source of PSW in the Canada Basin is thought to largely be a combination of ACW and ACC (Shimada et al. 2001, Steele et al. 2004) that primarily enters the basin through Barrow Canyon (for example, see Münchow and Carmack 1997, Weingartner et al. 1998, Woodgate et al. 2005a). Can I relate changes in the basin to changes in the salinity of the inflow?

I first examined the interannual variability of PSW in the Canada Basin. Since the temperature of PSW is non-conservative, I chose to compare the salinity at the temperature maximum. This temperature maximum was a consistent feature (a Gaussian-like PSW temperature peak was observed in 201 out of 204 temperature profiles) so I simply found the salinity at the highest PSW temperature. This salinity was plotted for all cruises (Figure 3.10) and the average salinity inside the gyre, outside the gyre and in the transition zone was calculated (Figure 3.11). The salinity at the PSW temperature maximum ranged from about 30.6 to 32.0. From 1993-2008, the salinities were freshest inside the gyre (average 30.8 to 31.6) and saltiest outside the gyre (average 31.1 to 31.9). Considerable interannual variability was observed, with the freshest salinities throughout the basin in 2006 (31.0) and 2002 (31.1) and the saltiest in 1993 and 2005 (31.6). In addition, the freshest salinities in 2006 were on the western side of the Canada Basin near the Northwind Ridge. This is the same region where Shimada et al. (2001) and Steele et al. (2004) observed the warmest PSW. Shimada et al. (2006) suggested this is because the warmest pulse of PSW is transported through Barrow Canyon at the same time that easterly winds become dominant, thereby pushing the warm PSW toward the western Canada Basin. It is thus likely that the region near the Northwind Ridge receives new PSW each year.

To compare the source PSW to that in the Canada Basin, the monthly average salinity and temperature were calculated from moorings A2, A3 and A4 and the data were smoothed with a three month running mean. These were plotted with the salinity and temperature of PSW at CB5 near

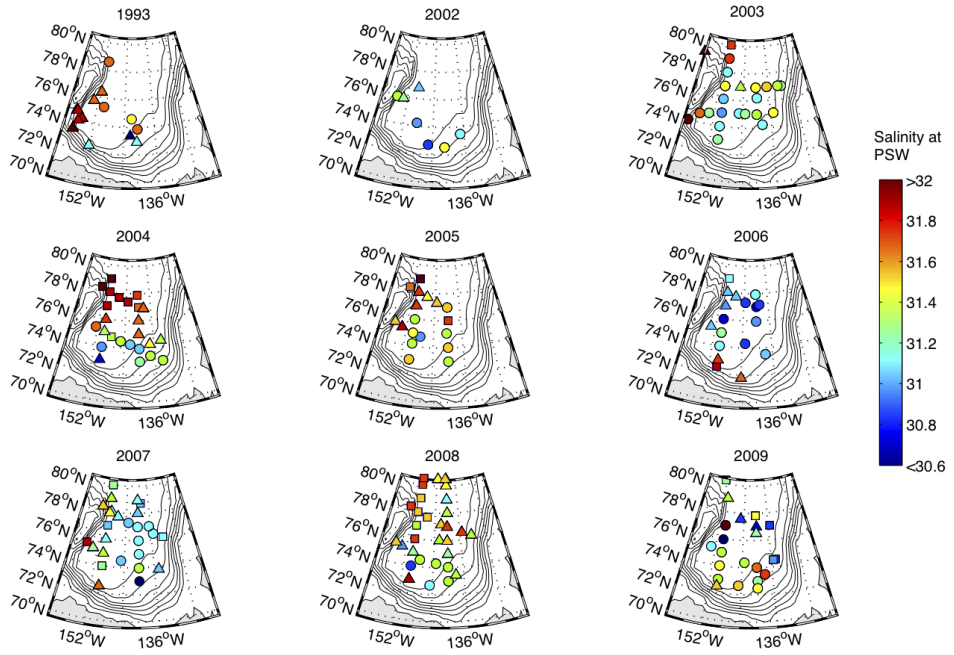

Figure 3.10: A comparison of the salinity at the PSW temperature maximum from the 1993-2009 summer cruises. Coloured circles represent stations that were inside the Beaufort Gyre, triangles represent stations that were in the transition zone, and squares represent stations that were outside of the gyre. Black lines show the bathymetry at 500 m intervals from 500 m to 3500 m.

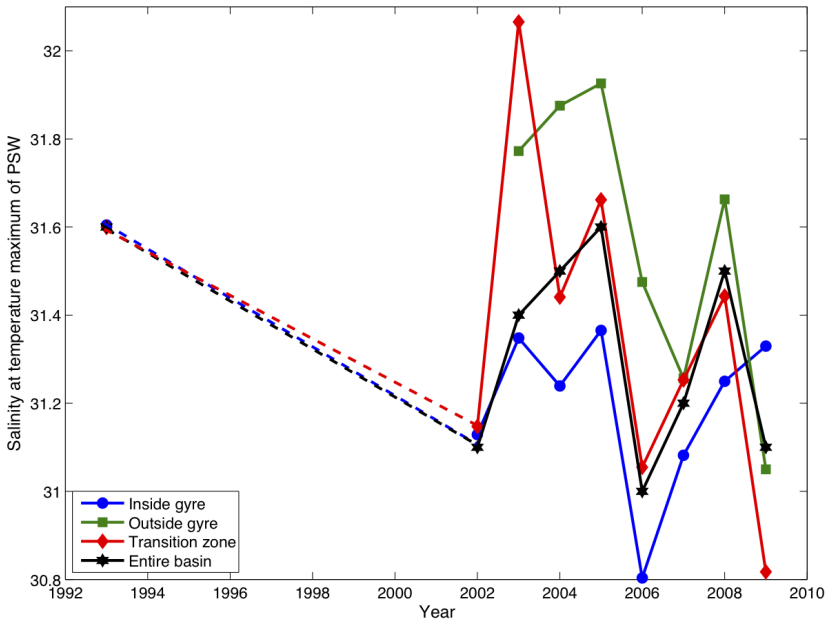

Figure 3.11: The average salinity at the temperature maximum of PSW from 1993-2009. The average salinity was calculated for stations inside the Beaufort Gyre (blue line), outside the gyre (green line), in the transition zone (red line), and for the entire Canada Basin (black line). Only stations that had a bottom depth greater than 3000 m were considered. The dashed line indicates years when no data were collected.

the southern Northwind Ridge (75.3°N, 153.3°W) during cruises 2002-09 to evaluate how they are related (Figure 3.12). From these data, I found that: i) A2 and A4 are in the same salinity range as PSW at CB5 (A3 is far saltier), however the timing of anomalous events (e.g. the 2004 fresh anomaly at A4 and the 2006 fresh anomaly at CB5) did not match; ii) the temperature at CB5 was much cooler than in the Bering Strait. This suggests substantial heat loss during transit from the Bering Strait into the Canada Basin that, as discussed by Woodgate et al. (2010), would affect sea ice and atmospheric conditions in the Chukchi Sea, and; iii) while the salinity of the PSW source waters vary interannually, there was no freshening trend over my study period that could account for the fresher salinity range surrounding PSW observed in the Canada Basin.

The joint examination of the mooring and CTD data allowed me to explore two questions about the relationship between Bering Strait waters and PSW - i) Is PSW at station CB5 most influenced by ACC, ACW or the mixed water at mooring A3?; and ii) Can the transport time from Bering Strait to station CB5 be estimated? To answer both questions, the average salinity and temperature mooring data from the months where the water had warm and fresh PSW properties (June through November) was calculated and a linear regression was run between the seasonally averaged mooring data and the summer data at CB5 (Figure 3.13). Data from the same year couldn't be compared as it would take time for water to travel from Bering Strait to the Canada Basin. Woodgate et al. (2005b) found that it takes several months for water to cross the Chukchi Sea from the Bering Strait to Barrow Canyon and, given typical near-surface velocities in the

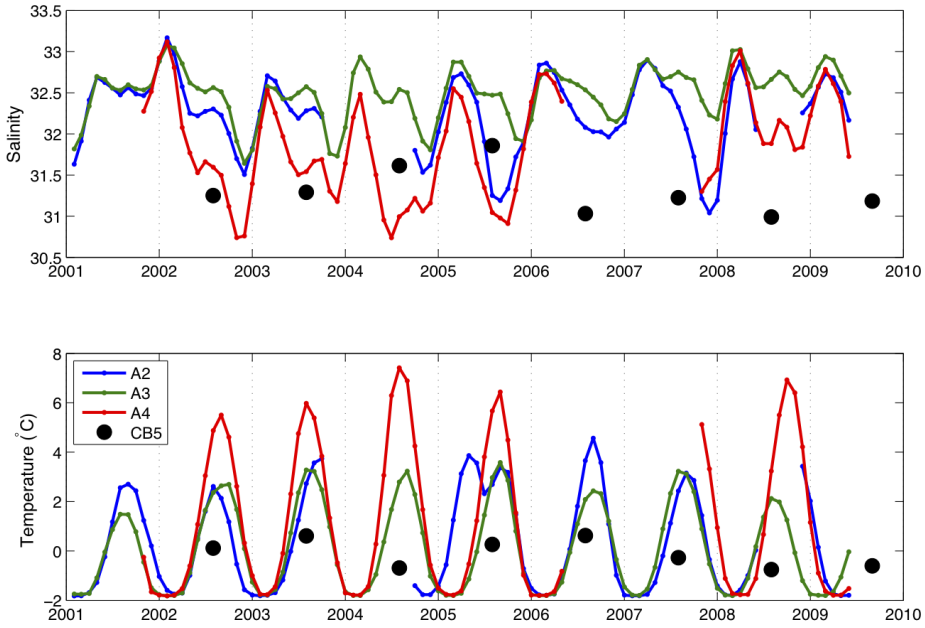

Figure 3.12: A comparison of the salinity (top) and temperature (bottom) at Bering Strait moorings A2, A3 and A4 with the salinity and temperature from the PSW temperature maximum at station CB5 (75.3°N, 153.3°W) in the western Canada Basin. The mooring data were averaged monthly and smoothed with a 3 month running mean.

Canada Basin of 1-5 cms^{-1} (Coachman and Barnes 1961, Jahn et al. 2010a), it would take up to 1 year for water to reach CB5 from Barrow Canyon. Thus, CB5 data were compared with Bering Strait data that were moved forward by 1 year (Figure 3.13a and b) and no significant relationship was found with a 1-year lag. A 2-year lag (i.e. 2002 Bering Strait data were compared with 2004 CB5 data; Figures 3.13c and d) showed that both the salinity (R^2=0.99; $S_{CB5} = 1.36 * S_{A4} - 11$) and temperature ($R^2$=0.82; $T_{CB5} = 0.843 * T_{A4} - 3.71°C$) at CB5 were very well-correlated with the five month averaged salinity and temperature at mooring A4. While only four data points are shown, these relationships appear to be robust since both temperature and salinity were well-correlated.

Based on these findings, several conclusions can be drawn. The first is that during my study period, ACC (sampled at mooring A4) primarily controlled the properties of PSW in the southwestern Canada Basin. The second is that a transit time of 2 years from the Bering Strait to the southern Northwind Ridge, at least during my study period, is reasonable. The third is that, since the relationship between water at A4 and CB5 was so consistent, there was little interannual variation in mixing of PSW between the Bering Strait and CB5 during my study period. The fourth conclusion is that ACC cooled and became saltier on its transit from A4 to CB5. An area of future research would be to study how ACC is modified between A4 and CB5 and the role that heat fluxes and the freeze-melt cycle (as discussed by Woodgate et al. (2010)) and diffusion play altering the properties of ACC. The fifth conclusion is that while there was no obvious warming or freshening trend, changing ACC may have a large impact on PSW at CB5. For

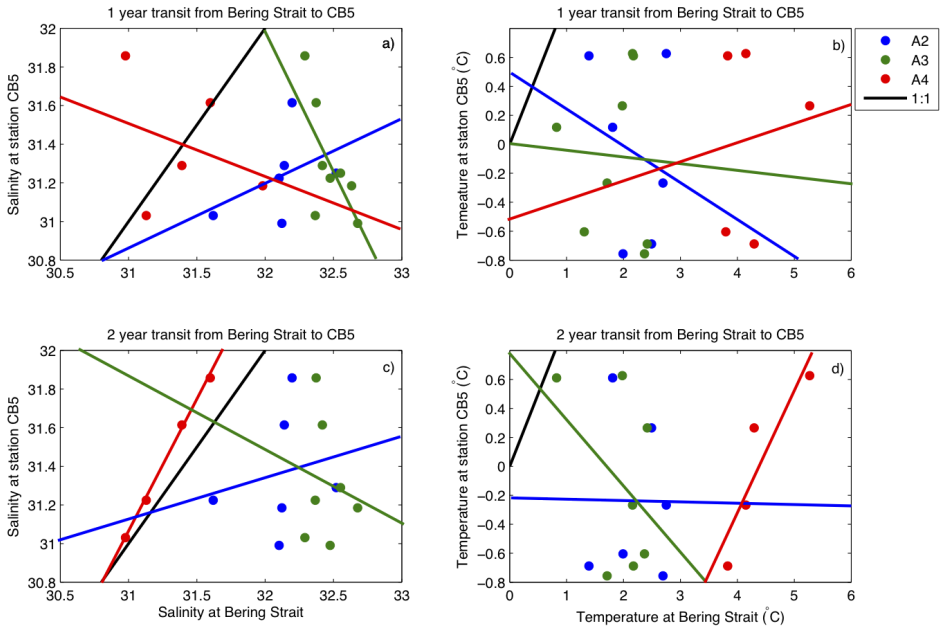

Figure 3.13: Linear regression between the 5 month average (June through November) from moorings A2, A3, and A4 (horizontal axes) and the PSW properties at station CB5 (horizontal axes). Here I compared the data from CB5 to data from the Bering Strait moorings that were collected 1 year (Figures a and b) and 2 years (Figures c and d) before. Lines represent the best fit between each different mooring and station CB5. Black line is the 1:1 ratio of the properties.

example, anomalously warm and fresh 2004 ACC waters caused the PSW to warm by about 0.5°C and freshen by about 0.5 salinity units from 2005 to 2006.

3.6.2 Changes to the Pathway and Velocity of Pacific Summer Water

Almost half (0.3 Sv) of the 0.8 Sv Pacific water that crosses through Bering Strait is thought to enter the Canada Basin through Barrow Canyon (Coachman and Barnes 1961, Shimada et al. 2001, Steele et al. 2004, Weingartner et al. 2005, Shimada et al. 2006). Thus, changes in the transport through Barrow Canyon could alter the properties of PSW within the basin. The water flowing through Barrow Canyon, which is about 2-4 months downstream of Bering Strait (Woodgate et al. 2005b, Panteleev et al. 2010), is warm enough and fresh enough to be PSW from the end of July through the beginning of November (Aagaard and Roach 1990, Woodgate et al. 2005b). Transport estimates through Barrow Canyon into the basin have ranged from an annual average of 0.14 Sv (Woodgate et al. 2005b) to about 0.3 Sv during summer and fall (Münchow and Carmack 1997, Nikolopoulos et al. 2009, Watanabe and Hasumi 2009). Münchow and Carmack (1997) found that PSW will follow three pathways out of Barrow Canyon - one that travels eastward along the shelf, one that travels eastward along the slope, and one that turns north into the Canada Basin. It has been estimated that the eastward slope current, which Nikolopoulos et al. (2009) call the western Arctic boundary current, transports about 0.13 Sv at a velocity of 5-10 cms^{-1} from mid-August to the beginning of October (Nikolopoulos et al. 2009). Mecha-

nisms that transport PSW from the boundary current out into the Canada Basin are largely unknown, although it has been suggested that hydrodynamic instabilities of the Barrow Canyon inflow and the slope current can form basin-bound eddies (D'Asaro 1988, Pickart 2004, Nikolopoulos et al. 2009). Also, upwelling events (which are most prevalent in late fall Pickart 2004) could feasibly move waters from the slope current into the basin. The fate of PSW that travels along the shelf is largely unknown but it is likely its properties are modified in fall and winter as sea ice forms.

The velocity of PSW that flows northward from Barrow Canyon into the Canada Basin has been estimated (based on 2 days in September 1993) as 5-10 cms^{-1} (Münchow and Carmack 1997) although specific details of this transport is unknown. Using a model, Watanabe and Hasumi (2009) suggested that more PSW is transported into the Canada Basin in summer when the sea ice concentration is reduced. They argue that reduced sea ice accelerates flow through Barrow Canyon, thereby creating more instabilities that form eddies that travel into the basin. Similarly, a simulation by Steele et al. (2010) found that Pacific water traveled further into the Canada Basin in 2007 than 2000-2006 and they suggest that the minimal 2007 sea ice cover led to faster spreading of PSW. Despite these findings, the strong correlation between mooring A4 and station CB5 suggest that how PSW is transported through Barrow Canyon has little effect on its properties once in the Canada Basin.

Based on a model of heat and salt diffusion (see Section 3.3.6 for details), PSW modification once in the gyre was examined. Once it leaves the southern Northwind Ridge, PSW is thought to be transported as part of the

anticyclonic Beaufort Gyre (Coachman and Barnes 1961, Steele et al. 2004). Station CB21 is downstream of CB5 and was within the gyre for every year of the study period (Figure 3.6) so the transport from CB5 to CB21 should give an estimate of PSW modification from its 'new' form (given the high correlation between ACC water and PSW at CB5) once in the gyre. Heat and salt diffusion (with two different diffusivities, $\kappa = 1 \text{ x } 10^{-6}$ m^2s^{-1} and $\kappa = 3 \text{ x } 10^{-6}$ m^2s^{-1}) was estimated for each summer cruise from station CB5 for 1 year and then compared to data from station CB21 sampled during the following cruise (Figure 3.14). In general, the properties at CB21 were quite similar to those at CB5 from one year earlier. For example, the cold PSW observed at CB5 in 2004 was seen during the following summer cruise at CB21. This suggests that it takes about 1 year to transport PSW from the southern Northwind Ridge to the centre of the gyre. If PSW traveled a straight path from CB5 to CB21, PSW would need to travel at a speed of about 1 cms^{-1} to cover the 415 km between the two stations in 1 year. This estimate is within the range of 1-5 cms^{-1} observed by Coachman and Barnes (1961) and less than the 5 cms^{-1} found by Jahn et al. (2010a). Results shown in Figure 3.14 also suggest that a diffusivity of 1 x 10^{-6} m^2s^{-1} gave the best estimate of heat loss from CB5 to CB21 between the annual cruises.

Although several mechanisms have been proposed for changing the velocity and pathway of PSW once it leaves the Chukchi Sea (the pathway of PSW at the mouth of Barrow Canyon, the sea ice cover offshore of Barrow Canyon, and the strength of the Beaufort Gyre), I found no evidence that this happened during my study period. The high correlation of properties

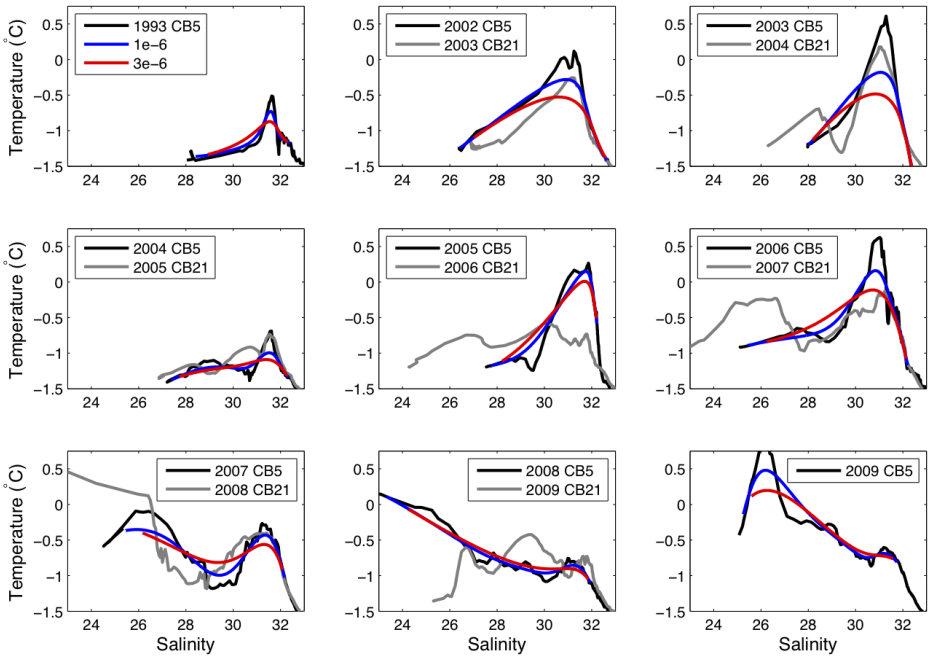

Figure 3.14: Temperature-salinity diagram of the upper 100 m for station CB5 (75.3°N, 153.3°W, solid black line) and station CB21 (74°N, 140°W, solid grey line) one year later. PSW travels from station CB5 to CB21 in the anticyclonic Beaufort Gyre so heat and salt should diffuse from CB5 to CB21. The diffusion of heat and salt from station CB5 were estimated from a 1-D vertical diffusion model calculated using a central derivative finite difference. The model was run separately for 1 year with two different diffusivities - 1x10^{-6} m^{2}s^{-1} (solid blue line) and 3x10^{-6} m^{2}s^{-1} (solid red line).

between mooring A4 in Bering Strait and station CB5 near the southern Northwind Ridge suggests (for the years examined) that transport between these regions did not change. In addition, although there was interannual variability, changes to PSW between CB5 and station CB21 inside of the gyre can partly be explained by vertical heat diffusion over ∼1 year, and there was little evidence for systematic change in the velocity or pathway to PSW during my study period. However, PSW appeared to propagate faster from 2003 at CB5 to 2004 at CB21 and propagate slower from 2005 at CB5 to 2006 at CB21.

3.6.3 Heat Diffusion from the NSTM and PSW to the rML

In previous sections, I found that successive NSTMs appear to be merging instead of stacking on top of each other (Figure 3.1), that the rML has warmed and freshened (Figures 3.4 and 3.5), and that the salinity range surrounding PSW freshened (Figures 3.8). These changes were greatest at stations located within the Beaufort Gyre. Since more heat has been stored below the summer halocline in recent years (Chapter 2), it is possible that some changes could have been caused by the diffusion of heat and salt between the NSTM, rML and PSW.

To estimate heat diffusion, a 1-D model of the heat equation was run for 1 year (Figure 3.15). The model was run at station CB21 since this was located within the gyre each year. This is different than the comparison in section 3.6.2 because here I am interested in the change to the rML that remains inside of the gyre whereas in section 3.6.2, I was interested in change to PSW as it is advected into the gyre. In general, the temperature change

was about double for the higher diffusivity (e.g PSW in 2004 lost about 0.25°C with the lower diffusivity and 0.5°C with the higher diffusivity). The rML gained heat each year while the NSTM and PSW lost heat. It was found that from 2002-05, the greatest heat loss was from PSW and the greatest heat gain was at the rML. Beginning in 2006, heat loss from the NSTM became equally important to that lost from PSW. My model shows that some of the heat lost from the NSTM was gained in the surface mixed layer, which suggests that even though Toole et al. (2010) found that a much larger diffusivity is needed to completely erode the summer halocline, small diffusion can bring some heat stored as the NSTM in contact with sea ice. From the heat equation, I conclude that much of the warming of the rML observed since 1993 can be attributed to heat diffusion from both the NSTM and PSW, with more heat being contributed from the NSTM since 2006. These results also imply that a diffusivity of 3 x 10^{-6} m^2s^{-1} explains most of the heat gained by the rML over 1 year. This is because the rML usually disappears during winter (Figure 3.3) and the higher diffusivity is more realistic in smoothing out the rML. The disappearance of the rML is likely from both heat diffusion and downwelling (the latter which thins the rML and makes it more susceptible to mixing) and the higher diffusivity accounts for both mechanisms.

Salt diffusion was also estimated for 1 year (Figure 3.16). In general, the greatest changes were seen above and below the summer and winter haloclines, with salt lost below each halocline and gained above it. This implies that in general, PSW became fresher, the rML became saltier (by up to 0.5 salinity units in 2002), the NSTM became fresher and the surface mixed

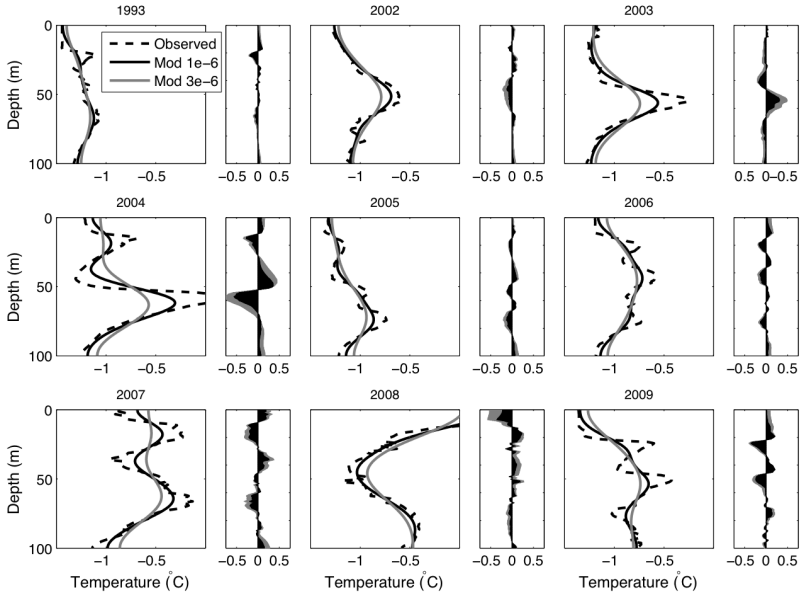

Figure 3.15: An estimate of vertical heat diffusion at station CB21 (74°N, 140°W) for 1993 and 2002-09. Using a central derivative finite difference, the heat equation was calculated in the upper 100 m for 1 year. Two experiments were run, one where the diffusivity (κ) was 1.0 x 10^{-6} m^2s^{-1} (solid black line) and one where κ was 3.0 x 10^{-6} m^2s^{-1} (solid grey line). The observed temperature profile (dashed black line) was also plotted. The horizontal bar graphs show where the temperature increased or decreased in 1 m increments within the range -0.75°C to 0.75°C.

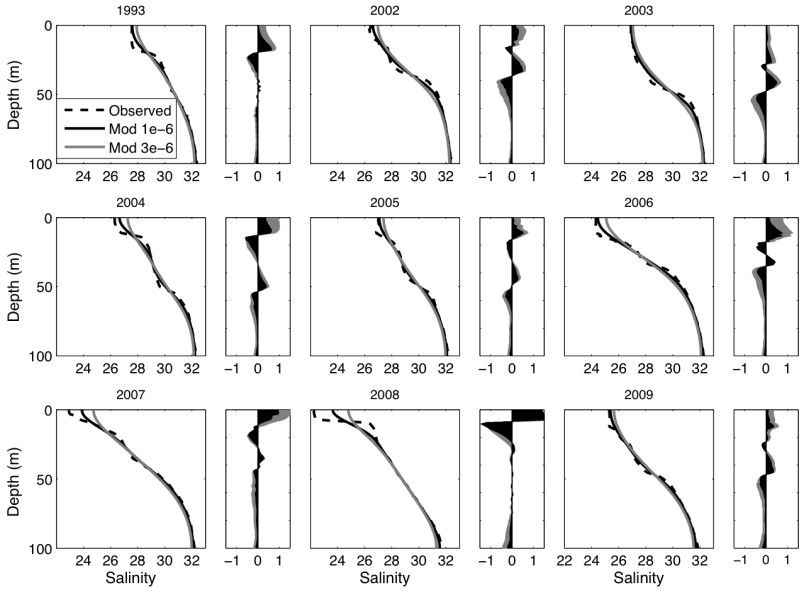

Figure 3.16: As in Figure 3.15 but for salt diffusion. The salinity range of the horizontal bar graphs is -1.5 to 1.5 salinity units.

layer became saltier. Thus, the freshening of the rML can not be explained by salt diffusion. It is important to note that there were no dynamics in this model to represent processes such as the freeze-melt cycle and wind mixing, thus the upper boundary condition is likely erroneous and over-represents salt diffusion. However, it is possible that some salt diffuses upwards to weaken the summer halocline during winter.

From this simple model I can then conclude that the diffusion of heat from PSW and the NSTM is likely what caused the rML to warm during my study period. It is likely that the warming of the rML, first noticed in 2006 (Figures 3.1, 3.4 and 3.8) was linked to the warming of the NSTM that was

caused by the increased absorption of solar radiation from sea ice melt. The freshening of the rML was different and was likely caused by the freshening of near-surface waters from sea ice melt and interannual changes to the strength of the Beaufort Gyre. The accumulation of freshwater within the Beaufort Gyre intensified the freshening and warming of the rML because it was formed at fresher salinities and because the higher stratification trapped more heat in the NSTM (Chapter 2) that can later diffuse to the rML. Since there was no freshening trend of PSW entering the Canada Basin and since the velocity and pathway of PSW seems not to have changed, I can conclude that the freshening of the salinity range surrounding PSW was caused by the freshening of the rML. The water mass structure from 2009 was different, with 3 temperature maxima inside the basin. My model predicts that these temperature maxima will diffuse into one temperature maximum by the summer of 2010.

3.7 Discussion and Summary

The near-surface waters of the Canada Basin changed dramatically from 1993-2009. These changes include the warming and freshening of the rML and the NSTM, the apparent freshening of the PSW temperature maximum, and the appearance of a third temperature maximum and second temperature minimum in 2009. I used CTD, mooring and sea ice concentration data and a 1-D model of heat and salt diffusion to examine several possible processes that could account for these changes.

A model of heat diffusion showed heat is diffused from the NSTM and

PSW to warm the rML. Before 2006, most of the heat to warm the rML was diffused from PSW. Since 2006, heat to warm the rML was diffused from both the NSTM and PSW. Thus, the warming of the NSTM through reduction of sea ice melt and the increased absorption of solar radiation indirectly warmed the rML (estimated at 30-50 m in summer).

My results suggest that the salinity of the rML was associated with the location of the Beaufort Gyre. It is likely that the location of the gyre can be attributed to changes in surface winds (Overland 2009, Proshutinsky et al. 2009), that are linked to the Arctic Ocean Oscillation (Proshutinsky and Johnson 1997). It was found that the rML was on average 1.9 salinity units fresher inside the gyre than outside of the gyre. Results from a vertical model of salt diffusion showed that over 1 year, salt would likely diffuse from below the winter halocline to the rML and from the NSTM to the surface, so salt diffusion would actually increase the salinity of the rML. Thus, I suggest that the freshening of the rML and NSTM is caused by a combination of sea ice melt and the repositioning of the Beaufort Gyre.

Three different processes were examined to explain the freshening of the salinity range surrounding PSW. The first theory was that the source waters of PSW were freshening. To examine this, the properties at three moorings in the Bering Strait were examined and no obvious freshening trend was observed. The second theory was that the pathway and velocity of PSW between Barrow Canyon and the Canada Basin had changed. There are many uncertainties in this transport, however, the properties between Bering Strait and station CB5 (near the southern Northwind Ridge) and CB5 and station CB21 (in the southeastern Canada Basin) were similar

and this suggests that there was little variation of PSW transport during my study period. The third theory was that the diffusion of heat and salt changed the properties of the rML, thereby appearing to widen the salinity range surrounding PSW. My model showed that once in the basin, PSW should be freshening because salt diffuses across the winter halocline from PSW to the rML. The salt gradient between PSW and rML has increased because the rML has freshened from sea ice melt. Thus, the widened salinity range for PSW can be explained by the loss of salt by diffusion from PSW to the freshened rML.

The near-surface waters in 2009 were different than other years because there was an extra temperature maximum between PSW and the NSTM. This extra feature was most prevalent within the gyre and I suggest it is linked to downwelling. Yang (2009) found that downwelling rates increased from 1979 to 2006 due to increased ice velocities. It is possible then that freshwater penetrated deeper within the Beaufort Gyre in 2007-2009 as the reduced sea ice cover lead to faster ice velocities. In addition, it was found that the Beaufort Gyre was very strong in 2008 and weakened in 2009 (Arndt et al. 2010). I found that PSW was deepest in 2008 at all stations and remained deep in 2009 for only stations within the gyre. Thus, I suggest that the increased downwelling for stations within the gyre in 2008 rapidly deepened the 2008 NSTM and rML. The 2009 NSTM and rML formed above the 2008 features so a third temperature maximum and second temperature minimum were observed. My model predicts that diffusion through the winter of 2009-2010 will cause the three temperature maxima to merge into one temperature maximum that occupies the near-surface waters from the

base of the surface mixed layer to PWW. A new NSTM will then form in 2010 so that the summer temperature profile will again have two temperature maxima.

The deepening of the nutrient-rich Pacific waters in the centre of the Beaufort Gyre will likely alter the ecosystem. In Chapter 4, I will show that the chlorophyll maximum deepened by 16 m from 2003 through 2008. This deepening can be explained by either increased solar radiation (from decreased sea ice cover) that would support phytoplankton at deeper depths or the deepening of the nutricline. Nutrient data from the same cruises show that the nutricline is deepening (McLaughlin and Carmack, in preparation) and this trend can explain why the foodweb structure transitioned to smaller picoplankton (Li et al. 2009) that require fewer nutrients (Agawin et al. 2000). Picoplankton mainly support the microbial loop (Barber 2007) that exports less carbon for grazing and burial than a nanoplankton-based foodweb (Li et al. 2009). Thus, changes to the water mass structure of the Canada Basin that are largely caused by sea ice melt also impact the foodweb structure and the sequestration of carbon.

During my study period, the near-surface water masses went through a period of dramatic transition - from a basin where the upper ∼40 m was seasonally heated and cooled in 1993 to a basin where the NSTM became stored year-round that then warmed the rML below, to a basin where in the winter the NSTM, rML and PSW were merged into one temperature maximum below a strongly stratified summer halocline. Is the merged temperature maximum the new reality for the winter near-surface water masses in the Canada Basin? If so then any erosion of the summer halocline will

entrain a significant store of heat that can further melt sea ice. Or, is the temperature maximum composed of merged water masses merely another step during the transition of near-surface water masses in the Canada Basin?

Chapter 4

Suspended Particles in the Canada Basin from Optical and Bottle Data, 2003-2008[2]

4.1 Chapter Summary

It is expected that coastal erosion, upwelling, and increased river runoff from Arctic warming will increase the concentration of suspended particles in the Arctic Ocean. Here I analyze in situ transmissometer and fluorometer data from the summers of 2003 through 2008 and bottle-derived particulate organic carbon (POC) and total suspended solids (TSS) measurements sampled in the summers of 2006 and 2007 from the Canada Basin and surrounding shelves. I divided my study area into five regions to account for the significant spatial variability and found that the highest attenuation, POC and TSS values were observed along the Beaufort shelf and the lowest values were located along the eastern shelf of the Canada Basin. I then ex-

[2]This paper is published as "Jackson, J.M., S.E. Allen, E.C. Carmack, and F.A. McLaughlin (2010), Suspended Particles in the Canada Basin from Optical and Bottle Data, 2003-2008, *Ocean Science,* **6,** 799-813."

plored the correlation of POC and TSS with beam attenuation coefficients to assess the viability of estimating POC concentrations from archived transmissometer data. POC (but not TSS) and attenuation were well-correlated over the Northwind Ridge, in the Canada Basin interior, and along the eastern shelf of the Canada Basin. From an interannual comparison, I found no evidence of increasing attenuation from the summers of 2003 through 2008 and, although not statistically significant, it even appeared that attenuation decreased over time in the upper 25 m of the Northwind Ridge and in the 25-100 m layer (that includes the chlorophyll maximum) of the eastern Beaufort shelf and within the Canada Basin. In the Canada Basin interior, the subsurface chlorophyll maximum deepened at a rate of 3.2 m per year from an average of 45 m in 2003 to 61 m in 2008, and this is likely linked to the freshening of the near-surface waters.

4.2 Introduction

Climate change is predicted to increase upwelling, coastal erosion and river runoff and these effects will likely increase suspended particle concentrations in the Arctic Ocean and its surrounding continental shelves (Carmack et al. 2006). Particles supplied by these processes in the western Arctic Ocean (see map in Figure 4.1) are primarily inorganic (Macdonald et al. 1998, O'Brien et al. 2006). Suspended particles influence the near-surface optical environment by scattering and absorbing sunlight, which may affect rates of primary productivity.

Historical measurements of total suspended solids (TSS i.e. both inor-

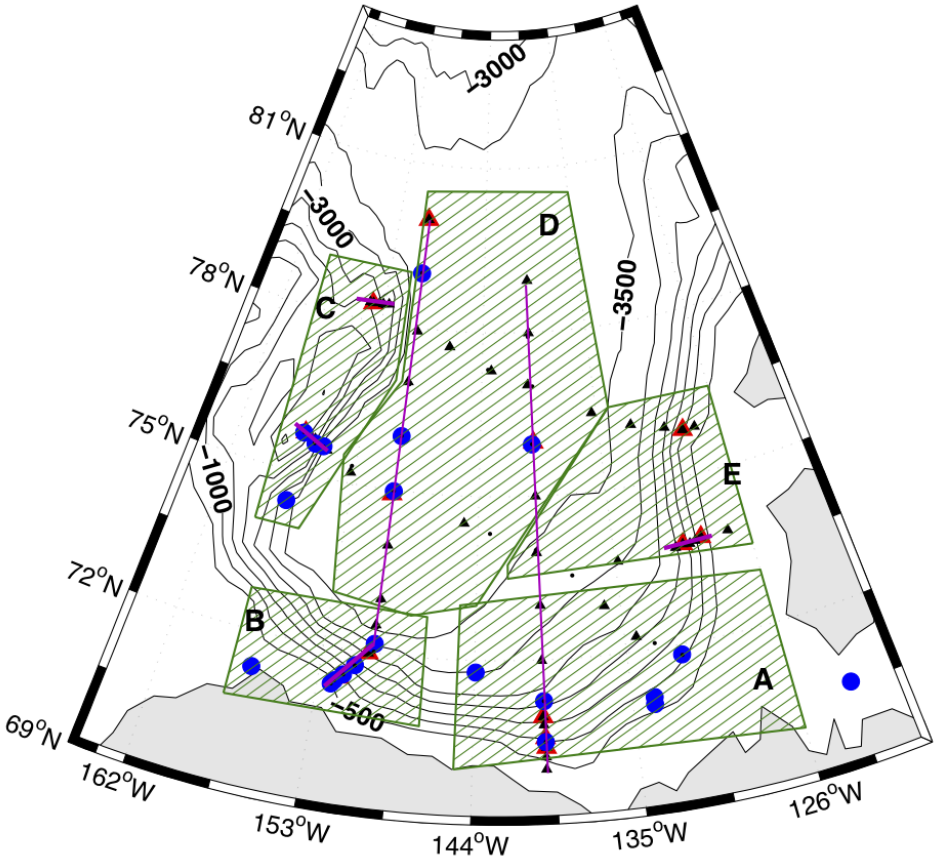

Figure 4.1: Bathymetric map of the stations where POC and TSS were sampled in 2006 (blue circles) and 2007 (red triangles). Contoured depths are labeled in meters at 500 m intervals. Small black circles (2006) and triangles (2007) represent stations where the CTD and sensors were deployed but no POC or TSS were sampled. This study area was separated into 5 regions over which the POC and TSS was averaged at each sampling level. These are A) the eastern Beaufort shelf that includes the Mackenzie Trough, B) the western Beaufort shelf that includes the Barrow Canyon, C) the eastern Northwind Ridge slope, D) the interior of the Canada Basin, and E) the eastern Canada Basin shelf between Banks Island and Prince Patrick Island. Purple lines indicate stations used to make section plots for Figures 4.7-4.11.

ganic and organic particles) and particulate organic carbon (POC) in the western Arctic Ocean are limited. The first reported TSS and POC data from the Canada Basin, collected in the spring of 1968 and 1969 at Ice Station T-3, were 9-56 μgkg^{-1} and 2-14 μgC kg^{-1}, respectively, with the highest values of both observed at 50 m (Kinney et al. 1971). Similar values for POC were found in April 1983 along the Alpha Ridge during the CESAR program (Gordon and Cranford 1985). The above concentrations were among the lowest ever observed for an open ocean system, and thus the Canada Basin was described as a biological desert (Kinney et al. 1971, Gordon and Cranford 1985). In 1994, POC samples were collected in summer during the joint Canada-US expedition from the Chukchi Sea to the North Pole and values in the upper 100 m were about five times greater than previous estimates, suggesting that the Canada Basin is seasonally productive (Wheeler et al. 1997) and actively cycles carbon (Wheeler et al. 1996).

Several studies have examined the transport of particles from Arctic shelves to the Canada Basin. During ice-island T3 from 1965-69, several nepheloid layers were identified along the Northwind Ridge that likely transported particles into the deep Canada Basin (Hunkins et al. 1969). At the surface, it has been found that particles in modified Mackenzie River runoff (O'Brien et al. 2006, Lalande et al. 2009) and in Lena River runoff (Burenkov 1993, Lalande et al. 2009) can end up in the Canada Basin (Yamamoto-Kawai et al. 2009a, Guay et al. 2009). Dirty sea ice can also release particles in situ if it melts (Darby 2003). During the 2002 Western Arctic Shelf-Basin Interactions (SBI) summer cruise, several plumes of particles at various depths below 50 m were identified that likely transported matter

from the Chukchi and western Beaufort shelf into the Canada Basin (Ashjian et al. 2005, Bates et al. 2005, Codispoti et al. 2005). Mechanisms to transport this material include advection through Barrow Canyon (Ashjian et al. 2005) and advection of eddies that are formed within the particle-rich along-shelf boundary current (Pickart 2004, Ashjian et al. 2005, Mathis et al. 2007).

Particle concentrations can also be approximated from transmissometer (measures light attenuation) and fluorometer (approximates chlorophyll *a*) data, both of which have been measured more extensively in the Canada Basin and surrounding shelves than POC and TSS. It has been found that POC and TSS are well correlated with attenuation in Puget Sound (Baker and Lavelle 1984), along the continental rise of the northwest Atlantic (Gardner et al. 1985), in the Gulf Stream (Bishop 1986), in the Laptev Sea near the Lena River delta (Burenkov 1993), in the equatorial Pacific (Bishop 1999) and in the subarctic Pacific (Bishop et al. 1999). However, these relationships have not been tested in the Canada Basin.

During the summers of 2003 through 2008, CTD, transmissometer and fluorometer data were collected at stations in the Canada Basin and its surrounding shelves. In addition, POC and TSS samples were taken during the 2006 and 2007 cruises (Figure 4.1). Here, I examine these data to i) identify regions of high attenuation, fluorescence, POC and TSS (section 4.3), to ii) examine the interannual variability of these data (section 4.4), and to iii) determine the correlation between TSS and attenuation and POC and attenuation (section 4.5). Developing a transmissometer-POC relationship would be highly valuable to look at changing particle distributions.

4.3 Data and Methods

4.3.1 CTD, Transmissometer and Fluorescence Data

For this study, researchers from Fisheries and Oceans Canada in collaboration with researchers from the Japan Agency for Marine-Earth Science and Technology and Woods Hole Oceanographic Institution collected temperature, salinity, chlorophyll *a* fluorescence, and transmissometer data from 2003 to 2008 (details in McLaughlin et al. 2008). The 24 10 L Niskin bottles and the sensors were deployed on the same rosette. During all years, a SeaBird SBE-911 Plus CTD, a Wetlabs C-star transmissometer, and a Seapoint fluorometer were used. The cruise dates were: 13 August - 3 September, 2003; 5-30 August, 2004; 3 - 31 August, 2005; 7 August - 12 September, 2006; 27 July - 28 August, 2007; and 23 July - 20 August, 2008. Transmissometer data were collected at 662 nm. The transmissometer was factory calibrated by a clean water reading test and a blocked path test. The Seapoint fluorometer measured chlorophyll *a* and its excitation and emission wavelengths were 470 nm and 685 nm, respectively. The fluorometer is calibrated each year by comparison with bottle-derived chlorophyll *a* samples.

An initial assessment of the transmissometer data revealed significant drift (up to 2%) between years and even during the same cruise, likely due to variable frequency of cleaning the optical window. In order to compare all transmissometer data, I calibrated all profiles to station CB11, sampled on 1 September, 2006 at 79°N, 150°W with a freshly calibrated Wetlabs C-star transmissometer. To perform the calibration, I set the transmission

at 2000 m at each station to 90.7% (the transmissometer value at CB11 at 2000 m in 2006). I then calculated the difference between the chosen station and 90.7% and added that difference to the entire profile. A depth of 2000 m was chosen because it was found to be the clearest water in the Arctic Ocean when the bottom depth was greater than 3000 m (Hunkins et al. 1969). For shallower stations, I averaged the calibration from the nearest basin stations. A similar calibration was done for fluorescence data. Here, the data were calibrated to the fluorometer value observed at 2000 m at CB11 in 2006 (0.0347 μgL^{-1}) and the basin profiles were calibrated based on the difference between the value at CB11 and the value at each station at 2000 m.

It has been shown that transmissometer output are affected by differences between the internal temperature of the transmissometer and the temperature of the seawater, especially in cold, clear water (Bishop 1986). In particular, Bishop (1986) found that a temperature difference of about 11°C amounts to 9-12 μgkg^{-1}of total suspended solids in open oceans. UBC's Wetlabs C-star transmissometer, subjected to temperature stability tests, had a maximum transmissometer error of 0.02% per degree Celsius difference, which is less than half of the 0.05% transmission error per degree Celsius found by Bishop (1986). To further minimize these effects, the transmissometer was soaked at 5 m for 3 minutes before each cast.

To determine the amount of light that is attenuated due to both scattering and absorption of particles, I calculated the beam attenuation coefficient (C) as $C = -ln(Tr)/r$ where Tr was the observed transmissometer value and r, the path length of the transmissometer, was 0.25 m (Bishop 1986).

4.3.2 POC and TSS Data

In 2006 and 2007, POC samples were taken at 5 m and 20 m, at the fluorometer maximum, at salinities 32.3, 32.6, 32.9, 33.1, 34.4, at the bottom and at any interesting transmissometer features. Nineteen stations were sampled in 2006 and 12 in 2007. Water was subsampled directly from 10 L Niskin bottles into two pre-calibrated, acid cleaned 2 L Nalgene bottles. The spigot was a few centimetres above the bottom of the Niskin bottles so, as found by Gardner (1977), it is possible that some of the particles could have settled to the bottom of the Niskin bottles before they were sampled. Onboard ship, the 4 L samples were filtered onto 47 mm Advantec GF75 filters in 2006 and 25 mm Advantec GF75 filters in 2007 that had been pre-combusted at 500°C for 4 hours. A vacuum pump whose pressure did not exceed 7 psi (4.82 Ncm^{-2}) was used during filtration. The filtration castles were rinsed down with double-filtered MilliQ water just before the filtration was complete. The filters were then placed in a labeled 50 mm glass Petri dish and frozen at -20°C. The filtration time and the volume of water filtered were recorded and filtration was performed within 4 hours of sampling.

Once on shore, the POC filters were dried for 24 hours at 50°C, HCl fumed for 48 hours, then dried again at 50°C for 24 hours, wrapped in aluminum foil and pressed into pellets. The pellets were analyzed using a Carlo Erba CN analyzer, located in the Department of Earth and Ocean Sciences at UBC, to determine POC. Sulfanilamide and blank cups were used as standards. Duplicates were taken at least once per cast in 2007 and the average standard deviation of the 10 duplicates was 6.3 $\mu\mathrm{gCkg}^{-1}$,

which was 29% of the average 2007 POC value of 21.4 μgCkg^{-1}. It should be noted that 9 POC samples were destroyed during analysis in 2007, including 3 duplicates.

TSS samples were taken at 5 m, 20 m, at the fluorometer maximum and at any interesting transmissometer feature in 2006. In 2007, samples were taken at the same depths as the POC samples. In 2006, 16 stations were sampled and in 2007, 12 stations were sampled. Water was subsampled directly from 10 L Niskin bottles into two or three pre-calibrated acid cleaned 2 L Nalgene bottles. Onboard ship, 4-6 L were filtered onto 47 mm Poretics 0.4 μm polycarbonate nucleopore filters that had been acid cleaned, rinsed with double-filtered MilliQ water, dried at 50°C and pre-weighed to 0.001 mg. A vacuum pump that did not exceed 7 psi (4.82 Ncm^{-2}) was used during filtration. The filtration castles were rinsed down with double-filtered MilliQ water just before the filtration was complete. The filters were rinsed with 3% ammonium carbonate solution after filtration was complete, placed in a labeled 50 mm plastic Petri dish, and frozen at -20°C. The time of filtration and the volume of water filtered were recorded and filtration was performed within 4 hours of sampling.

Once on shore, the TSS samples were dried at 50°C for 24 hours and then weighed. The TSS concentration was equal to the final weight minus the initial weight divided by the volume of water filtered. In 2006, the Satorius LE225D scale used to pre-weigh the filters was not available and a Mettler Toledo XP205 scale was used instead. By comparison of pre-weighed Petri dishes, it was found that the Petri dishes weighed on average (with standard deviation) 0.00057 ($\pm$ 0.00009) g less on the new scale so 0.00057 g was added

to the final weight of the filters. The Mettler Toledo XP205 scale was used in 2007. Duplicates were taken at least once per cast in 2007 and the average standard deviation of these 13 duplicates was 25.5 μgkg^{-1}, which was 25% of the average 2007 TSS value of 103 μgkg^{-1}.

4.4 Results

An initial evaluation of the sensor and bottle data showed substantial spatial variability, so I chose to divide the data into five different geographic regions of the Canada Basin for analysis (Figure 4.1). These are i) the eastern Beaufort shelf, a shelf-slope region in the southeastern Canada Basin with a bottom depth less than 3500 m that is influenced by outflow from the Mackenzie River; ii) the western Beaufort shelf, a shelf-slope area with a bottom depth less than 3500 m that includes Barrow Canyon; iii) the eastern Northwind Ridge slope, a feature with depths from about 950-3500 m between the Northwind Abyssal Plain and the Canada Basin, iv) the Canada Basin interior, with a bottom depth greater than 3500 m; and v) the eastern Canada Basin shelf, a shelf-slope area with a bottom depth less than 3500 m that lies between Banks and Prince Patrick Islands. Average profiles of beam attenuation, fluorescence, POC and TSS within each region were prepared for comparison (Figures 4.2-4.6).

4.4.1 The Eastern Beaufort Shelf

Overall, the highest TSS concentrations (maximum 1789 μgkg^{-1} in the surface water in 2006) were observed in the eastern Beaufort shelf. The average

profiles of beam attenuation (Figure 4.2) showed that the water was relatively clear below about 250 m, with the most particle-rich water in the upper 25 m. In this region, the highest attenuation, POC and TSS were seen above 10 m in 2006. In 2007, the surface water also had high attenuation but relatively low TSS and POC concentrations. It is likely that the source of particles in this area was the Mackenzie River. Based on oxygen isotopes and alkalinity, Yamamoto-Kawai et al. (2009a) found about double the amount of Mackenzie water here in 2007 than 2006, which suggests that the quantity of Mackenzie water itself is not a good indicator of TSS or POC concentration. O'Brien et al. (2006) attribute much of the spatial and temporal variability of suspended particles here to both the strength of the Mackenzie plume during freshet and to variable wind transport, which may cause either the resuspension of particles during north-westerly winds or the erosion of coastlines during south-easterly winds. Proshutinsky et al. (2009) found that the winds were more upwelling favourable in 2007 so more coastal erosion would be expected that year. Thus, since neither the resuspension of particles nor coastal erosion were greater in 2006, it is likely that the higher surface particle concentrations observed were due to a higher Mackenzie River particle load. Below the surface, attenuation was low in 2006 although a fluorescence and POC signal at about 50 m indicate the ubiquitous deep chlorophyll maximum (Lee and Whitledge 2005, Nishino et al. 2008, Martin et al. 2010). Both the near-surface and subsurface fluorescence maxima were deeper in 2007 than 2006. In general, the water column had higher attenuation and TSS concentrations in 2006 than 2007.

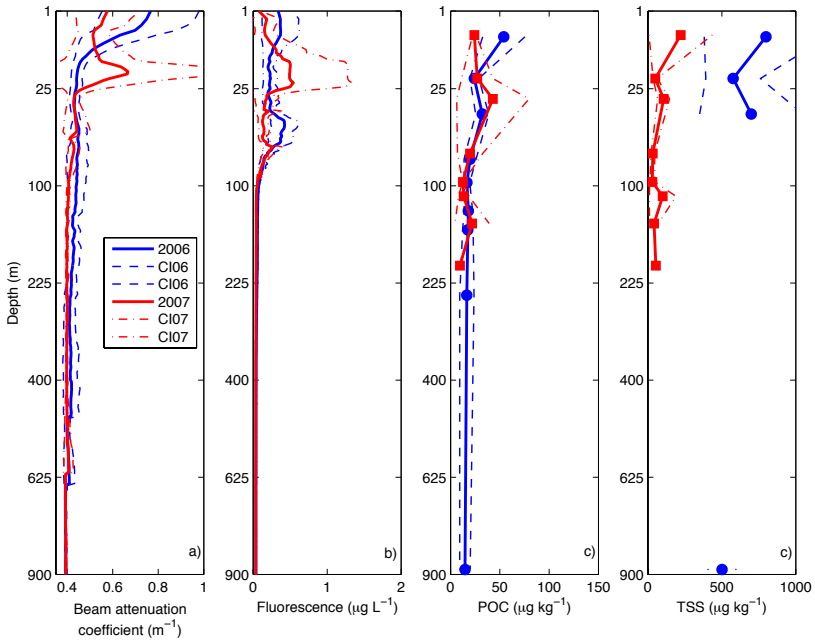

Figure 4.2: Average profiles of a) beam attenuation coefficient, b) fluorescence, c) POC, and d) TSS in the eastern Beaufort shelf region for 2006 (blue lines) and 2007 (red lines). The vertical axis is nonlinear (square root) to emphasize the near-surface features. Only the upper 900 m are shown because there were no attenuation features or bottle samples below this depth. The red and blue dashed lines represent the 95% confidence intervals for 2006 and 2007, respectively. For beam attenuation coefficient only, the 5 m centred running mean is plotted to smooth the data. The blue circles and red squares represent the average sampling depth for POC and TSS in 2006 and 2007, respectively.

4.4.2 The Western Beaufort Shelf

The western Beaufort shelf had the highest observed POC concentrations of the study area (Figure 4.3), with a maximum value of 192 μgCkg^{-1} at 5 m over the shelf in 2006. This is similar to surface water values sampled at the same location during the 2002 SBI project (Bates et al. 2005). In 2007, the surface water also had high attenuation, however, POC was low and TSS was high, which indicates that most of the particles were inorganic. Below the surface, the western Beaufort shelf also had the most variable attenuation profile of the regions sampled, with three main attenuation features above 1000 m in 2006 and five in 2007.

In 2006, the three features were i) A high POC, high fluorescence signal at about 25 m that represents the chlorophyll maximum; ii) High attenuation from about 75-100 m that had low POC; and iii) A high POC layer from about 100-200 m that was observed in an eddy of cold Pacific winter water (PWW, defined by a salinity of 33.1 as per Coachman and Barnes 1961). During the 2002 SBI project, Ashjian et al. (2005) found high concentrations of marine snow (up to about 20 μgCkg^{-1}) within PWW at the same location. I found similar POC concentrations of up to 29 μgCkg^{-1} within PWW. No TSS samples were taken in this layer in 2006. In 2007, the five subsurface attenuation features were i) The high fluorescence, high POC chlorophyll maximum from 30-50 m; ii) Near 100 m, there was non-fluorescent water with a very high TSS concentration of 806 μgkg^{-1}. This feature was within Pacific Summer Water (salinity of 32.7) and, as described by Pickart (2004), the sloping isohalines (not shown) indicate the eastward

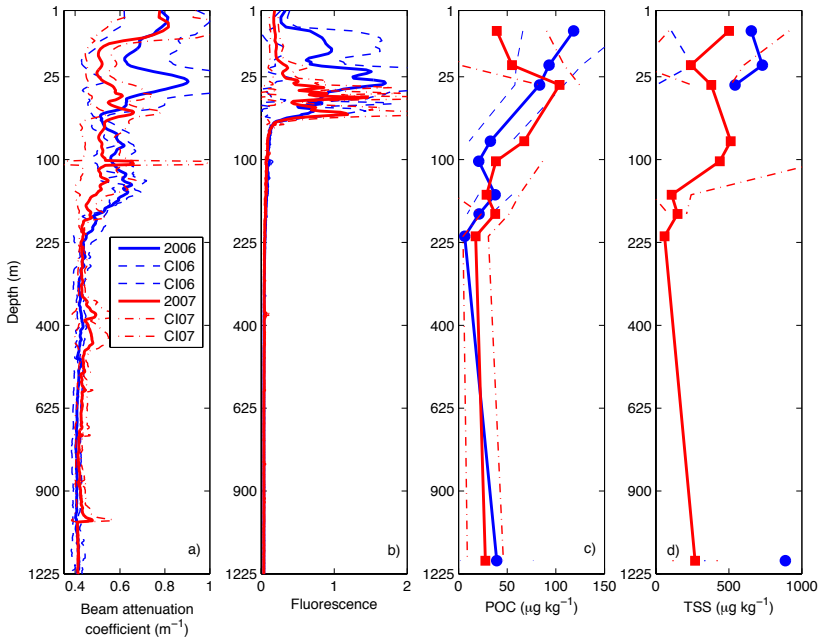

Figure 4.3: As in Figure 4.2 but for the western Beaufort shelf region. The upper 1600 m are shown to include all attenuation features and bottle samples.

flowing Beaufort shelfbreak jet. High concentrations can thus be explained by shear-induced re-suspension of particles caused by the current; iii) A POC (up to 46 μgCkg^{-1}) and TSS (up to 180 μgkg^{-1}) signal within PWW that was likely marine snow; iv) An attenuation feature at about 400 m within Atlantic water (salinity of 34.83). This feature was most apparent in the shallow station (bottom depth of 500 m), thus it could be from particle resuspension associated with a boundary current of Atlantic water; v) An attenuation feature at about 1000 m. This water had a salinity of 34.88 and the station had a bottom depth of 2000 m.

4.4.3 The Eastern Northwind Ridge Slope

The attenuation features on the eastern Northwind Ridge slope were all above 100 m (Figure 4.4). In 2006, a non-fluorescent, low-POC feature was observed at about 20 m that was not apparent in 2007. From the same 2006 cruise, I found a summer halocline at this depth (Chapter 2) and Yamamoto-Kawai et al. (2009a) observed a relatively high fraction of sea ice melt at the surface. Thus I suggest that the particles at 20 m were primarily inorganic and were released from melting sea ice, then trapped within the strong summer halocline that formed as the ice melted. The attenuation maximum in this region had high-fluorescence, high POC, and was at a depth of about 50 m. This deep chlorophyll maximum had much higher fluorescence values in 2006 than 2007, however the average POC (with 95% confidence interval) was 64$\pm$22 μgCkg^{-1} in 2006 and 47$\pm$8 μgCkg^{-1} in 2007, so there was no apparent statistical difference in POC concentrations.

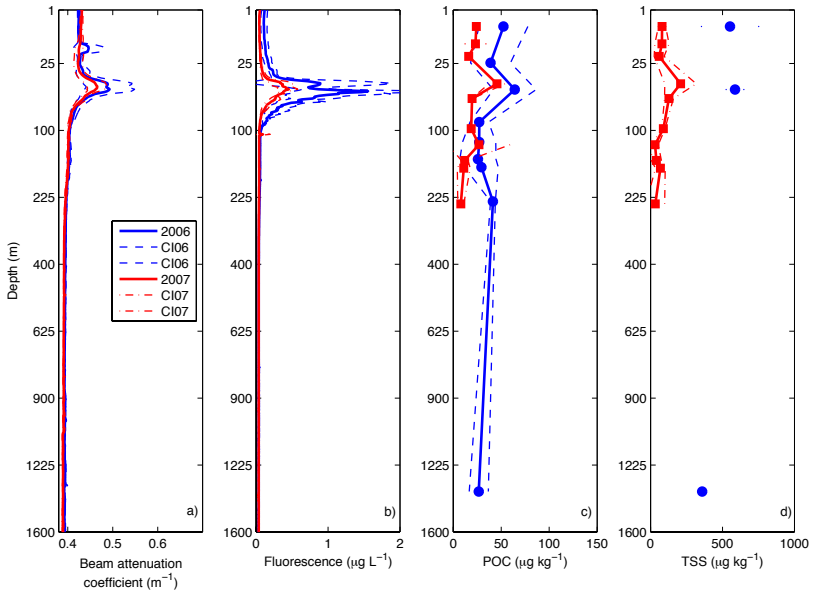

Figure 4.4: As in Figure 4.2 but for the eastern Northwind Ridge slope region. The upper 1600 m are shown to include all attenuation features and bottle samples.The value on the horizontal axis for beam attenuation coefficient is about half of the value in Figures 4.2a and 4.3a.

4.4.4 The Interior of the Canada Basin

Similar to the Northwind Ridge, the main attenuation features in the Basin region were observed in the near-surface waters (Figure 4.5). An non-fluorescent attenuation feature that had relatively high POC was observed at the surface in 2006 and at about 10 m in 2007. There was considerable sea ice melt during my sampling in both years, thus the particles observed in the upper 10 m could have been recently deposited from the melting ice and trapped in the surface summer halocline. The relationship between these particles and stratification is explored in Appendix A. The highest attenuation was the deep chlorophyll maximum at about 50 m. Similar to the Northwind Ridge, fluorescence (but not POC) was greater in 2006 than 2007. The average POC concentrations (with 95% confidence intervals) were 31±11 μgCkg^{-1} in 2006 and 27±4 μgCkg^{-1} in 2007, which is lower than the values found near the Northwind Ridge but about double those found in the central Basin in April and May by Kinney et al. (1971) and Gordon and Cranford (1985). An anomalous attenuation feature was observed at a depth of about 150 m within PWW (salinity = 33.1) in 2006 that was correlated with slightly higher POC values. Although not apparent in the attenuation profile, the highest average TSS concentrations were also observed within PWW in 2007. These results suggest that some particles are transported into the basin within PWW.

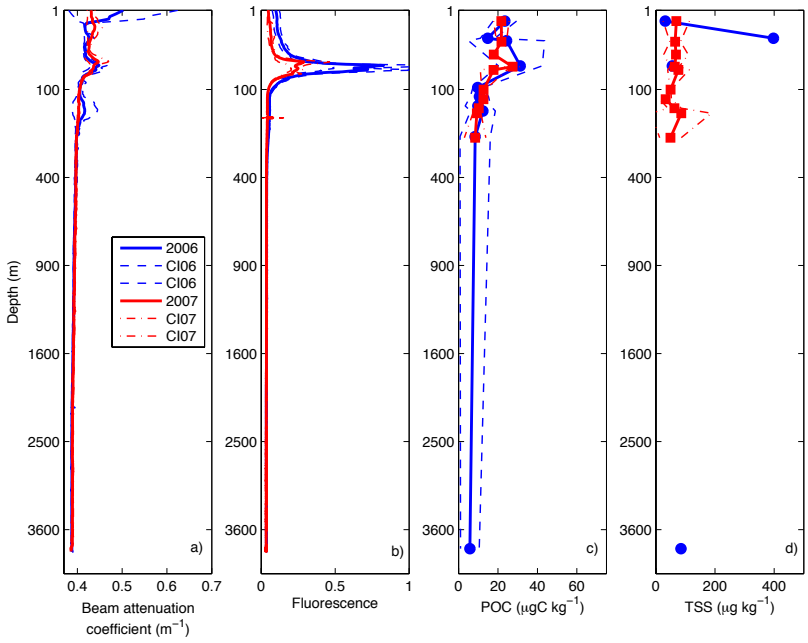

Figure 4.5: As in Figure 4.2 but for the interior of the Canada Basin. The upper 3800 m are shown to include all attenuation features and bottle samples. The scales on the horizontal axes are half of those in Figures 4.2 and 4.3.

4.4.5 The Eastern Shelf of the Canada Basin

The eastern shelf region was sampled only in 2007 because this region is usually inaccessible due to ice thickness. A general observation of this area was that the attenuation, fluorescence, POC and TSS concentrations in the upper 100 m were lower than in any other non-basin region (Figure 4.6). Overall, four attenuation features were observed. These were i) The attenuation maximum, which was located at the surface and had low fluorescence and relatively high POC concentrations; ii) The fluorescence maximum that was at a depth of about 60 m. Here, both the fluorescence and POC were much lower than other shelf-slope regions, suggesting that this is one of the least productive areas of the Canada Basin; iii) An attenuation feature at about 200 m that was above the TSS maximum. This feature is difficult to see in Figure 4.6a and is more obvious in the individual station profile (not included). The TSS maximum was centred at 129.2°W and was observed from about 320-370 m, within the salinity range 34.74-34.78. This feature had the highest observed TSS concentration of the region (263 μgkg^{-1}), and given the slightly tilted isopycnals (not shown), could be from re-suspension due to the passage of a boundary current transporting Atlantic water. It is interesting to note that there was a TSS peak at the salinity 32.9 and a POC peak at the salinity 33.1 that were not observed in the attenuation profiles. iv) The fourth feature was within the salinity range 34.82 - 34.86 from 446 m to the bottom (492 m) and suggest the presence of a bottom nepheloid layer at the 500 m depth station.

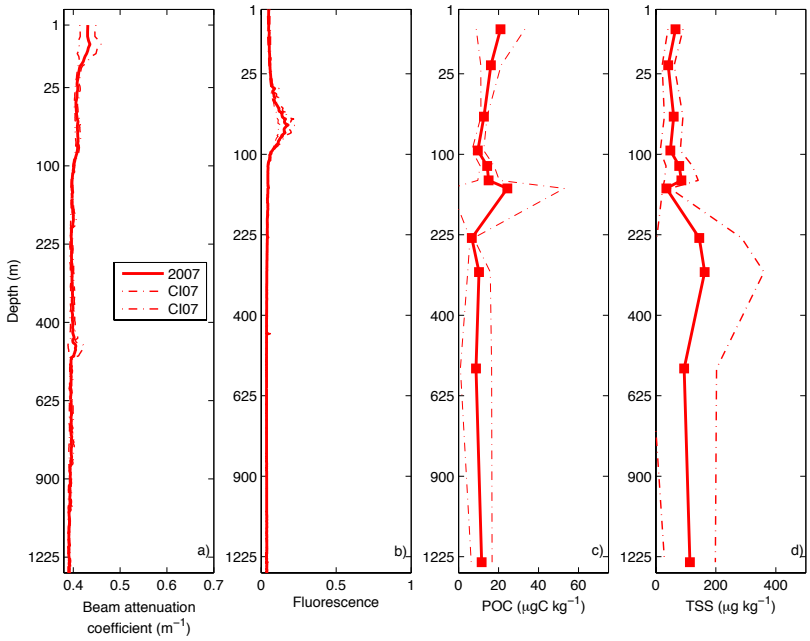

Figure 4.6: As in Figure 4.2 but for the eastern shelf of the Canada Basin. The upper 1300 m are shown to include all attenuation features and bottle samples. This region was sampled only in 2007. The scales on the horizontal axes are half of those in Figures 4.2 and 4.3.

4.4.6 Attenuation from the Shelf to the Basin

My results showed that there were several profiles along the continental slope that had high attenuation either along the bottom as nepheloid layers or in the water column within different water masses. To compare these features among regions, I contoured attenuation from shelf to basin for the eastern Beaufort shelf region, the western Beaufort shelf region, the eastern Northwind Ridge slope region and the eastern shelf of the Canada Basin region in 2007 (Figure 4.7). In the eastern Beaufort shelf region, most of the particles were observed at the surface and there was a small nepheloid layer along the slope. Overall, the western Beaufort shelf region had the highest attenuation below 100 m. Here, I found that particles at about 400 m (salinity 34.83) and 1500 m (salinity 34.92) extended to at least 72°N in the basin. The lowest attenuation below 100 m was seen at the Northwind Ridge and no nepheloid layer was found. Along the eastern shelf, I found the highest attenuation along the slope after the western Beaufort shelf, suggesting the presence of a significant nepheloid layer to about 800 m.

Results from the attenuation, fluorescence, POC and TSS data collected during the summers of 2006 and 2007 indicate six relatively consistent attenuation features and several irregular attenuation features in the Canada Basin. The six main features are found within i) surface water, ii) the summer halocline, iii) water that has high fluorescence, iv) cold water within the salinity range 32.9 - 33.1 of Pacific Winter Water, v) Atlantic water within the salinity range 34.4-34.85, and vii) samples taken at the bottom. Of these features, only the first three were found in the basin region and

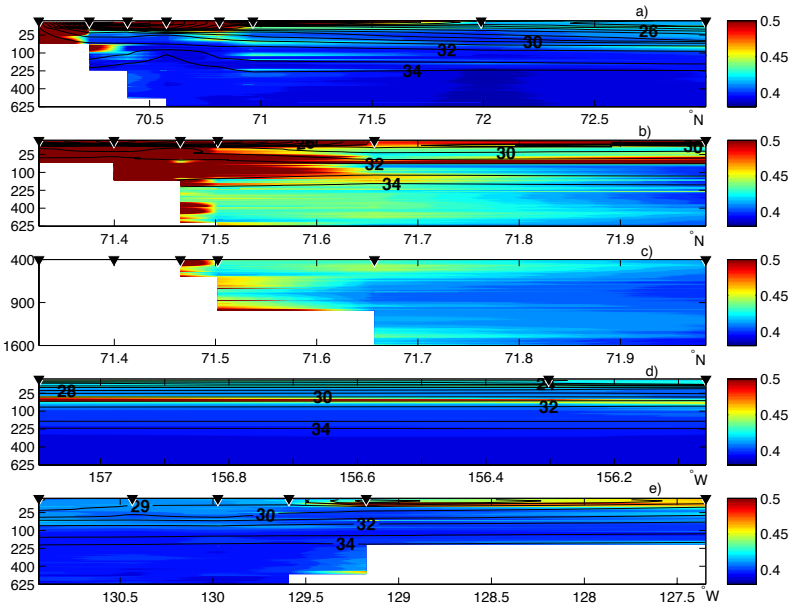

Figure 4.7: A comparison of the beam attenuation coefficient (m^{-1}) along four different shelf-basin sections. All data are from the summer of 2007. These are a) the eastern Beaufort shelf region along the longitude 140 °W, b) the western Beaufort shelf region along the longitude 150-152 °W. Here, the near-surface (1-625 m) attenuation features are shown c) The deep attenuation features (400-1600 m) along the western Beaufort shelf, d) The eastern Northwind Ridge slope region along the latitude 75-76 °N, and e) the eastern shelf of the Canada Basin region along the latitude 73-74 °N. The vertical axis is nonlinear (square root). Black horizontal lines represent the isohalines with 1.0 salinity resolution and black triangles denote the station locations.

were generally at depths less than 70 m. These near-surface features can have both high POC and TSS concentrations. All six features are found at various locations on the shelves and slopes surrounding the Canada Basin and generally had high TSS concentrations. Thus, particle concentrations within the Canada Basin have significant spatial variability.

4.5 Interannual Variation of Beam Attenuation Coefficient and Fluorescence from 2003 to 2008

Here, I will examine the interannual variation of beam attenuation coefficient and fluorescence within the six consistent attenuation features in the eastern and western Beaufort shelf, along the eastern slope of the Northwind Ridge, and in the interior of the Canada Basin from 2003 to 2008.

4.5.1 The Eastern Beaufort Shelf

Similar to the 2006 and 2007 analysis in Section 4.4.1, I found that the greatest attenuation in the eastern Beaufort shelf was near the coast and at the surface (Figure 4.8). At the surface, attenuation was highest (up to 1.5 m^{-1}) at 70.5°N in 2006. Surface waters in this region during these cruises were found to have a high fraction of runoff from the Mackenzie River (Yamamoto-Kawai et al. 2009a, Guay et al. 2009) and the attenuation variability again emphasizes the inconsistent location of the Mackenzie River plume and its changing particle load. The summer halocline was

indistinguishable from Mackenzie River water, thus I could not compare attenuation within the summer halocline. Water that had high fluorescence was observed both on the shelf and within the subsurface chlorophyll maximum. The highest shelf fluorometer values (with chlorophyll *a* estimates up to 5 μgL^{-1} at 15-25 m) were seen at 70°N in 2007 while the highest subsurface chlorophyll values (0.65 μgL^{-1} at 55-60 m) were seen at 72°N in 2006. The fluorescence values were lowest in 2008 throughout the region (not shown). High attenuation was observed within cold (temperature range -1.4 to -1.7°C) water in the salinity range 32.9 - 33.2 in 2005, 2006 and 2008, with highest values (0.55 m^{-1} at 133 m) in 2008. Melling and Lewis (1982) found that cold, dense water is formed along the Beaufort shelf in winter that descends into the Canada Basin, thus, these high attenuation plumes could be Beaufort shelf-derived winter water instead of PWW. There were several high attenuation features within Atlantic water and these were especially evident from 2005 to 2007. These features could be nepheloid layers, however, the isohalines in 2007 suggest upwelling near the shelf so the 2007 attenuation could have been due to particles entrained into Atlantic water from resuspension.

4.5.2 The Western Beaufort Shelf

In the western Beaufort shelf region, much of the attenuation variability was observed near the shelf and in subsurface plumes that appear to extend into the Canada Basin (Figure 4.9). Similar to the eastern Beaufort shelf, the highest attenuation at the surface (up to 1.4 m^{-1} at 71.4°N) was in 2006. This high surface attenuation in 2006 was correlated with high POC (see

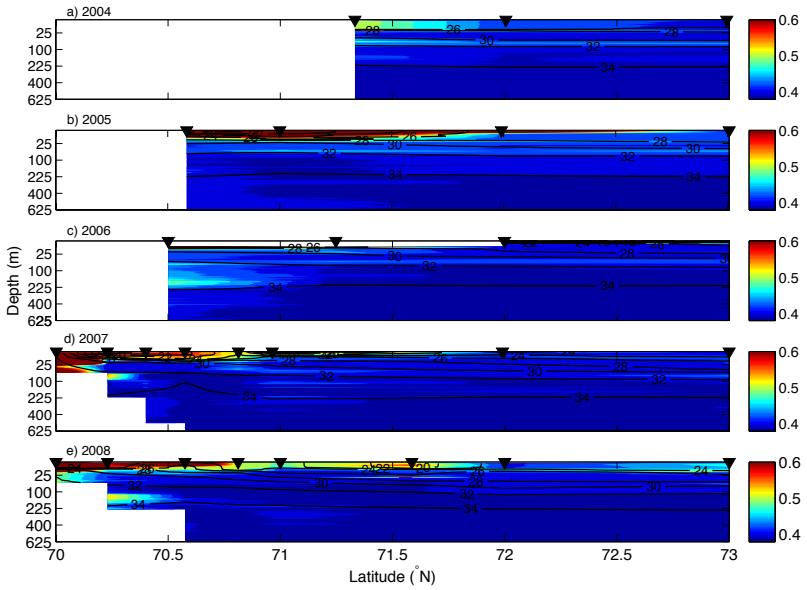

Figure 4.8: An interannual comparison of beam attenuation coefficient (in m^{-1}) from a section along the longitude 140 °W in the eastern Beaufort shelf region for the years a) 2004, b) 2005, c) 2006, d) 2007, and e) 2008. This section was not sampled in 2003. Here, the vertical axis is nonlinear (square root) to emphasize the near-surface features. The black lines show isohalines at 2 salinity unit intervals. The black triangles represent station locations for each year. Note that the attenuation range is about double that in Figure 4.7.

Section 4.4.2) and fluorescence (chlorophyll *a* estimates up to 3.9 μgL^{-1} at 22 m), which indicates that attenuation was mainly due to phytoplankton. Surface attenuation was lowest in 2003. Due to the high fraction of sea ice meltwater and meteoric water, with sources likely from Russian Rivers (Yamamoto-Kawai et al. 2009a), it was difficult to discern surface waters from the summer halocline. The subsurface chlorophyll maximum had the highest values in 2007 with chlorophyll *a* estimates up to 4.8 μgL^{-1} at 52 m at 72°N. Several high attenuation plumes were evident in waters with salinity greater than 32.5. The most obvious was the cold core eddy in 2006 (with a maximum attenuation value of 0.67 m^{-1} at 157 m) that had high POC concentrations (discussed in Section 4.4.2). Other high attenuation layers were observed at 400 m in 2005 with maximum attenuation of 0.54 m^{-1} at the salinity 34.82 and at 162 m in 2008 with maximum attenuation of 0.62 m^{-1} at the salinity 33.3. There was evidence of a bottom nepheloid layer, particularly in 2007 and 2008.

4.5.3 The Eastern Northwind Ridge Slope Region

The summer cruises over the Northwind region sampled both a southern (latitudes 75-76°N) and a northern (latitude 78-78.5°N) section (see Figure 4.1) so I contoured these sections separately (Figure 4.10). During my study, high attenuation was seen near the surface that could have been due to particles deposited from melting ice. Unlike the basin region, the summer halocline was weaker here and the high attenuation was spread throughout the upper 25 m, suggesting that particles did not accumulate in the strong stratification. In the surface waters, attenuation was highest (with a maxi-

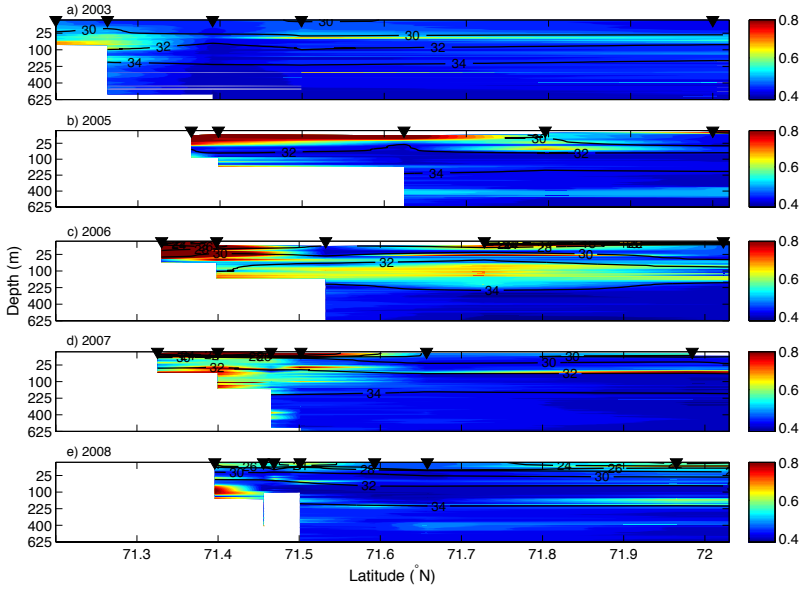

Figure 4.9: As in Figure 4.8 but for the western Beaufort shelf region for the years a) 2003, b) 2005, c) 2006, d) 2007, and e) 2008. This section was not sampled in 2004. Note that the attenuation range is about double what it was in Figure 4.8.

mum attenuation of 0.45 m^{-1} at 2 m) along the northern line in 2005. High attenuation within the summer halocline was most prevalent in the southern section in 2006. The predominant feature along the Northwind Ridge was the subsurface chlorophyll maximum. I found that fluorescence was higher along the southern Northwind Ridge, with the highest estimated chlorophyll *a* value of 3.4 μgL^{-1} at 52 m in the southern region in 2006. Below 100 m, there was little interannual variability, however, the attenuation here was higher than either the basin interior or eastern shelf regions. This indicates that particles could be transported from the Chukchi Sea to Northwind Ridge in deeper waters, as was suggested by Nishino et al. (2008).

4.5.4 The Interior of the Canada Basin

Most of the variability along 150°W within the Canada Basin was observed in the upper 100 m and near the southern end (Figure 4.11). At the surface, attenuation was highest from 2003-05, particularly north of 75°N. From 2006 to 2008, although not obvious in Figure 4.11, attenuation was higher in the summer halocline and lower at the surface. This suggests that the strengthened summer halocline from 2006 to 2008 (Chapter 2) trapped suspended particles that may have otherwise descended into the basin. The chlorophyll maximum was variable, with the highest chlorophyll *a* estimate of 3.3 μgL^{-1} at 60 m in 2006.

The chlorophyll maximum also appeared to deepen over my study period. To elucidate this trend, the average depth of the chlorophyll maximum was calculated at basin stations (i.e. bottom depth greater than 3500 m) along the 140°W and 150°W section lines (Figure 4.12). I found that the

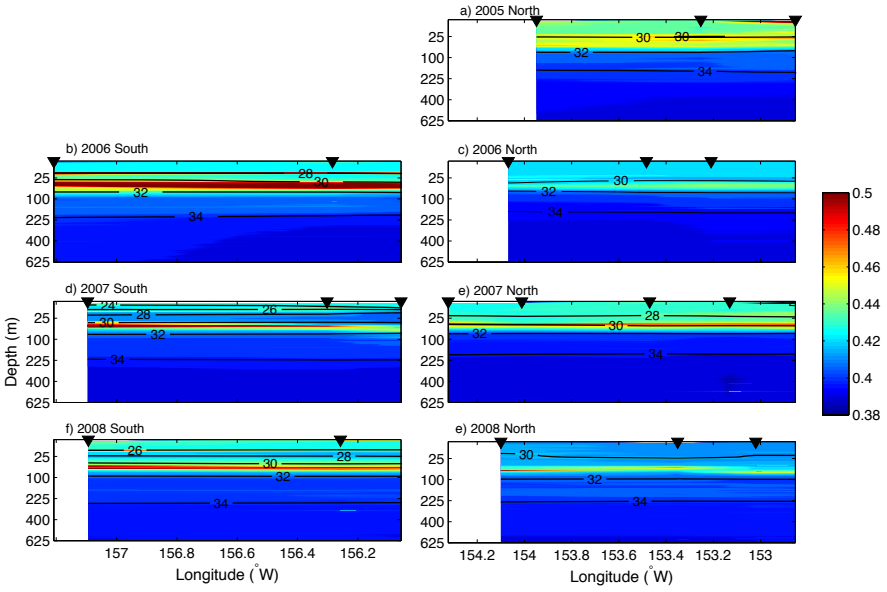

Figure 4.10: As in Figure 4.8 but for the eastern Northwind Region slope region. This region was sampled along a southern line (latitudes 75-76°N) and along a northern line (latitudes 78-79°N). Here, the northern line is shown on the right for a) 2005, c) 2006, e) 2007, and g) 2008 and the southern line is shown on the right for b) 2006, d) 2007, and f) 2008. Only one station was sampled along each line in 2003, 2004 and the southern region in 2005. The attenuation range is about half what it is in Figure 4.8.

subsurface chlorophyll maximum deepened at a rate of 3.2 m per year from an average of 45 m in 2003 to an average of 61 m in 2008, with the greatest difference observed between 2007 and 2008. The deepening of the chlorophyll maximum could be caused by two different processes. The first is that the decreased summer sea ice cover has allowed photosynthetically active radiation to penetrate deeper and phytoplankton have been able to utilize nutrients at deeper depths. The second is that the nutricline itself descended and this is likely since I found that the nutrient-rich PSW deepened during the same period. Nutrient data from the same cruises also show a deepening of the nutricline (McLaughlin and Carmack, in preparation). Understanding why the chlorophyll maximum has deepened is an important area of future research since the first process would cause depth-integrated primary production to increase while the second would cause it to decrease.

Below 100 m, attenuation features were observed at the southern end of the section. In particular, high attenuation was observed at 73°N in 2005 (with values up to 0.50 m^{-1}) from about 350-430 m within the salinity range 34.76 to 34.81 and in 2006 (with values up to 0.48 m^{-1}) from about 150-200 m within the salinity range 33 to 33.5. These regions of high attenuation have the same properties as the subsurface plumes observed in the western Beaufort shelf region (Section 4.5.2) and suggest that particles can be transported as far as 150 km from the shelf into the basin.

To examine whether attenuation has changed from 2003 to 2008, attenuation was averaged each year for all stations within each region (Figure 4.13). The water column was separated into three layers to see if there were any changes near the surface (1-25 m), in waters that contain the subsurface

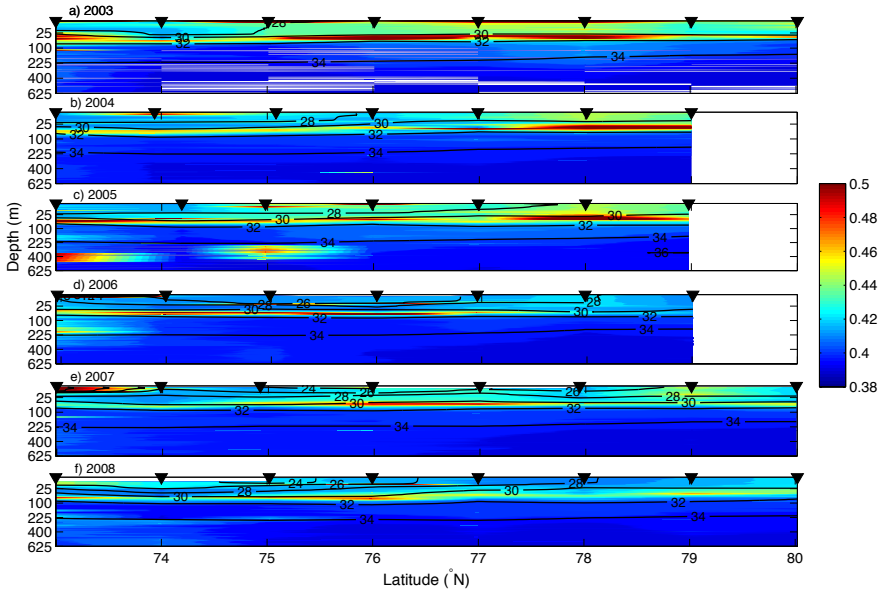

Figure 4.11: As in Figure 4.8 but for the interior of the Canada Basin for the years a) 2003, b) 2004, c) 2005, d) 2006, e) 2007, and f) 2008. These stations were located along the 150°W section, which is a continuation of the western Beaufort shelf section. Note that the attenuation range is about half what it was in Figure 4.8.

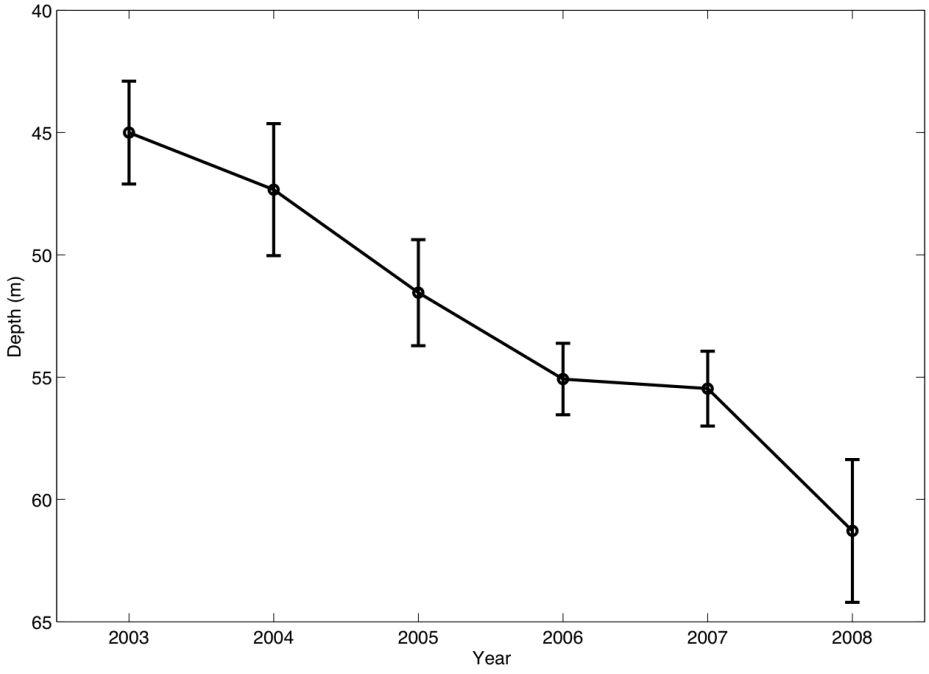

Figure 4.12: The average depth (with standard error bars) of the subsurface chlorophyll maximum in the interior of the Canada Basin from 2003 to 2008. Here, only stations that had a bottom depth greater than 3500 m and were along the 140°W or 150°W section within the latitudes 73°-80°N were used to calculate the average. The number of stations that fit these criteria was 11 in 2003, 12 in 2004, 11 in 2005, 13 in 2006, 15 in 2007, and 14 in 2008.

chlorophyll maximum (26-100 m) and in deeper waters (101-500 m for the eastern and western Beaufort shelf and the east shelf of the Canada Basin, 101-900 m for the Northwind Ridge and 101-3500 m for the interior of the Canada Basin). There are several conclusions that can be drawn from this figure, i) With the exception of the surface layer in 2007 and 2008, attenuation was always highest in the western Beaufort shelf, ii) In the intermediate and deeper layers, attenuation was generally higher in the Northwind Ridge than the interior of the Canada Basin, iii) Attenuation in the surface layer may have decreased at the Northwind Ridge from 2005-08, however the error on the trend is large enough that even its sign is not significant, and iv) Attenuation may have decreased over the study period in the intermediate layer at the eastern Beaufort shelf and in the interior of the Canada Basin but the high standard error again made the trends not statistically significant. Thus I conclude that attenuation did not increase during my study period as was suggested by Carmack et al. (2006).

4.6 Correlation Between Attenuation and POC and TSS

One of the main objectives of this project was to determine whether a relationship between transmission and POC and transmission and TSS exists in the Canada Basin. The overall attenuation and TSS relationship (Figure 4.14a and Table 4.1, R^2=0.54) was less-correlated than observed in the Gulf Stream and Sargasso Sea (R^2 = 0.76 - 0.89; Bishop 1986), in Puget Sound (R^2 = 0.78 - 0.90; Baker and Lavelle 1984), along the continental rise of the

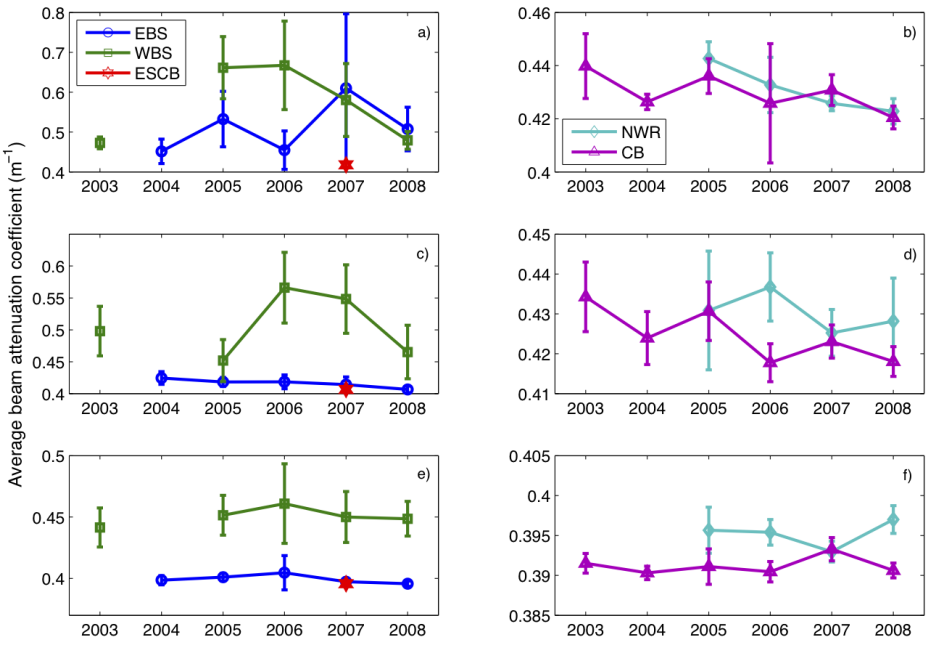

Figure 4.13: The average attenuation within the five different regions - the eastern Beaufort shelf (EBS), the western Beaufort shelf (WBS), the eastern shelf of the Canada Basin (ESCB), the eastern slope of the Northwind Ridge (NWR) and the interior of the Canada Basin (CB). The error bars represent the standard error. The average attenuation was plotted for shelf stations EBS, WBS and ESCB (a, c and e) and basin stations NWR and CB (b, d and f). To understand how attenuation varied with depth, the average was calculated for a and b) 1-25 m, c and d) 26-100 m, and e) 101-500 m for the shelf stations and f) 101-900 m for NWR and 101-3500 m for CB.

northwest Atlantic (R^2 = 0.97 - 0.98; Gardner et al. 1985), in the Equatorial Pacific (R^2 = 0.60 - 0.91; Bishop 1999), and in the Laptev Sea near the Lena River delta (R^2 = 0.96; Burenkov 1993). My attenuation and POC relationship (Figure 4.14b and Table 4.2, R^2=0.48) was less-correlated than observed in the Equatorial Pacific (R^2 = 0.75 - 0.95; Bishop 1999) and subarctic Pacific (R^2 = 0.95; Bishop et al. 1999) when POC was sampled with a Multiple Unit Large Volume in situ Filtration System but better correlated than when POC was sampled in the Equatorial Pacific using rosette bottles (R^2 = 0.41; Bishop 1999). In addition, the slope of the line of best fit for my samples was less steep than observed by Bishop (1999) in the Equatorial Pacific, suggesting that the particles in the Canada Basin are both heavier and less efficient at scattering light. I also compared the correlation in 2006 and 2007 and found that in general both TSS (R^2=0.64) and POC (R^2=0.58) were more correlated with attenuation in 2007 than in 2006. The relatively poor correlation in the Canada Basin and its surrounding shelves could be caused by i) scatter due to hydrographic variability (i.e. variability associated with the physical environment such as upwelling) (Bishop et al. 1999); ii) the use of rosette bottles instead of large volume pumps to collect POC and TSS samples (Bishop 1999), although Gardner et al. (2003) suggest the bottle sampling method is better in polar oceans; iii) an inconsistent particle size (Kitchen et al. 1982, Boss et al. 2001, Bowers et al. 2009), particle composition (Kitchen et al. 1982) , or particle density (Bowers et al. 2009); or iv) increased absorption of coloured dissolved organic material in the Arctic Ocean (Pegau 2002) compared to other regions, which could affect attenuation.

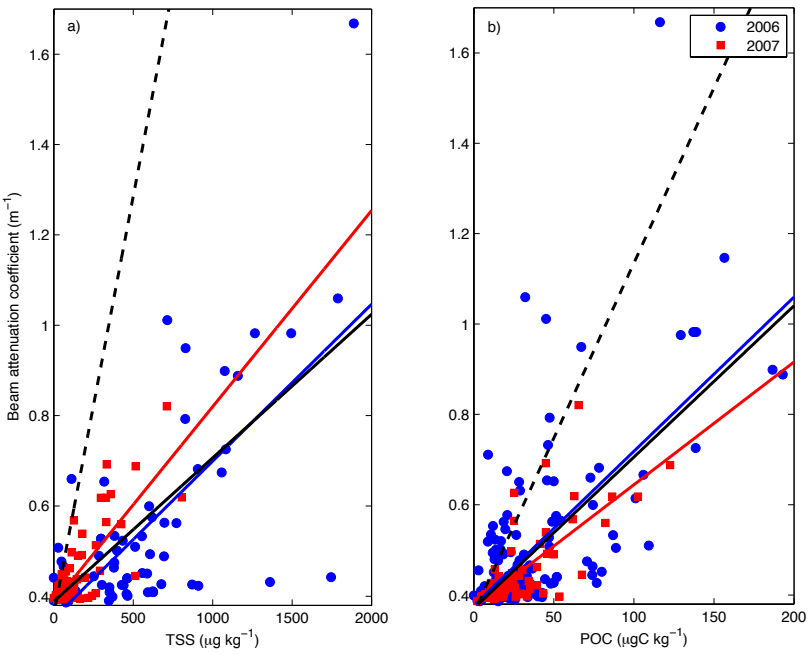

Figure 4.14: Linear least squares regression of a) the relationship between beam attenuation coefficient and total suspended solids, and b) the relationship between beam attenuation coefficient and particulate organic carbon. The blue dots represent samples taken in 2006 and the red squares are samples taken in 2007. The blue and red lines represent the line of best fit for 2006 and 2007, respectively. The solid black line represents the line of best fit from both years together and the dashed black line represents the linear regression (bac = 0.00755(POC) + 0.36 and bac = 0.00185(TSS) + 0.36) from Bishop (1999) based on JGOFS Equatorial Pacific data.

Table 4.1: A comparison of the relationships between beam attenuation coefficient and total suspended solids. The symbol n represents the number of samples in each linear regression. The units for slope and intercept are $m^{-1}(\mu g kg^{-1})^{-1}$ and m^{-1}, respectively.

Region	year	n	slope (x 10^{-3})	intercept	R^2
all	2006	62	0.347	0.35	0.44
	2007	130	0.434	0.39	0.64
	2006, 2007	295	0.318	0.39	0.54
Eastern Beaufort	2006	26	0.147	0.42	0.13
	2007	22	0.517	0.39	0.47
	2006, 2007	48	0.153	0.41	0.23
Western Beaufort	2006	21	0.496	0.34	0.75
	2007	20	0.425	0.40	0.56
	2006, 2007	41	0.468	0.38	0.75
Northwind Ridge	2006	6	0.350	0.28	0.39
	2007	19	0.453	0.38	0.74
	2006, 2007	25	0.143	0.40	0.36
Canada Basin	2006	9	0.035	0.44	0.02
	2007	35	0.050	0.41	0.02
	2006, 2007	44	0.087	0.41	0.14
East shelf	2007	33	0.044	0.40	0.03

Table 4.2: A comparison of the relationships between beam attenuation coefficient and particulate organic carbon. The symbol n represents the number of samples in each linear regression. The units for slope and intercept are $m^{-1}(\mu gCkg^{-1})^{-1}$ and m^{-1}, respectively.

Region	year	n	slope (x 10^{-2})	intercept	R^2
all	2006	174	0.341	0.38	0.45
	2007	121	0.272	0.37	0.58
	2006, 2007	295	0.335	0.37	0.48
Eastern Beaufort	2006	63	0.235	0.41	0.11
	2007	23	0.216	0.38	0.30
	2006, 2007	86	0.238	0.40	0.12
Western Beaufort	2006	37	0.320	0.43	0.44
	2007	20	0.254	0.41	0.46
	2006, 2007	57	0.314	0.46	0.41
Northwind Ridge	2006	27	0.152	0.37	0.37
	2007	20	0.19	0.38	0.59
	2006, 2007	47	0.14	0.38	0.39
Canada Basin	2006	47	0.142	0.39	0.32
	2007	29	0.206	0.38	0.75
	2006, 2007	76	0.152	0.39	0.37
East shelf	2007	32	0.166	0.38	0.52

To determine the effect of hydrographic variability on the relationship between attenuation and TSS and POC concentrations, I separated the data into the five different regions. For TSS, I found that there was significant variability between these regions (Figure 4.15, Table 4.1). Part of this variability was because TSS concentrations were much higher in 2006 than 2007. Overall, the best fits were observed in the western Beaufort shelf in 2006 and in the Northwind Ridge in 2007. The worst fits were seen within the Basin and on the eastern shelf.

Examining each region separately, I found that in the eastern Beaufort shelf, most of the outlier points were observed at 5 m. These outliers were removed but the correlation worsened (R^2=0.13). An assessment of particles measured in sediment traps offshore of the Mackenzie River showed substantial compositional diversity (O'Brien et al. 2006). The transmissometer gives the most accurate readings when the particles are small and have a low density (Bowers et al. 2009) so I suggest that some of the variability in the TSS and attenuation correlation is from inconsistent particle size and composition. Thus, the eastern Beaufort shelf is not a good candidate for finding a linear relationship between TSS and attenuation. Along the western Beaufort shelf, the relationship was best in 2006, even in the shallow shelf stations. This suggests that the particles in the western Beaufort shelf are small and of low density and the relationship found in this area can be used to estimate past TSS concentrations. There was significant interannual variability at the Northwind Ridge, with much higher TSS concentrations observed in 2006. However, TSS was well-correlated with attenuation in 2007 when more data points were available, thus I attribute some of the

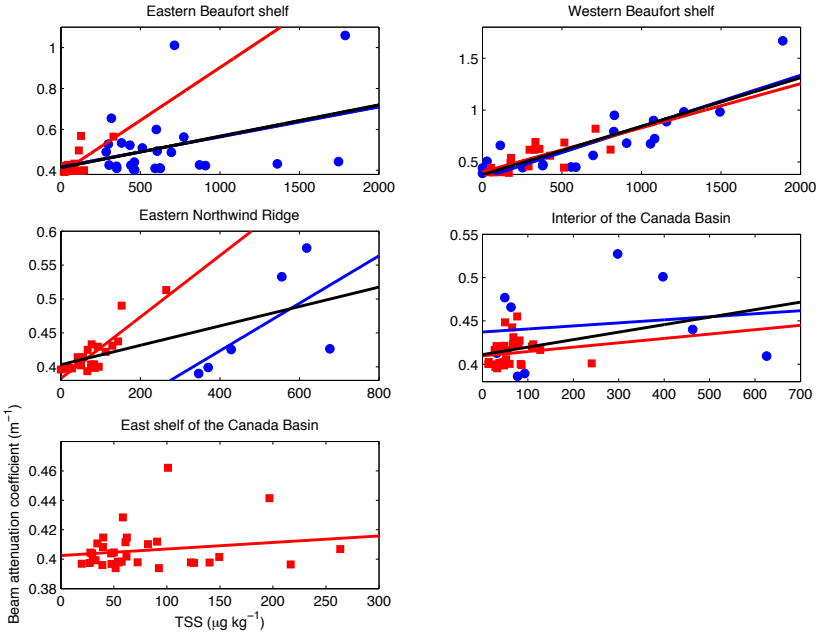

Figure 4.15: Linear regression of the relationship between beam attenuation coefficient and total suspended solids (μgkg^{-1}) in the five different regions. Here, the blue circles are samples from 2006 and the red squares are from 2007. The lines denote the linear least square regression from 2006 (blue lines), 2007 (red lines) and both 2006 and 2007 (black lines). Linear relations and R^2 values are listed in Table 4.1. Note that the scales are different in each figure.

interannual variability to insufficient sampling in 2006. In the interior of the Canada Basin, the outlying points could be placed into 3 groups i) Those with high TSS concentrations and low attenuation. These were found either near the surface in the southern basin or near the bottom; ii) Those with high TSS concentrations and high attenuation. These were found above 20 m in the south-central basin; iii) Those with low TSS concentrations and high attenuation. These were all found at the deep chlorophyll maximum throughout the basin. Similar to Bishop (1999), these results suggest that the transmissometer does not linearly represent TSS and it is likely that the attenuation values depend on the percentage of organic matter. Along the eastern shelf of the basin, I found that there were two types of outlying points i) those with high TSS concentrations and low attenuation, found in water below 100 m.; ii) those with high TSS concentrations and high attenuation, found primarily at 5 m. Unlike the interior of the basin, there were no low TSS, high attenuation particles found within the deep chlorophyll maximum and this is likely because the chlorophyll *a* fluorescence concentrations (and thus POC) were very low here. From these evaluations, I suggest that a reasonable relationship between TSS and attenuation can only be found in the western Beaufort shelf region.

Linear regressions to determine the relationship between attenuation and POC within each region were also run (Figure 4.16, Table 4.2). I found the best relationship within the basin and on Northwind Ridge in 2007, confirming results from Bishop (1999) who found that attenuation was much better correlated with POC than TSS in open ocean areas. POC and attenuation were least correlated along the eastern Beaufort shelf.

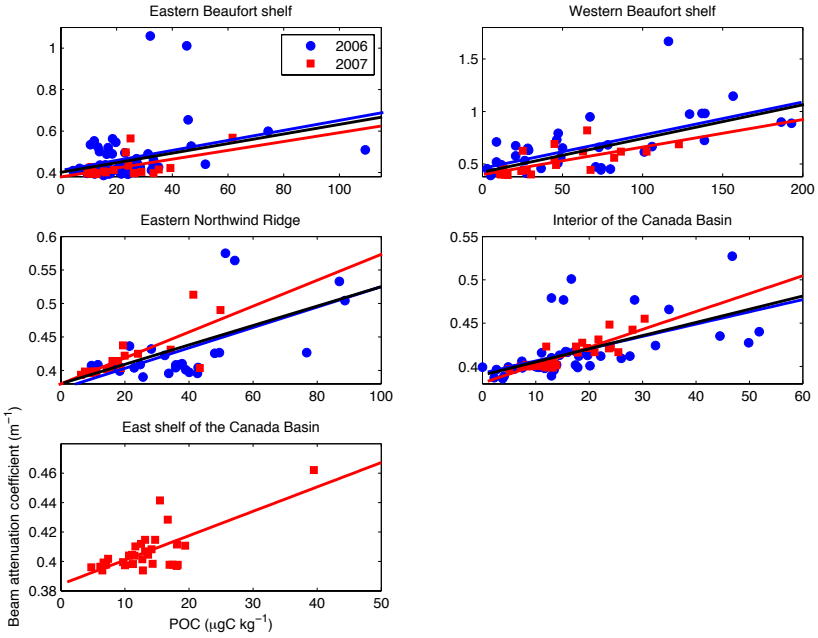

Figure 4.16: As in Figure 4.15 but for correlations between attenuation and POC. Linear relations and R^2 values are listed in Table 4.2. Note that the scales are different in each figure.

An examination of the outliers in the eastern Beaufort shelf found that they were generally from samples that had high TSS concentrations. Thus, I conclude that the particle composition of the eastern Beaufort shelf is too variable to be represented by a linear relationship between POC and attenuation. In the western Beaufort shelf, attenuation and POC were well correlated below an attenuation of 1.1 m^{-1}. When I removed the outlier at attenuation 1.6 m^{-1}, the relationship for both 2006 and 2007 improved to R^2=0.53. Within the basin, I found that many of the outliers were within the upper 20 m, which corresponded to the summer halocline. To examine this relationship, I calculated first the Brunt-Väisälä-frequency as a measurement of stratification (Figure 4.17a) and found that several of the high attenuation, low POC points were located within the highly stratified water of the summer halocline. I suggest these particles are deposited in the surface ocean when sea ice melts and are trapped by the strong stratification. Previous studies have found that, although there is considerable variability, most of the particles in sea ice are inorganic (Pfirman et al. 1989, Dethleff et al. 2000). Thus, the ratio of POC:TSS was calculated to confirm that the outliers within the summer halocline also had high TSS concentrations relative to POC (Figure 4.17b). Although some particles within the summer halocline had a high POC:TSS ratio, much of the variability can be explained by removing all particles that were found in water with a Brunt-Väisälä-frequency greater than 0.001 s^{-1}. The relationship improved to R^2=0.59. Along the Northwind Ridge, I noticed that there were several samples that had low attenuation and high POC concentrations. Upon closer examination, I found that these POC samples had very high blank

values so may have been contaminated in the lab. This contamination would have only affected the three Northwind Ridge stations in 2006. Thus, I decided to base the correlation between POC and attenuation solely on the 2007 relationship. Unlike the stations in the basin, the summer halocline over the Northwind Ridge was not very stratified and there were fewer particles trapped in this layer. This is likely because there was less ice cover here than in the basin region, so there was likely more mixing. Because of this, the POC-attenuation relationship was likely suitable for the entire water column. Along the eastern shelf of the Canada Basin, I found that the high attenuation, low POC outlier occurred within the nepheloid layer at a depth of 500 m. Since the data show that the nepheloid layer along the eastern shelf has low POC concentrations, the nepheloid layer was excluded from the correlation. I defined the eastern shelf nepheloid layer as water within 50 m of the bottom along the slope (with bottom depths between about 250 and 3000 m) that had attenuation higher than 0.43 m^{-1}. Once this outlier was removed, the relationship improved to R^2=0.60.

I have defined one TSS-attenuation relationship and four POC-attenuation relationships that can be applied to attenuation profiles to estimate past TSS and POC concentrations (Table 4.3). Upon comparison of the observed to the estimated TSS and POC values, I found that the root mean square error was very high for both TSS and POC in the western Beaufort shelf. This is likely because despite a good linear correlation, the variable particle composition here did not allow for an accurate estimate of TSS and POC values from transmission. The method error estimates in the Northwind, basin and eastern shelf regions were all within the same order of magnitude

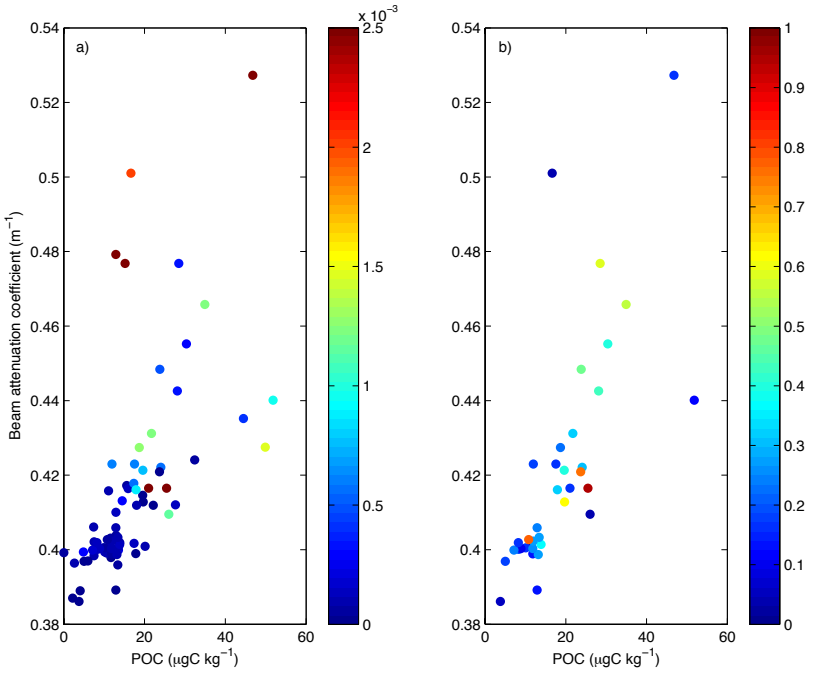

Figure 4.17: Relationship for the stations within the interior of the Canada Basin between a) attenuation and POC with the Brunt-Väisälä-frequency (s^{-1}) in colour and b) attenuation and POC with the ratio of POC to TSS in colour. There are fewer points in plot b) because TSS was sparsely sampled in 2006.

Table 4.3: TSS-attenuation and POC-attenuation statistics for regions that had good relationships (R^2 value greater than 0.50 for all samples) between the bottle and sensor data. The symbols WBS stand for western Beaufort shelf, NWR for Northwind Ridge, CB for the interior of the Canada Basin, ESCB for the eastern shelf of the Canada Basin and BV the Brunt-Väisälä frequency. Units are (μgkg^{-1})m for TSS slope, (μgCkg^{-1})m for POC slope, μgkg^{-1} for TSS intercept and μgCkg^{-1} for POC intercept. Note that the relationships are written in opposite direction to those in Tables 4.1 and 4.2 so that TSS and POC are calculated from beam attenuation coefficient.

Particles	Region	Slope	Intercept	R^2	RMSE	Comments
TSS	WBS	1595	-472	0.75	233	
POC	WBS	188	-55	0.53	33.1	For attenuation < 1.1 m^{-1}
POC	NWR	306	-108	0.59	8.3	
POC	CB	410	-153	0.59	6.1	For water with BV < 0.001 s^{-1}
POC	ESCB	378	-140	0.60	4.1	Not for nepheloid layers

of the average standard error for POC duplicates (4.4 μgCkg^{-1}). These POC estimates are also similar to previous studies. In the summer of 1994, Wheeler et al. (1997) sampled POC along a transect from the Chukchi Sea to the North Pole. They crossed the Canada, Makarov, Amundsen and Nansen Basins and found that there was an average of 4.6 gCm^{-2} in the upper 100 m. These values were almost 5 times greater than the 1 gCm^{-2} that Kinney et al. (1971) and Gordon and Cranford (1985) found in April and May in the Canada Basin. To compare, I also integrated POC each year in the upper 100 m and, estimated that there was 2.1 to 2.6 gCm^{-2} in summer in the Canada Basin.

4.7 Conclusions

As the Arctic Ocean undergoes rapid change, one of the projected transitions is an increase in suspended particle concentrations (Carmack et al.

2006). For this paper, I examined suspended particle concentrations from both sensor (transmissometer and fluorometer) and bottle (POC and TSS) data from the summers of 2003 through 2008 to first locate regions of high attenuation, then to examine interannual variability within those regions, and finally to investigate whether simple linear relationships existed between TSS and attenuation, and POC and attenuation.

To account for spatial variability, I divided my study area into five regions. I observed the highest attenuation, TSS and POC concentrations along the Beaufort shelf. The eastern Beaufort shelf was characterized by high near-surface attenuation and POC and TSS concentrations and the particles were likely from the Mackenzie River. The western Beaufort shelf was more variable, with several attenuation features throughout the water column, including plumes that appeared to transport particles from the shelf up to 150 km north in the Canada Basin. Along the Northwind Ridge and within the Canada Basin, I observed that most of the particles were found above 100 m and were dominated by the subsurface chlorophyll maximum. The eastern shelf was the least productive region and had minimal fluorescence and POC values, however, a nepheloid layer at about 400-900 m suggested the transport of particles from shelf into the Canada Basin.

Common attenuation features within the Canada Basin and its surrounding shelves were placed into six categories. These are i) Particles in surface water; ii) Particles within the summer halocline. These particles are likely transported to the region in ice and deposited as the ice melts; iii) Particles within high fluorescent water; iv) Particles in the salinity range 32.9 to 33.1 that is either PWW or Beaufort shelf-derived winter water. These are likely

transported from the shelf into the basin through canyons or as eddies that are formed along the shelf; v) Particles within Atlantic water in the salinity range 34.4-34.85 that are likely deposited by resuspension due to upwelling or the passage of a boundary current.; and vi) Particles at the bottom that are often found within nepheloid layers.

In the interior of the Canada Basin, I found that the subsurface chlorophyll maximum deepened at a rate of 3.2 m per year from an average depth of 45 m in 2003 to 61 m in 2008. This deepening could be the result of either increased photosynthetically available radiation (caused by the decreased summer sea ice cover) that would support phytoplankton at deeper depths or the deepening of the nutricline. Deeper light absorption would be expected to increase primary productivity while a deeper nutricline would decrease primary productivity. This is an important area of future research as these changes would be expected to have a significant impact on the Arctic Ocean ecosystem.

The annual differences in the average attenuation were calculated. I found that in all regions, most of the variability was above 100 m. In general, the greatest attenuation was observed in the western Beaufort shelf. I found no evidence of increased attenuation from the summers of 2003 through 2008. Instead, there were examples where attenuation appeared to decrease over time - in the surface layer over the Northwind Ridge and in the intermediate layer (that includes the chlorophyll maximum) in both the eastern Beaufort shelf and in the interior of the chlorophyll maximum. These trends were not statistically significant because the standard error was high. I think that this work provides a baseline estimate of attenuation in the Canada Basin

to which future changes can be compared.

One of the main goals of this paper was to find a relationship between attenuation and bottle (POC and TSS) data that could be applied to past transmissometer data. I found that there was no consistent relationship that could be applied to the entire study region so I again analyzed the five regions separately. In the eastern Beaufort shelf, I found that attenuation was not well-correlated with either POC or TSS and suggest that the transmissometer cannot account for the particle variability in terms of both size and density. Along the western Beaufort shelf, both TSS and POC appeared to be well-correlated with attenuation, however, the error measurements were very high and thus not statistically significant. Along the Northwind Ridge, within the basin and on the eastern shelf, POC and attenuation were well-correlated with the following exceptions - i) Within the summer halocline in the interior of the Canada Basin. Here, it appears that both organic and inorganic particles are being trapped in the strong stratification so POC cannot be accurately estimated; ii) Within the bottom nepheloid layer along the eastern shelf. Again, the particles here are primarily inorganic so POC cannot be estimated.

Chapter 5

Conclusions

There are two main properties that make the near-surface waters of polar oceans different from temperate or tropical oceans. The first is that the salinity range is relatively much greater than the temperature range, which, combined with the fact that the thermal expansion coefficient is small at low temperatures, results in salinity having a greater impact on the density structure than temperature. These so-called beta oceans are found poleward of the subpolar front, are permanently stratified by salinity, and have a relatively shallow surface mixed layer above a strong halocline (Carmack 2007). The second main difference between polar and low latitude oceans is that interactions between the atmosphere and ocean are modified by sea ice. These interactions include destabilizing mechanical mixing (in the form of wind stress, tidal energy and surface cooling) and stabilizing surface buoyancy flux (in the form of surface warming and freshwater input). The depth of the surface mixed layer is used as an indicator of the balance of these processes - a deep surface mixed layer implies that mechanical mixing is stronger and a shallow surface mixed layer suggests that the surface buoyancy flux is stronger. Sea ice adds a quasi-permeable barrier between the atmosphere and ocean. It has been found that an ice-covered oceans receive less kinetic

energy from wind stress (Yang 2009) and less stabilizing solar radiation due to the reflectivity of sea ice (Maykut 1986). In addition, the formation of sea ice throughout fall and winter greatly decreases stability (through increased outgoing heat fluxes and brine rejection) while the melting of sea ice in spring and summer increases stabiliity (Maykut 1986).

Interactions between the atmosphere and ocean have largely been studied for either ice-free or ice-covered oceans. For my Ph.D. thesis, I examined changes to the near-surface (upper 100 m) waters of the Canada Basin from 1993-2009. This was a period of rapid change that was largely due to atmospheric and oceanic warming and the resulting sea ice melt. This gave me the unprecedented chance to study the near-surface waters during the transition of a substantial fraction of the Canada Basin from a perennially ice-covered to a seasonally ice-covered ocean.

Changes to the properties of the near-surface waters in the Canada Basin began at the surface. In the 1970s, the depth of the surface mixed layer in the Canada Basin was an average of about 40 m in summer and 50 m in winter (Morison and Smith 1981). Data from 2004-2008 showed that the surface mixed layer had shoaled dramatically since the 1970s to an average depth of just 24 m in winter and at most 16 m in summer (Toole et al. 2010). I suggested that a large input of freshwater from sea ice melt caused the summer halocline to strengthen, which prevented the deepening of the surface mixed layer (Chapter 2). In other words, the near surface waters were stabilized by sea ice melt and this was greater than mechanical mixing from wind stress, outgoing heat fluxes, and brine rejection, so the surface mixed layer shoaled year-round.

Solar radiation warms about the upper 50 m (Figure 2.13), which includes water that is below the surface mixed layer. The transfer of heat fluxes between the ocean, ice and atmosphere moderate the temperature of the surface mixed layer. The water below the mixed layer is not in direct contact with the atmosphere and partial ice cover so solar radiation is essentially trapped below the summer halocline. This forms a temperature maximum that I call the near-surface temperature maximum or NSTM (Chapter 2). The loss of sea ice has allowed more stabilizing solar radiation to enter the ocean (Perovich et al. 2007) and the shoaling of the surface mixed layer has trapped even more heat as the NSTM. From 1993-2009, the NSTM warmed, freshened, expanded northwards and formed at successively shallower depths (Chapters 2 and 3). The NSTM was first observed year-round during the winter of 2007-2008 and I suggest that this is because the strengthened summer halocline (from increased sea ice melt) could not be eroded in winter so that solar radiation was stored throughout the year as the NSTM (Chapter 2). It is likely that the NSTM would be more persistent in stations located inside the anticyclonic Beaufort Gyre and this is because downwelling (at a rate of about 29 m per year, Yang 2006) further isolates the NSTM from surface processes (Chapter 2). In addition, the NSTM was fresher at stations inside of the Beaufort Gyre and this is because freshwater is accumulated within the gyre so the NSTM was formed in fresher waters than outside the gyre (Chapter 3). The year-round presence of the NSTM is a unique example of how a change in the sea ice cover can alter near-surface waters below the surface mixed layer.

Below the NSTM is a temperature minimum that I call the remnant of

the previous winter's surface mixed layer or rML (Chapters 2 and 3). The NSTM forms in the upper about 30 m (Figures 2.3 - 2.6) - first as a warmed surface mixed layer and then as a temperature maximum as the summer halocline isolates the NSTM beneath the surface mixed layer. When the winter surface mixed layer is deeper than about 30 m, a remnant of the previous winter's mixed layer remains trapped as a temperature minimum below the NSTM. This rML should have similar properties to the previous winter's mixed layer (i.e. be relatively cold and fresh). From 1993-2008, I found that the rML warmed by about 0.5°C and freshened by about 2 salinity units (Chapter 3). Using a 1-D model of heat diffusion, I found that heat from both the NSTM and Pacific Summer Water (PSW) is diffused to the rML at a diffusion rate of about $3x10^{-6}$ m^2s^{-1}(Chapter 3). Before 2006, more heat from PSW was diffused to the rML but since 2006, the warming NSTM began to transfer more heat to the rML. The freshening of the rML can be explained by sea ice melt. Stations that were located inside the Beaufort Gyre were fresher than those outside of the gyre and this can be attributed to downwelling and subsequent accumulation of freshwater within the gyre.

Pacific Summer Water (PSW) forms a temperature maximum at a depth of about 40-80 m in the Canada Basin (Coachman and Barnes 1961). The source of PSW is Pacific-origin water that is modified in the Chukchi Sea during summer, thus is warmer (temperature up to 1°C) and fresher (salinity 31-32) than water that is modified in the winter (Coachman and Barnes 1961). Several recent papers have suggested that heat transferred to the surface from warming PSW could explain why sea ice is melting faster in

the Canada Basin than in other parts of the Arctic Ocean (Shimada et al. 2006, Watanabe and Hasumi 2009, Woodgate et al. 2010). Using mooring data located in Bering Strait, I examined the Pacific-origin source of PSW to determine whether it changed over my study period. I found that there were no obvious warming or freshening trends and concluded that changes to PSW could not explain changes to the NSTM or rML (Chapter 3). In addition, by comparing the Bering Strait data to CTD data near the southern Northwind Ridge, I found that the primary source of PSW is from the Alaskan Coastal Current water and that it takes about 2 years for PSW to travel from Bering Strait to the southern Northwind Ridge. Once in the basin, there was evidence of interannual variation in transport time of PSW (faster transport from 2003-2004 and slower from 2005-2006), however there was little evidence of a systematic change in the velocity or pathway of PSW during my study period.

How will this warming and freshening effect primary productivity in the Canada Basin? Phytoplankton are limited by light and nutrients so on the one hand, the reduced sea ice cover allows light to penetrate deeper into the water column and on the other hand, the increased stratification from sea ice melt limits mixing and nutrient replenishment in the euphotic zone. Carmack et al. (2006) suggested that climate change will likely increase suspended particle concentrations in the Arctic Ocean due to increased coastal erosion, upwelling and river runoff - all processes that would likely have a greater impact on Arctic shelves. Based on transmissometer data from 2003-2008, I found no evidence of increased attenuation and my data even suggested that attenuation decreased in some regions (Chapter 4). I did not

look at data from before 2000 so could not examine attenuation before the rapid warming of the past decade. In the interior of the Canada Basin, I found that the average depth of the chlorophyll maximum deepened by 16 m from 2003 to 2008 and this could be caused by either by a deepening of the euphotic zone or by a deepening of the nutricline. During the same period, the nutrient-rich PSW (Jones and Anderson 1986) also appeared to deepen, particularly at stations that were located within the Beaufort Gyre (Chapter 3), and this implies that the nutricline is descending. If the nutricline continues to deepen then even less light will be available for phytoplankton and primary production in the Canada Basin will decrease. The deepening of the chlorophyll maximum likely explains the shift from a foodweb that is based primarily on nanoplankton to one that is dominated by picoplankton (Li et al. 2009). This is an example of how changes to the near-surface water mass structure from climate warming has impacted the Arctic Ocean ecosystem.

During my study period from 1993-2009, the sea ice cover of the southern Canada Basin was drastically reduced from being perennially ice-covered in 1993 to almost ice-free in the summers of 2007-2009 (Figure 3.4). During this time, I witnessed the rapid warming of the NSTM and rML and by 2009, three temperature maxima and two temperature minima were present. My heat diffusion model suggests that by the summer of 2010, all of these features will merge into one temperature maximum. This prediction was confirmed by data from ITP33 (not shown). Is this one temperature maximum the end state of the transition of Canada Basin's near-surface water mass structure? Will this temperature maximum continue to warm as sum-

mer sea ice melt traps and then stores solar radiation? Will heat from this temperature maximum melt ice throughout winter? How will these changes affect primary production and the ecosystem structure of the Canada Basin? These questions and many more are sure to arise as the Canada Basin continues its transition to a seasonally ice-free ocean.

Bibliography

K. Aagaard and A.T. Roach "Arctic-Ocean shelf exchange: Measurements in Barrow Canyon" *Journal of Geophysical Research,* **95,** C10, 18163-18175. (1990).

K. Aagaard, J.H. Swift, and E.C. Carmack "Thermohaline circulation in the Arctic mediterranean seas" *Journal of Geophysical Research,* **90,** C3, 4833-4846. (1985).

N.S.R. Agawin, C.M. Duarte, and S. Agusti "Nutrient and Temperature Control of the Contribution of Picoplankton to Phytoplankton Biomass and Production" *Limnology and Oceanography,* **45,** 3, 591-600. (2000).

M.B. Alkire and J.H. Trefry "Transport of spring floodwater from rivers under ice to the Alaskan Beaufort Sea" *Journal of Geophysical Research,* **111,** C12008, doi:10.1029/2005JC003446. (2006).

D.S. Arndt, M.O. Baringer, and M.R. Johnson "State of the Climate in 2009" *Bulletin of the American Meteorological Society,* **91,** 7, s1-s222. (2010).

K.R. Arrigo, G. van Dijken, and S. Pabi "Impact of a shrinking Arctic ice

cover on marine primary productiion" *Geophysical Research Letters,* **35,** 19, L19603, doi:10.1029/2008GL035028. (2008).

C.J. Ashjian, S.M. Gallager, and S."Transport of plankton and particles between the Chukchi and Beaufort Seas during summer 2002, described using a Video Plankton Recorder" *Deep-Sea Research II,* **52,** 3259-3280. (2005).

E.T. Baker, J.W. Lavelle "The effect of particle size on the the light attenuation coefficient of natural suspensions" Journal of Geophysical Research, **89,** 8179-8203. (1984).

R.T. Barber "Picoplankton Do Some Heavy Lifting" *Science,* **315,** 5813, 777-778. (2007).

N.R. Bates, D.A. Hansell, S.B. Moran, and L.A. Codispoti "Seasonal and spatial distribution of particulate organic matter (POM) in the Chukchi and Beaufort Seas" *Deep-Sea Research II,* **52,** 3324-3343. (2005).

J.K.B. Bishop "The correction and suspended particulate matter calibration of Sea Tech transmissometer data" *Deep-Sea Research,* **33,** 1, 121-134. (1986).

J.K.B. Bishop "Transmissometer measurement of POC" *Deep-Sea Research I,* **46,** 353-369. (1999).

J.K.B. Bishop, S.E. Calvert, and M.Y.S. Soon "Spatial and temporal variability of POC in the northeast Subarctic Pacific" *Deep-Sea Research II,* **46,** 2699-2733. (1999).

E. Boss, M.S. Twardowski, and S. Herring "Shape of the particulate beam attenuation spectrum and its inversion to obtain the shape of the particulate size distribution" *Applied Optics,* **40,** 4885-4893. (2001).

D.G. Bowers, K.M. Braithwaite,W.A.M. Nimmo-Smith, and G.W. Graham "Light scattering by particles suspended in the sea: The role of particle size and density" *Continental-Shelf Research,* **29,** 1748-1755. (2009).

V.I. Burenkov "Optical properties of the Laptev Sea near the Lena River delta" *Underwater Light Measurements,* **2048,** Eilertsen, H.C. (Ed.), The Society of Photo-Optical Instrumentation Engineers Proceedings Series, Bellingham Washington, USA, 175-183. (1993).

W.-J. Cai, L. Chen, Z. Gao, S.H. Lee, J. Chen, D. Pierrot, K. Sullivan, Y. Wang, X. Hu, W.-J. Huang, Y. Zhang, S. Xu, A. Murata, J.M. Grebmeier, E.P. Jones, and H. Zheng "Decrease in the CO_2 uptake capacity in an ice-free Arctic Ocean basin" *Science,* **329,** 556-559. (2010).

E.C. Carmack "The alpha/beta ocean distinction: A perspective on freshwater fluxes, convection, nutrients and productivity in high-latitude seas" *Deep-Sea Research II,* **54,** 2578-2598. (2007).

E. Carmack, and P. Wassmann "Food webs and physical-biological coupling on pan-Arctic shelves: Unifying concepts and comprehensive perspectives" *Progress in Oceanography,* **71,** 446-477. (2006).

E. Carmack, D. Barber, J. Christensen, R. Macdonald, B. Rudels, and E. Sakshaug "Climate variability and physical forcing of the food webs and

the carbon budget on panarctic shelves" *Progress in Oceanography,* **71,** 145-181. (2006).

D. Cavalieri, C. Parkinson, P. Gloersen and H. J. Zwally. "Sea ice concentrations from Nimbus-7 SMMR and DMSP SSM/I passive microwave data, [1993, 1997, 2002-7]". Boulder, Colorado USA: National Snow and Ice Data Center. Digital media. (1996, updated 2008).

M. Chen, Y. Huang, P. Cai, and L. Guo "Particulate Organic Carbon Export Fluxes in the Canada Basin and Bering Sea as Derived from $^{234}Th/^{238}U$ Disequilibria" *Arctic,* **56(1),** 32-44. (2003).

L.K. Coachman "On the flow field in the Chirikov Basin" *Continental Shelf Research,* **13,** 481-508. (1993).

L.K. Coachman and C.A. Barnes "The contribution of Bering Sea water to the Arctic Ocean" *Arctic,* **14,** 146-161 (1961).

L.K. Coachman, K. Aagaard,and R. B. Tripp *Bering Strait: The Regional Physical Oceanography,* 72 pp., University of Washington Press, Seattle. (1975).

L.A. Codispoti, C. Flagg, V. Kelly, and J.H. Swift "Hydrographic conditions during the 2002 SBI process experiments" *Deep-Sea Research I,* **52,** 3199-3226. (2005).

J.C. Comiso, C.L. Parkinson, R. Green and L. Stock "Accelerated decline in the Arctic sea ice cover" *Geophysical Research Letters,* **35,** L01703, doi:10.1029/2007GL031972 (2008).

D.A. Darby "Sources of sediment found in sea ice from the western Arctic Ocean, new insights into processes of entrainment and drift patterns" *Journal of Geophysical Research,* **108,** C8, 3257, doi:10.1029/2002JC001350. (2003).

E. D'Asaro "Observations of Small Eddies in the Beaufort Sea" *Journal of Geophysical Research,* **93,** C6, 6669-6684. (1988).

D. Dethleff, V. Rachold, M. Tintelnot, and M. Antonow "Sea-ice transport of riverine particles from the Laptev Sea to Fram Strait based on clay mineral studies" *International Journal of Earth Sciences,* **89,** 496-502. (2000).

K.H. Dunton, T. Weingartner, and E.C. Carmack "The nearshore western Beaufort Sea ecosystem: Circulation and importance of terrestrial carbon in arctic coastal food webs" *Progress in Oceanography,* **71,** 362-378. (2006).

W.D. Gardner "Incomplete extraction of rapidly settling particles from water samplers" *Limnology and Oceanography,* **22,** 764-768. (1977).

W.D. Gardner, P.E. Biscaye, J.R.V. Zaneveld, and M.J. Richardson "Calibration and comparison of the LDGO nephelometer and the OSU transmissometer on the Nova Scotian Rise" *Marine Geology,* **66,** 323-344. (1985).

W.D. Gardner, M.J. Richardson, C.A. Carlson, D. Hansell, and A.V. Mishonov "Determining true particulate organic carbon: bottles, pumps and methodologies" *Deep-Sea Research II,* **50,** 655-674. (2003).

A. Gargett "Differential diffusion: an oceanographic primer" *Progress in Oceanography,* **56 (3-4),** 559-570. (2003).

A.E. Gill "Properties of Seawater" *Atmosphere-Ocean Dynamics,* 599-603, Academic Press, New York, USA (1982).

D.C. Gordon and P.J. Cranford "Detailed distribution of dissolved and particulate organic matter in the Arctic Ocean and comparison with other ocean regions" *Deep-Sea Research,* **32,** 10, 1221-1232. (1985).

J.M. Grebmeier, L.W. Cooper, H.M. Feder, and B.I. Sirenko "Ecosystem dynamics of the Pacific-influenced Northern Bering and Chukchi Seas in the Amerasian Arctic" *Progress in Oceanography,* **71,** 331-361. (2006a).

J.M. Grebmeier, J.E. Overland, S.E. Moore, E.V. Farley, E.C. Carmack, L.W. Cooper, K.E. Frey, J.H. Helle, F.A. McLaughlin, and S.L. McNutt "A major ecosystem shift in the northern Bering Sea" *Science,* **311,** 1461-1464. (2006b).

C.K.H. Guay, F.A. McLaughlin, and M. Yamamoto-Kawai "Differentiating fluvial components of upper Canada Basin waters on the basis of measurements of dissolved barium combined with other physical and chemical tracers" *Journal of Geophysical Research,* **114,** C00A09, doi:10.1029/2008JC005099. (2009).

K. Hunkins, E.M. Thorndike, and G. Mathieu "Nepheloid Layers and Bottom Currents in the Arctic Ocean" *Journal of Geophysical Research,* **74,** 28, 6995-7008. (1969).

J.M. Jackson, P.G. Myers, and D. Ianson "An examination of mixed layer sensitivity in the Northeast Pacific Ocean from July 2001 - July 2005 using the General Ocean Turbulence Model and Argo data" *Atmosphere-Ocean,* **47,** 139-153. (2009).

A. Jahn, B. Tremblay, L.A. Mysak, and R. Newton "Effect of the large-scale atmospheric circulation on the variability of the Arctic Ocean freshwater transport" *Climate Dynamics,* **34 (2-3),** 201-222. (2010a).

M. Jakobsson "Hypsometry and volume of the Arctic Ocean and its constituent seas" *Geochemistry, geophysics and geosystems,* **3,** 5, doi:10.1029/2001GC000302. (2002).

E.P. Jones and L.G. Anderson "On the origin of the chemical properties of the Arctic Ocean halocline" *Journal of Geophysical Research,* **91,** C9, 10759-10767. (1986).

E.P. Jones, L.G. Anderson, and J.H. Swift "Distribution of Atlantic and Pacific waters in the upper Arctic Ocean: Implications for circulation" *Geophysical Research Letters,* **25,** 6, 765-768. (1998).

D. Kadko "Modeling the evolution of the Arctic mixed layer during the fall 1997 Surface Heat Budget of the Arctic Ocean (SHEBA) Project using measurements of ^{7}Be" *Journal of Geophysical Research,* **105,** C2, 3369-3378 (2000).

D. Kadko and P. Swart "The source of the high heat and freshwater content of the upper ocean at the SHEBA site in the Beaufort Sea in 1997" *Journal of Geophysical Research,* **109,** C01022, doi:10.1029/2002JC001734 (2004).

E. Kalnay, M. Kanamitsu, R. Kistler, W. Collins, D. Deaven, L. Gandin, M. Iredell, S. Saha, G. White, J. Woollen, Y. Zhu, A. Leetmaa, B. Reynolds, M. Chelliah, W. Ebisusaki, W. Higgins, J. Janowiak, K.C. Mo, C. Ropelewski, J. Wang, R. Jenne and D. Joseph "The NCEP/NCAR 40-Year Reanalysis Project" *Bulletin of the American Meteorological Society,* **77**, 3, 437-471 (1996).

P.J. Kinney, T.C. Loder, J. and Groves "Particulate and dissolved organic matter in the Amerasian Basin of the Arctic Ocean" *Limnology and Oceanography,* **16,** 132-137. (1971).

J.C. Kitchen, J.R.V. Zaneveld, and H. Pak "Effect of particle size distribution and chlorophyll content on beam attenuation spectra" *Applied Optics,* **21,** 3913-3918. (1982).

R. Krishfield, J. Toole, A. Proshutinsky and M.-L. Timmermans "Automated Ice-Tethered Profilers for Seawater Observations under Pack Ice in All Seasons"*Journal of Atmospheric and Oceanic Technology,* **25,** 11, 2091-2105 (2008).

C. Lalande, A. Forest, D.G. Barber, Y. Gratton, and L. Fortier, "Variability in the annual cycle of vertical particulate organic carbon export on the Arctic shelves: Contrasting the Laptev Sea, Northern Baffin Bay and the Beaufort Sea" *Continental Shelf Research,* **29,** 2157-2165. (2009).

D. Lavoie, K.L. Denman, and R.W. Macdonald "Effects of future climate change on primary productivity and export fluxes in

the Beaufort Sea" *Journal of Geophysical Research,* **115,** C04018, doi:10.1029/2009JC005493. (2010).

S.H. Lee and T.E. Whitledge " Primary and new production in the deep Canada Basin during summer 2002" *Polar Biology,***28,** 190-197, doi:10.1007/s003000-004-0676-3. (2005).

W.K.W. Li, F.A. McLaughlin, C. Lovejoy, and E.C. Carmack "Smallest algae thrive as the Arctic Ocean freshens" *Science,* **326,** 539. (2009).

B. Light, T. C. Grenfell, D. K. Perovich "Transmission and absorption of solar radiation by Arctic sea ice during the melt season" *Journal of Geophysical Research,* **113,** C03023, doi:10.1029/2006JC003977 (2008).

R.W. Macdonald, D.W. Paton, E.C. Carmack, and A. Omstedt "The freshwater budget and under-ice spreading of Mackenzie River water in the Canadian Beaufort Sea based on salinity and $^{18}O/^{16}O$ measurements in water and ice" *Journal of Geophysical Research,* **100,** C1, 895-919. (1995).

R.W. Macdonald, M. O'Brien, E.C. Carmack, R. Pearson, F.A. McLaughlin, D. Sieberg, J. Barwell-Clarke, D.W. Paton, D. Tuele "Physical and chemical data collected in the Beaufort, Chukchi and east Siberian seas, August-September 1993" *Canadian data report of hydrography and ocean sciences,* **139,** 287 pp. (1995).

R.W. Macdonald, S.M. Solomon, R.E. Cranston, H.E. Welch, M.B. Yunker, and C. Gobeil "A sediment and organic carbon budget for the Canadian Beaufort Shelf" *Marine Geology,* **144,** 255-273. (1998).

R.W. Macdonald, E.C. Carmack, F.A. McLaughlin, K.K. Falkner, and J.H. Swift "Connections among ice, runoff and atmospheric forcing in the Beaufort Gyre" *Geophysical Research Letters,* **26,** 15, 2223-2226. (1999).

R.W. Macdonald, F.A. McLaughlin, and E.C. Carmack "Fresh water and its sources during the SHEBA drift in the Canada Basin of the Arctic Ocean" *Deep-Sea Research I,* **49,** 1769-1785 (2002).

T. Markus, J. C. Stroeve, and J. Miller "Recent changes in Arctic sea ice melt onset, freezeup, and melt season length" *Journal of Geophysical Research,* **114,** C12024, doi:10.1029/2009JC005436.

J. Matrin, J.-E. Tremblay, J. Gagnon, G. Tremblay, A. Lapoussire, C. Jose, M. Poulin, M. Gosselin, Y. Gratton, and C. Michel "Prevalence, structure and properties of subsurface chlorophyll maxima in Canadian Arctic waters" *Marine Ecology Progress Series,* **412,** 69-84, doi: 10.3354/meps08666. (2010).

J. Maslanik, and J. Stroeve. "Near-Real-Time DMSP SSM/I Daily Polar Gridded Sea Ice Concentrations, [list dates of data used]". Boulder, Colorado USA: National Snow and Ice Data Center. Digital media. (1999, updated daily).

J.A. Maslanik, C. Fowler, J. Stroeve, S. Drobot, J. Zwally, D. Yi, and W. Emery "A younger, thinner Arctic ice cover: Increased potential for rapid, extensive sea-ice loss" *Geophysical Research Letters,* **34,** L24501, doi:10.1029/2007GL032043. (2007).

J.T. Mathis, R.S. Pickart, D.A Hansell, D. Kadko, and N.R. Bates "Eddy transport of organic carbon and nutrients from the Chukchi Shelf: Impact on the upper halocline of the western Arctic Ocean" *Journal of Geophysical Research,* **112,** C05011, doi:10.1029/2006JC003899. (2007).

G.A. Maykut "The surface heat and mass balance" in *The Geophysics of Sea Ice,* **146,** N. Untersteiner, NATO ASI Series, Plenum Press, New York, 395-459. (1986).

G.A. Maykut and M.G. McPhee "Solar heating of the Arctic mixed layer" *Journal of Geophysical Research,* **100,** C12, 24691-2470. (1995).

F. McLaughlin, E. Carmack, R. Macdonald, A.J. Weaver, and J. Smith "The Canada Basin, 19891995: Upstream events and far-field effects of the Barents Sea" *Journal of Geophysical Research,* **107,** C7, 3082, doi:10.1029/2001JC000904. (2002).

F.A. McLaughlin, E.C. Carmack, R.G. Ingram, W.J. Williams, and C. Michel "Oceanography of the Northwest Passage" in *The Sea,* **14,** eds. A.R. Robinson and K.H. Brink, ??. (2006).

F. McLaughlin, K. Shimada, E. Carmack, M. Itoh, and S. Nishino "The hydrography of the southern Canada Basin, 2002" *Polar Biology,* **28,** 182-189. (2005).

F.A. McLaughlin, E.C. Carmack, S. Zimmerman, D. Sieberg, L.White, J. Barwell-Clarke, M. Steel and W.K.W. Li "Physical and chemical data from the Canada Basin, August 4-16 2004" *Can. Data Rep. Hydrogr. Ocean. Sci,* **140,** 185p (2008).

F.A. McLaughlin, E.C. Carmack, W.J. Williams, S. ZImmerman, K. Shimada, and M. Itoh "Joint effects of boundary currents and thermohaline intrusions on the warming of Atlantic water in the Canada Basin, 19932007" *Journal of Geophysical Research,* **114,** C00A12, doi:10.1029/2008JC005001. (2009).

M.G. McPhee, T.P. Stanton, J.H. Morison and D.G. Martinson "Freshening of the upper ocean in the Arctic: Is perennial sea ice disappearing?" *Geophysical Research Letters,* **25,** 10, 1729-1732. (1998).

M.G. McPhee, A. Proshutinsky, J.H. Morison, M. Steele and M.B. Alkire "Rapid change in freshwater content of the Arctic Ocean" *Geophysical Research Letters,* **36,** L10602, doi:10.1029/2009GL037525. (2009).

H. Melling and E.L. Lewis "Shelf drainage flows in the Beaufort Sea and their effect on the Arctic Ocean pycnocline" *Deep Sea Research,* **29,** 8A, 967-985. (1982).

G.H. Miller, J. Brigham-Grette, R.B. Alley, L. Anderson, H.A. Bauch, M.S.V. Douglas, M.E. Edwards, S.A. Elias, B.P. Finney, J.J. Fitzpatrick, S.V. Funder, T.D. Herbert, L.D. Hinzman, D.S. Kaufman, G.M. MacDonald, L. Polyak, A. Robock, M.C. Serreze, J.P. Smol, R. Spielhagen, J.W.C. White, A.P. Wolfe and E.W. Wolff "Temperature and precipitation history of the Arctic" *Quaternary Science Reviews,* **29 (15-16),** 1679-1715. (2010).

G. H. Miller, R. B. Alley, J. Brigham-Grette, J.J. Fitzpatrick, L. Polyak, M.C. Serreze and J.W.C. White "Arctic amplification: can the past con-

strain the future?" *Quaternary Science Reviews,* **29 (15-16),** 1779-1790. (2010).

J. Morison and J.D. Smith "Seasonal variations in the upper Arctic Ocean as observed at T-3" *Geophysical Research Letters,* **8,** 7, 753-756. (1981).

R.P, Mulligan, W. Perrie, and S. Soloman "Dynamics of the Mackenzie River plume on the inner Beaufort shelf during an open water period in summer" *Estuarine, Coastal and Shelf Science,* **89,** 3, 214-220. (2010).

A. Munchow and E.C. Carmack "Synoptic flow and density observations near and Arctic shelf break" *Journal of Physical Oceanography,* **27,** 1402-1419. (1997).

A. Nikolopoulos, R.S. Pickart, P.S. Fratantoni, K. Shimada, D.J. Torres, and E.P. Jones "The western Arctic boundary current at 152°W: Structure, variability and transport" *Deep Sea Research II,* **56,** 1164-1181. (2009).

S. Nishino, M. Itoh, M. Yamamoto-Kawai, and S. Chiba "East-west differences in water mass, nutrient, and chlorophyll *a* distributions in the sea ice reduction region of the western Arctic Ocean" *Journal of Geophysical Research,* **113,** C00A01, doi:10.1029/2007JC004666. (2008).

M.C. O'Brien, R.W Macdonald, H. Melling, and K. Iseki "Particle fluxes and geochemistry on the Canadian Beaufort Shelf: Implications for sediment transport and deposition" *Continental Shelf Research,* **26,** 41-81. (2006).

S.R. Okkonen, C.J. Ashjian, R.G. Campbell, W. Maslowski, J.L. Clement-Kinney, and R. Potter "Intrusion of warm Bering/Chukchi waters onto

the shelf in the western Beaufort Sea" *Journal of Geophysical Research,* **114,** C00A11, doi:10.1029/2008JC004870. (2009).

M. Ogi and J.M. Wallace "Summer minimum Arctic sea ice extent and the associated summer atmospheric circulation" *Geophysical Research Letters,* **34,** L12705, doi:10.1029/2007GL029897. (2007).

J.E. Overland "Meteorology of the Beaufort Sea" *Journal of Geophysical Research,* **114,** C00A07, doi:10.1029/2008JC004861. (2009).

J.E. Overland, M. Wang and S. Salo " The recent Arctic warm period" *Tellus, Series A,*, **60,** 589-597. (2008).

G. Panteleev, D. A. Nechaev, A. Proshutinsky, R. Woodgate, and J. Zhang "Reconstruction and analysis of the Chukchi Sea circulation in 19901991" *Journal of Geophysical Research,* **115,** C08023, doi:10.1029/2009JC005453. (2010).

C.L. Parkinson, D.J. Cavalieri, P. Gloersen, H.J. Zwally and J.C. Comiso "Arctic sea ice extents, areas, and trends, 1978-1996" *Journal of Geophysical Research,* **104,** C9, 20 837 - 20 856. (1999).

W.S. Pegau "Inherent optical properties of the central Arctic surface waters" *Journal of Geophysical Research,* **107,** C10, doi:10.1029/2000JC000382. (2002).

D.K. Perovich, B. Light, H. Eicken, K.F. Jones, K. Runciman and S.V. Nghiem "Increasing solar heating of the Arctic Ocean and adjacent seas,

1979-2005: Attribution and role in the ice-albedo feedback" *Geophysical Research Letters,* **34,** L19505, doi:10.1029/2007GL031480. (2007).

D.K. Perovich, J.A. Richter-Menge, K.F. Jones and B. Light "Sunlight, water, and ice: Extreme Arctic sea ice melt during the summer of 2007" *Geophysical Research Letters,* **35,** L11501, doi:10.1029/2008GL034007. (2008).

S. Pfirman, J.C. Gascard, I. Wollenburg, P. Mudie, and A. Abelmann "Particle-laden Eurasian Arctic sea ice: observations from July and August 1987" *Polar Research,* **7,** 59-66. (1989).

R.S. Pickart "Shelfbreak circulation in the Alaskan Beaufort Sea: Mean structure and variability" *Journal of Geophysical Research,* **109,** C04024, doi:10.1029/2003JC001912. (2004).

R.S. Pickart, W.K. Moore, D.J. Torres, P.S. Fratantoni, R.A. Goldsmith, and J. Yang "Upwelling on the continental slope of the Alaskan Beaufort Sea: Storms, ice, and oceanographic response" *Journal of Geophysical Research,* **114,** C00A13, doi:10.1029/2008JC005009. (2009).

L. Polyak, R. B. Alley, J.T. Andrews, J. Brigham-Grette, T.M. Cronin, D.A. Darby, A.S. Dyke, J.J. Fitzpatrick, S. Funder, M. Holland, A.E. Jennings, G.H. Miller, M. O'Regan, J. Savelle, M. Serreze, K. St. John, J.W.C. White and E. Wolff "History of sea ice in the Arctic" *Quaternary Science Reviews,* **29 (15-16),** 1757-1778. (2010).

A.Y. Proshutinksy and M. Johnson "Two circulation regimes of the wind

driven Arctic Ocean" *Journal of Geophysical Research,* **102,** 12,493-12,514. (1997).

A. Proshutinsky, R.H. Bourke, and F.A. McLaughlin "The role of the Beaufort Gyre in Arctic climate variability: Seasonal to decadal climate scales" *Geophysical Research Letters,* **29,** 23, 2100, doi:/10.1029/2002GL015847. (2002).

A. Proshutinsky, R. Krishfield, M-L. Timmermans, J. Toole, E. Carmack, F. McLaughlin, W.J. Williams, S. Zimmerman, M. Itoh, and K. Shimada "Beaufort Gyre freshwater reservoir: State and variability from observations" *Journal of Geophysical Research,***114,** C00A10, doi:10.1029/2008JC005104. (2009).

D.A. Rothrock, Y. Yu, and G.A. Maykut "Thinning of the Arctic sea-ice cover" *Geophysical Research Letters,* **26,** 23, 3469-3472. (1999).

B. Rudels, L.G. Anderson, and E.P. Jones "Formation and evolution of the surface mixed layer and halocline of the Arctic Ocean" *Journal of Geophysical Research,* **101,** C4, 8807-8821. (1996).

M.C. Serreze, J.A. Maslanik, T.A. Scambos, F. Fetterer, J. Stroeve, K. Knowles, C. Fowler, S. Drobot, R.G. Barry, and T.M. Haran "A record minimum arctic sea ice extent and area in 2002" *Geophysical Research Letters,* **30,** 3, 1110, doi:10.1029/2002GL016406. (2003).

M.C. Serreze, M.M. Holland and J. Stroeve"Perspectices on the Arctic's Shrinking Sea-Ice Cover" *Science,* **315,** 1533, doi: 10.1126/science.1139426. (2007).

K. Shimada K., E.C. Carmack, K. Hatakeyama and T. Takizawa "Varieties of Shallow Temperature Maximum Waters in the Western Canadian Basin of the Arctic Ocean" *Geophysical Research Letters,* **28,** 18, 3441-3444. (2001).

K. Shimada K., M. Itoh, S. Nishino, F. McLaughlin, E. Carmack, and A. Proshutinsky "Halocline structure in the Canada Basin of the Arctic Ocean" *Geophysical Research Letters,* **32,** L03605, doi:10.1029/2004GL021358. (2005).

K. Shimada, T. Kamoshida, M. Itoh, S. Nishino, E. Carmack, F. McLaughlin, S. Zimmerman and A. Proshutinsky "Pacific Ocean inflow: Influence on catastrophic reduction of sea ice cover in the Arctic Ocean" *Geophysical Research Letters,* **33,** L08605, doi:10.1029/2005GL025624. (2006).

M. Steele, J. Morison, W. Ermold, I. Rigor, M. Ortmeyer and K. Shimada "Circulation of summer Pacific halocline water in the Arctic Ocean" *Journal of Geophysical Research,* **109,** C02027, doi:10.1029/2003JC002009. (2004).

M. Steele, W. Ermold and J. Zhang "Arctic Ocean surface warming trends over the past 100 years" *Geophysical Research Letters,* **35,** L02614, doi:10.1029/2007GL031651. (2008).

M. Steele, J. Zhang, and W. Ermold "Mechanisms of summertime upper Arctic Ocean warming and the effect on sea ice melt" *Journal of Geophysical Research,* in press. (2010).

J. Stroeve, M.M. Holland, W. Meier, T. Scambos, and M. Serreze "Arctic sea ice decline: Faster than forecast" *Geophysical Research Letters,* **34,** L09501, doi:10.1029/2007GL029703. (2007).

M.-L. Timmermans and C. Garrett "Evolution of the Deep Water in the Canadian Basin in the Arctic Ocean" *Journal of Physical Oceanography,* **36,** 866-874. (2006).

J. Toole, R. Krishfield, A. Proshutinsky, C. Ashjian, K. Doherty, D. Frye, T. Hammar, J. Kemp, D. Peters, M.-L. Timmermans, K. von der Heydt, G. Packard and T. Shanahan "Ice Tethered-Profilers Sample the Upper Arctic Ocean" *EOS, Transactions of the American Geophysical Union,* **87,** 41, 434, 438 . (2006).

J.M. Toole, M.-L. Timmermans, D. K. Perovich, R. A. Krishfield, A. Proshutinsky, and J. A. Richter-Menge "Influences of the Ocean Surface Mixed Layer and Thermohaline Stratification on Arctic Sea Ice in the Central Canada Basin" *Journal of Geophysical Research,* doi:10.1029/2009JC005660. in press.

J.-. Tremblay, Y. Gratton, E. C. Carmack, C. D. Payne, and N. M. Price "Impact of the large-scale Arctic circulation and the North Water Polynya on nutrient inventories in Baffin Bay" *Journal of Geophysical. Research,* **107,** C8, 3112, doi:10.1029/2000JC000595. (2002).

J.-E. Tremblay, K. Simpson, J. Martin, L. Miller, Y. Gratton, and N.M. Price "Vertical stability and the annual dynamics of nutrients and chloro-

phyll fluorescence in the coastal, southeast Beaufort Sea" *Journal of Geophysical Research,* **113,** C07S90, doi:10.1029/2007JC004547. (2008).

Unesco "Background papers and supporting data on the Practical Salinity Scale 1978" *Unesco Technical Papers in Marine Science,* **37,** 144 pp. (1981b).

E. Watanabe and H. Haumi "Pacific water transport in the western Arctic Ocean simulated by an eddy-resolving coupled sea ice-ocean model" *Journal of Physical Oceanography,* **39,** 2194-2211. (2009).

T.J. Weingartner, D.J. Cavalieri, K. Aagaard, and Y. Sasaki "Circulation, dense water formation, and outflow on the northeast Chukchi shelf" *Journal of Geophysical Research,* **103,** C4, 7647-7661. (1998).

T. Weingartner, K. Aagaard, R. Woodgate, S. Danielson, Y. Sasaki, and D. Cavalieri "Circulation on the north central Chukchi Sea shelf" *Deep-Sea Research II,* **52,** 3150-3174. (2005).

P.A. Wheeler, M. Gosselin, E. Sherr, D. Thibault, D.L. Kirchman, R. Benner, and T.E. Whitledge "Active cycling of organic carbon in the central Arctic Ocean" *Nature,* **380,** 697-699. (1996).

P.A. Wheeler, J.M. Watkins, and R.L. Hansing "Nutrients, organic carbon and organic nitrogen in the upper water column of the Arctic Ocean: implications for the sources of dissolved organic carbon" *Deep-Sea Research II,* **44(8),** 1571-1592. (1997).

J.W.C. White, R.B. Alley, J. Brigham-Grette, J.J. Fitzpatrick, A.E. Jen-

nings, S.J. Johnsen, G.H. Miller, R.S. Nerem and L. Polyak "Past rates of climate change in the Arctic" *Quaternary Science Reviews,* **29 (15-16),** 1716-1727. (2010).

W.J. Williams, E.C. Carmack, K. Shimada, H. Melling, K. Aagaard, R.W. Macdonald, and R.G. Ingram "Joint effects of wind and ice motion in forcing upwelling in Mackenzie Trough, Beaufort Sea" *Continental Shelf Research, 26,* 2352-2366. (2006).

P. Winsor and D.C. Chapman "Pathways of Pacific water across the Chukchi Sea: A numerical model study" *Journal of Geophysical Research,* **109,** C03002, doi:10.1029/2003JC001962. (2004).

M. Winton "Does the Arctic sea ice have a tipping point?" *Geophysical Research Letters,* **33,** L23504, doi:10.1029/2006GL028017. (2006).

R.A. Woodgate. and K. Aagaard "Revising the Bering Strait freshwater flux into the Arctic Ocean" *Geophysical Research Letters,* **32,** L02602, doi:10.1029/2004GL021747. (2005).

R.A. Woodgate, K. Aagaard, and T.J. Weingartner "A year in the physical oceanography of the Chukchi Sea: Moored measurements from autumn 1990-1991" *Deep Sea Research II,* **52,** 3116-3149. (2005a).

R.A. Woodgate, K. Aagaard and T.J. Weingartner "Monthly temperature, salinity, and transport variability of the Bering Strait through flow" *Geophysical Research Letters,* **32,** L04601, doi:10.1029/2004GL021880. (2005b).

R.A. Woodgate, K. Aagaard, and T.J. Weingartner " Interannual changes in the Bering Strait fluxes of Volume, Heat and Freshwater between 1991 and 2004" *Geophysical Research Letters,* **33,** L15609, doi:10.1029/2006GL026931. (2006).

R.A. Woodgate, T. Weingartner, and R. Lindsay "The 2007 Bering Strait oceanic heat flux and anomalous Arctic sea?ice retreat" *Geophysical Research Letters,* **37,** L01602, doi:10.1029/2009GL041621. (2010).

M. Yamamoto-Kawai, N. Tanaka, and S. Pivovarov "Freshwater and brine behaviours in the Arctic Ocean deduced from historical data of δ^{18}O and alkalinity (1929-2002 A.D.) *Journal of Geophysical Research,* **110,** C10003, doi:10.1029/2004JC002793. (2005).

M. Yamamoto-Kawai, F.A. McLaughlin, E.C. Carmack, S. Nishino, K. Shimada, and N. Kurita "Surface freshening of the Canada Basin, 2003-2007: River runoff versus sea ice meltwater" *Journal of Geophysical Research,* **114,** C00A05, doi:10.1029/2008JC005000. (2009a).

M. Yamamoto-Kawai, F.A. McLaughlin, E.C. Carmack, S. Nishino, and K. Shimada "Aragonite undersaturation in the Arctic Ocean: Effects of ocean acidification and sea ice melt" *Science,* **326,** 1098. (2009b).

J. Yang "The Seasonal Variability of the Arctic Ocean Ekman Transport and Its Role in the Mixed Layer Heat and Salt Fluxes" *Journal of Climate,* **19,** 5366-5387. (2006).

J. Yang "Seasonal and interannual variability of downwelling in the

Beaufort Sea" *Journal of Geophysical Research,* **114,** C00A14, doi:10.1029/2008JC005084. (2009).

J. Yang, J. Comiso, D. Walsh, R. Krishfield, and S. Honjo "Storm-driven mixing and potential impact on the Arctic Ocean" *Journal of Geophysical Research,* **109,** C04008, doi:10.1029/2001JC001248. (2004).

J. Zhang and M. Steele "Effect of vertical mixing on the Atlantic Water layer circulation in the Arctic Ocean" *Journal of Geophysical Research,* **112,** C04S04, doi:10.1029/2006JC003732. (2007).

Appendix A

Particles Within the Summer Halocline

Several recent papers have described the increased freshwater content within the Canada Basin (McPhee et al. 2009, Proshutinsky et al. 2009, Yamamoto-Kawai et al. 2009a) and have discussed how this has affected the upper ocean stratification (Chapter 2; Toole et al. 2010). In particular, the near-surface summer halocline is believed to be a manifestation from increased freshwater content whose intense stratification forms a barrier between the near-surface waters and Pacific waters below. Observations from Chapter 4 suggested that the concentration of particles trapped within the summer halocline in the Canada Basin increased from 2003-2008 as the stratification strengthened. To explore this, I calculated the average profiles of both the Brunt-Väisälä frequency and beam attenuation coefficient at stations located in the basin for each year (Figure A.1). I calculated the Brunt-Väisälä frequency (N) as $N^2 = -g/\rho \ \delta\rho/\delta z$. For this equation, a value of 9.8 ms^{-2} was used for gravity (g), ρ represents the observed density and z was the vertical distance measured upwards. To smooth the Brunt-Väisälä frequency, I ran a centred 5 m running mean.

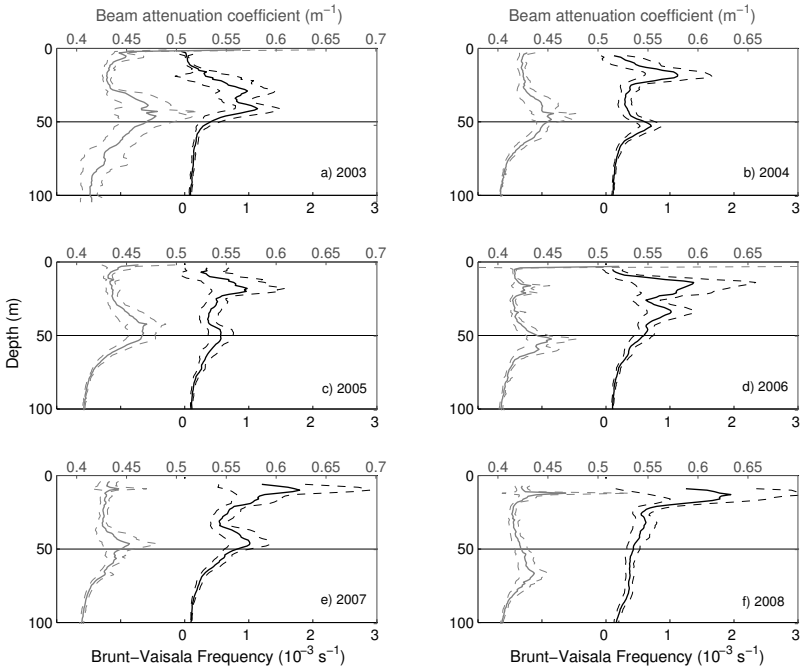

Figure A.1: A comparison of the average profiles within the Canada Basin of the Brunt-Väisälä frequency (black solid lines) and the beam attenuation coefficient (grey solid lines) during each summer cruise in a) 2003, b) 2004, c) 2005, d) 2006, e) 2007 and f) 2008. For the Brunt-Väisälä frequency, a 5 m centered running mean was calculated to smooth the data. To compute the average within the basin, only stations that were within the latitude range 73°-80°N and had a bottom depth greater than 3500 m were included. The black dashed lines and grey dashed lines indicate the 95% confidence interval for the Brunt-Väisälä frequency and beam attenuation coefficient, respectively. To compute this, 17 profiles in 2003, 21 profiles in 2004, 16 profiles in 2005, 17 profiles in 2006, 21 profiles in 2007 and 21 profiles in 2008 were used.

This analysis showed two trends. The first was the widening of a high stratification layer. As was discussed in Chapter 2, this layer grew from depths of 15-58 m in 2003 to 3-93 m in 2008. The second was changes to the depth of the attenuation maximum. In 2003-4, the attenuation maximum was correlated with the deeper chlorophyll maximum near 50 m. From 2005-7, an attenuation feature was observed in the summer halocline at 19 m, 16 m, and 9 m, respectively, but the attenuation maximum was associated with the chlorophyll maximum. In 2008, I observed for the first time that the attenuation maximum at 12 m was located within the summer halocline at 11 m.

The appearance of particles within the summer halocline starting in 2005 raises several important questions. The first is whether the same number of particles are simply becoming concentrated in the summer halocline or if there are actually more particles being deposited into the Canada Basin. In Chapter 4, I observed that most of the particles within the summer halocline were inorganic (Figure 4.5). Inorganic particles are transported to the near-surface waters of the Canada Basin in river runoff (O'Brien et al. 2006) and in sea ice (Darby 2003). If river runoff were the main source of the particles, I would expect to see the highest attenuation features in 2007 since this was when there were the greatest fractions of Mackenzie and Russian river water in the Canada Basin (Yamamoto-Kawai et al. 2009a). Since this was not the case, it is more likely that the rapid sea ice melt observed in the Canada Basin (Comiso et al. 2008) resulted in a greater source of particles that, coupled with the increased stratification, led to the attenuation feature in the summer halocline. In addition, I suggest

that climate change will increase the number of particles deposited into the Canada Basin from melting sea ice because it is expected that increased coastal erosion will result in increased suspended particle concentrations in coastal regions (Carmack et al. 2006) that would be entrained into sea ice as it forms in fall.

The second main question is how the increased suspended particles could affect the underwater light environment. Until recently it was thought that phytoplankton in the Canada Basin are primarily nutrient-limited (Carmack et al. 2006), however, with the deepening of PSW (Figure 3.11), it is possible that phytoplankton could become more light-limited. This light limitation could be compounded if the increased particles within the summer halocline were shading the deeper phytoplankton. To approximate this effect, I consider two different scenarios. In both cases, there is a 50 m chlorophyll maximum (the average depth of the chlorophyll maximum from 2003-7) located at 2% of the surface light intensity. Based on this information, I can calculate the extinction coefficient (k) as:

$$k = (ln(I_o) - ln(I_D))/D \tag{A.1}$$

where I_o is the irradiance at 1 m (which I estimate as 42 Wm^{-2} following Chapter 2), I_D is the irradiance at the 2% surface light intensity (0.8 Wm^{-2}) at the 50 m (D) chlorophyll maximum.

In the first scenario there are no particles within the summer halocline so k over the upper 50 m is 0.078 m^{-1}. In the second case there is a 10 m summer halocline with an extinction coefficient, based on the 2008 average

beam attenuation coefficient profiles (Figure A.1) that is 0.02 m^{-1} greater than the clear water so the average extinction coefficient over the upper 50 m is 0.082 m^{-1}. I can then calculate the depth of the 2% surface light intensity as:

$$D = (ln(I_o) - ln(I_D))/k \tag{A.2}$$

I find that the addition of particles in the summer halocline that increase the extinction coefficient by 0.02 m^{-1} for 10 m would cause the depth of the 2% surface light intensity to shoal from 50 m to 48.3 m. While 2 m does not seem like a great difference, it could be important if the PSW continues to descend, thereby causing the phytoplankton to choose between light and nutrient limitation. It is important to note that I did not consider the effects of decreased sea ice on the underwater light environment and suggest that this would have a larger impact than the increased particles in the summer halocline.